

# **CRUSTAL AND UPPER MANTLE IMAGING OF BOTSWANA USING MAGNETOTELLURIC METHOD**

STEPHEN AKINWUMI AKINREMI

June 2021

SUPERVISORS:

Dr. Islam Fadel

Prof.Dr. Mark van der Meijde



# **CRUSTAL AND UPPER MANTLE IMAGING OF BOTSWANA USING MAGNETOTELLURIC METHOD**

**STEPHEN AKINWUMI AKINREMI**

Enschede, The Netherlands, June 2021

Thesis submitted to the Faculty of Geo-Information Science and Earth Observation of the University of Twente in partial fulfilment of the requirements for the degree of Master of Science in Geo-information Science and Earth Observation.

Specialization: Applied Remote Sensing for Earth Sciences

**SUPERVISORS:**

Dr Islam Fadel

Prof.Dr Mark van der Meijde

**THESIS ASSESSMENT BOARD:**

Dr. C. A. Hecker (Chair)

Prof. Dr. Michael Becken (External Examiner, University of Munster)

#### DISCLAIMER

This document describes work undertaken as part of a programme of study at the Faculty of Geo-Information Science and Earth Observation of the University of Twente. All views and opinions expressed therein remain the sole responsibility of the author, and do not necessarily represent those of the Faculty.



## ABSTRACT

There exist some unclear and debated hypotheses about important tectonic features and the geodynamics of Botswana. There are open debates on the existence of a buried Maltahohe microcraton in the southwest region, termination of the East African Rift System in northern Botswana (Okavango Rift Zone), the extension of the East African Rift System to central Botswana, and its influence on the 03 April 2017 earthquake. Further exploration of the crust and upper mantle beneath Botswana in these highlighted tectonic domains would fundamentally improve our understanding of the two main features of the south African lithosphere, the African superswell and the East African Rift System. Besides understanding these features, it would improve the understanding of the current tectonic settings of Botswana and the deformation history.

This research presents a homogenous 3-D electrical model with an unprecedented spatial coverage, using a robust methodological scheme that requires no assumption about the directionality of the subsurface structure. The result of this study shows a resistive structure in southwest Botswana, which suggests the existence of the Maltahohe microcraton as a separate cratonic unit from the adjacent geologic terranes. In northern Botswana, the electrical conductivity model reveals a high conductivity structure around the Okavango Rift Zone, which connects with a deeper high conductivity structure that corresponds to the East African Rift System's extension to northern Botswana. This gives a piece of evidence to the role of ascending hot fluids or melt, leading to weakening of the lithosphere and subsequent rifting in the Okavango Rift Zone. Finally, the result of the electrical model could not establish the link between the high conductivity structures due to the East African Rift System in northern Botswana and beneath central Botswana (location of the 03 April 2017 earthquake) because of poor constrain of the model due to sparse magnetotelluric site distribution in the area.

The results of this study provides straightforward, connected, and precise geologic interpretations about different arguments raised in the literature on the tectonics and structure of the crust and upper mantle beneath Botswana. This work underscores the need to complement, confirm or refute findings from other geophysical data about the structure of the crust and upper mantle with electrical models derived from the magnetotelluric method.

## ACKNOWLEDGEMENTS

First and foremost, thanks be to God Almighty for the gift of life, strength, and grace to complete this work.

Sincere gratitude to my supervisors: Dr. Islam Fadel and Prof. Dr. Mark Meijde. I appreciate the mentorship and guide I enjoyed from you both. Your advice, discussions, critical comments, reviews, and commendations contributed to the success of my thesis. Thank you, Islam. You sharpened my programming skills, which helped me in achieving more in this research than I would have done ordinarily. You made me believe I could learn it and do it, even without prior programming knowledge. Islam, thanks a lot. Words are not enough to express my sincere and special appreciation to Dr. Harald van der Werff, my academic mentor. Our discussion in November 2019, the early guides, and supports you gave immensely solidified my interest and choice of MSc research. Beyond books, you are always there to check how I was doing in an unusual virtual learning time. Thank you, Harald.

Thanks to the staff members of the Earth Systems Analysis department for the quality lectures, guides, and administrative supports. Special thanks to my friends and colleagues at the ITC. I am glad to have met amazing and bright minds like you. Thank you, Ken Witherly, for sponsoring my magnetotelluric short course with Prof. Alan Jones. This opportunity indeed helped to sharpen my understanding of the magnetotelluric method. Thanks to the management of the Dutch National Supercomputer, Cartesius, for providing fast computing facilities (Grant Number: EINF-1468) that accelerated the successful completion of this research.

Many thanks to the ITC Foundation Special Scholarship for fully financing my MSc study. I still stand astounded at the merit selection for the scholarship award without an application, when all hopes of graduate school funding were lost. It was indeed a life-changing opportunity.

Special thanks to my dad and mum for your love, support, and encouragement from day one. Thank you, my siblings, Adebola, Christianah, John, and John (Jnr.) – much love. Thank you, Mummy Debbie, for the motherly support and love. Thank you, Tashingirira, my beautiful gem.

# TABLE OF CONTENTS

---

1.	INTRODUCTION.....	1
1.1.	Background.....	1
1.1.1.	Some Existing Hypotheses on the Tectonics of Botswana .....	3
1.1.2.	Geophysical Investigation of the Crust and Upper Mantle .....	4
1.1.3.	Magnetotelluric Method for Crust and Upper Mantle Imaging .....	5
1.2.	Problem Statement .....	6
1.3.	Research Objectives.....	7
1.3.1.	Main Objective .....	7
1.3.2.	Sub-objectives.....	7
1.4.	Research Questions .....	7
1.5.	Thesis Structure.....	7
2.	STUDY AREA AND GEOPHYSICAL STUDIES .....	8
2.1.	Study Area.....	8
2.2.	Geological Terranes of Botswana .....	8
2.2.1.	Cratons.....	8
2.2.2.	Mobile Belts .....	10
2.2.3.	Passarge and Nosop Basins .....	11
2.3.	Previous Geophysical Studies .....	11
2.3.2.	Seismological and Seismic Studies.....	12
2.3.3.	Magnetotelluric Studies .....	14
2.3.4.	Joint Velocity-Conductivity Inversion and Interpretation Efforts .....	17
3.	DATASET AND METHODOLOGY.....	18
3.1.	The Magnetotelluric Method .....	18
3.1.1.	Overview .....	18
3.1.2.	Basic Theoretical Concepts of Electromagnetics .....	18
3.1.3.	Transfer Functions of Magnetotelluric Response .....	19
3.1.4.	Dimensionality Distortion of Magnetotelluric Data .....	21
3.1.5.	Distortion of the Magnetotelluric Data.....	21
3.1.6.	What can the Magnetotelluric Method Image? .....	23
3.2.	Dataset .....	24
3.3.	Methodology.....	25
3.3.1.	Codes .....	25
3.3.2.	Data Correction and Preparation .....	25
3.3.3.	Data Analysis .....	27
3.3.4.	3-D Inversion .....	28
3.3.5.	Model Visualization and Assessment.....	31
4.	RESULTS AND DISCUSSION .....	32
4.1.	Magnetotelluric Data Analysis .....	32
4.1.1.	Resolution Depth and Horizontal Adjustment Length .....	32
4.1.2.	Apparent Resistivity.....	33

4.1.3. Dimensionality of the Magnetotelluric Data.....	34
4.2. Results and Discussion on Sensitivity Tests.....	34
4.2.1. Data Period Resolution.....	36
4.2.2. Effects of Short Period Data in Inversion Process.....	36
4.2.3. Model Grid Resolution.....	37
4.2.4. ModEM Inversion Damping Parameter.....	39
4.3. Nationwide 3-D Electrical Conductivity Model of Botswana.....	40
4.3.1. Evaluation of Data Fit of the 3-D Nationwide Electrical Conductivity Model.....	41
4.3.2. Overview of the Electrical Structure of the Crust and Upper Mantle.....	42
4.3.3. Imaging the Geological Provinces of Botswana.....	44
4.3.4. The Maltahohe Microcraton – Okavango Rift Zone – East African Rift System.....	51
4.4. Velocity-Conductivity Interpretation.....	54
5. CONCLUSION AND RECOMMENDATION.....	57
5.1. Conclusion.....	57
5.2. Research Limitations.....	58
5.3. Recommendations.....	58

## LIST OF FIGURES

---

Figure 1.1: Topographic map of Africa showing Botswana in black contour, African Superswell, and the East African Rift System (EARS) rift lines in red lines. ....	2
Figure 1.2: Map showing the main tectonic units in Botswana (McCourt, Armstrong, Jelsma, & Mapeo, 2013; Singletary et al., 2003). Transparent grey area = Okavango Rift Zone, MC = Suggested location of Maltahohe microcraton, and the focal mechanism represents the location and orientation of the 2017 6.5 Mw earthquake. ....	2
Figure 2.1: (a) Map showing the main tectonic units in Botswana from McCourt et al. (2013) and Singletary et al. (2003). (b) Sedimentary thickness map derived from aeromagnetic data (Pretorius 1984). Transparent grey area = Okavango Rift Zone, MC = Suggested location of Maltahohe microcraton, and the focal mechanism represents the location and orientation of the 2017 6.5 Mw earthquake. ....	8
Figure 2.2: Table summarizing the main tectonic events that formed the tectonics units in Botswana after Fadel (2018) .....	9
Figure 2.3: Regional tectonic map of southern Africa showing the distribution of seismic and MT data in the region. SAMTEX = Southern Africa Magnetotelluric Experiment (Jones et al., 2009), NARS = Network of Autonomously Recording Seismographs (NARS-Botswana) (Fadel et al., 2018), SASE = Southern Africa Seismic Experiment, SAFARI = Seismic Arrays for African Rift Initiation (Carlson et al., 1996), AfricaArray = Africa Array Initiative (Nyblade et al., 2008), GSN = Global Seismological Network. ....	12
Figure 2.4: Location of SAMTEX sites across Botswana showing previously interpreted sites in magenta squares: (a) Muller et al., (2009) (b) Miensopust et al., (2011) (c) Khoza et al., (2012) (d) Khoza et al., (2013) (e) Evans et al., (2019) (f) Moorkamp et al., (2019). Other MT sites are shown in black squares. Transparent grey area = Okavango Rift Zone, MC = Suggested location of Maltahohe microcraton, and the focal mechanism represents the location and orientation of the 2017 6.5 Mw earthquake. ....	15
Figure 2.5: Electrical conductivity models derived from 2-D smooth inversion of decomposed MT station responses by Muller et al. (2009) for (a.) 25° E of N strike azimuth and (b.) 45° E of N azimuth (c) Map of MT stations covering Botswana. The magenta squares show the MT sites profile published by Muller et al. (2009). ....	16
Figure 2.6: (a) Electrical conductivity model cross-section across Limpopo Belt-Kaapvaal Craton and Zimbabwe Craton in Botswana derived from 3-D inversion of MT data by Khoza et al., (2012) (b) Map of MT stations covering Botswana. The magenta squares show the MT sites across the profile presented in (a). SPTSS=Sunnyside-Palala-Tshipise Shear System.....	16
Figure 2.7: (a) Electrical conductivity model cross-section in northwest Botswana derived from 3-D inversion of MT data by Khoza et al., (2013) (b) Map of MT stations covering Botswana. The magenta squares show the MT sites across the profile presented in (a). ....	17
Figure 3.1: Volumetric sensitivity of the MT data in the subsurface .....	24
Figure 3.2: Apparent resistivity and impedance phase curves showing the effects of laterally displaced structure on MT data (Simpson & Bahr, 2005). In a simple 2-D MT model interpretation, E-pol.= E-polarisation mode in which electric fields parallel to the strike direction and B-pol.= B polarisation mode in which magnetic fields is parallel to the strike direction. ....	24
Figure 3.3: (a) Map of full SAMTEX sites. Red squares represent MT sites (b) SAMTEX data subset covering Botswana used in this research. ....	25
Figure 3.4: Methodology workflow .....	26
Figure 3.5: Examples of data correction of MT data through the galvanic distortion removal, static shift correction and data smoothening processing steps. Products are plotted as apparent resistivity and impedance phases against period (in logarithm scale). (a) Raw MT response from station Bot 409 (b)	

Corrected Bot 409 MT data after galvanic distortion, static shift correction and data smoothening. (c) Raw MT response from station Bot 417. (d) Corrected Bot 417 MT data (similar to (b)).	27
Figure 3.6: Map of SAMTEX data covering 355 stations in Botswana used for the nationwide 3-D electrical conductivity modelling (MT station represented with black squares).	30
Figure 3.7: (a) Map of SAMTEX data covering 127 stations used for data period and model grid resolution sensitivity tests (b) Map of SAMTEX data covering 28 stations used for ModEM inversion damping parameter sensitivity test (MT station represented with black squares).	31
Figure 4.1: Depth of penetration of the MT data at periods of 100, 250, 500, and 1,000 seconds. The MT sites are represented in circles and the corresponding depths of penetration are indicated by the colour.	33
Figure 4.2: Apparent resistivity maps for principal off-diagonal components ( $\rho_{xy}$ and $\rho_{yx}$ ) at representative periods of 100, 250, 500, and 1,000 seconds.	34
Figure 4.3: Phase tensor analysis result for three representative profiles. (a-c) Phase tensor ellipses for all periods in MT sites plotted. The corresponding profile location are also shown below each phase tensor ellipse plot. The phase tensors are plotted left-right or top to bottom along the profiles. The pseudo sections are plotted as circles and ellipses, while the colour indicates the skew value of the phase tensor.	35
Figure 4.4: nRMS plot per station for impedance tensor and tipper data components derived for 10 km, 15 km, and 30 km model grid resolutions. The MT sites are represented in circles and the corresponding nRMS are indicated by the colour. Masked sites (shown in black colour) =no data.	38
Figure 4.5: (a) Plan view of electrical conductivity model depth slices at 19 km derived for 10 km, 15 km, and 30 km grid resolution (b) Location Map. Red bounding box = location of models presented in (a).	39
Figure 4.6: (a) Plan view of electrical conductivity model depth slices at 49 km derived for 10 km, 15 km, and 30 km grid resolution (b) Location Map. Red bounding box = location of models presented in (a).	39
Figure 4.7: Plan view of electrical conductivity model depth slices at 49 km derived for 10 km, 15 km, and 30 km grid resolution. (b) Location Map. Red bounding box = location of models presented in (a).	40
Figure 4.8: nRMS plot per station for all components of the MT data, impedance ( $Z$ ) and VTFs. The MT sites are represented in circles, and the corresponding nRMS are indicated by the colour. Masked sites (shown in black colour) = no data.	41
Figure 4.9: Observed and predicted responses for three representative MT Sites. Location map shows the MT sites analysed.	42
Figure 4.10: Plan view of electrical conductivity model depth slices at 13 km, 20 km, 32 km, 50 km, 92 km, 120 km, 186 km, and 222 km depths. MT sites are represented in black dots.	43
Figure 4.11: Nationwide electrical conductivity model vertical profiles across the Rehoboth Province - Kheis Belt - Okwa Block - Kaapvaal Craton in southwest Botswana. KC=Kaapvaal Craton, KB=Kheis Belt, OB=Okwa Block, and RP=Rehoboth Province.	45
Figure 4.12: Electrical conductivity model from MT site profile across Congo Craton and Damara-Ghanzi-Chobe Terrane northwest Botswana. CC=Congo Craton, DGC=Damara-Ghanzi-Chobe Belt, and RP=Rehoboth Province.	48
Figure 4.13: Electrical conductivity model from MT site profile across Magondi Belt, Zimbabwe Craton and Limpopo Belt in southeast Botswana. DGC=Damara-Ghanzi-Chobe Belt, KC=Kaapvaal Craton, LB = Limpopo Belt, MB=Magondi Belt, and ZC = Zimbabwe Craton.	50
Figure 4.14: Electrical conductivity model cross-sections across southwest Botswana, ORZ, and Central Botswana. The red star = location of the 6.5 Mw earthquake in Central Botswana. CC=Congo Craton, DGC=Damara-Ghanzi-Chobe Belt, KC=Kaapvaal Craton, KB=Kheis Belt, MB=Magondi Belt, and RP=Rehoboth Province.	52
Figure 4.15: (a) The 3-D shear wave velocity model of Botswana after Fadel et al. (2020). (b) Electrical conductivity model derived from MT data. The red star = location of the 6.5 Mw earthquake in 2017. The	

cross-sections are shown in relative (left) and absolute (right) shear wave velocity. The highlighter features are; CC=Congo Craton, DGC=Damara-Ghanzi-Chobe Belt, ER = East African Rift System, KC=Kaarvaal Craton, KB=Kheis Belt, MB=Magondi Belt, MC = Maltahohe microcraton, NB = Nosop Basin, OK = Okavango Rift Zone, PB = Passarge Basin, and RP=Rehoboth Province. .... 56

# LIST OF TABLES

---

Table 4.1: Summary of the nRMS for the Data Period Sensitivity Test.....36  
Table 4.2: Summary of the nRMS for the Model Grid Resolution Sensitivity Test.....37  
Table 4.3: Summary of the nRMS for Initial Damping Parameter Sensitivity Test .....40

# 1. INTRODUCTION

## 1.1. Background

The lithosphere is the Earth's rigid outer layer composed of the crust and the upper mantle. The Earth's lithosphere is divided into several lithospheric plates of varying composition, thicknesses, and densities. The African lithospheric plate is a major tectonic plate composed of large cratons of the Archean age and other smaller cratonic fragments sutured together by younger mobile belts and sedimentary basins (Begg et al., 2009). Cratons are stable blocks of the lithosphere that have survived various tectonic activities, while mobile belts and sedimentary basins are formed through extension, accretion, and rifting of the stable cratonic blocks (Cooper & Miller, 2014; Lenardic, 2003). These tectonic units all play essential roles in the geodynamics of the continent. The study of the cratons and the relationship with the African plate's mobile belts is essential to understand the tectonic evolution and geodynamics of the continent. As a result, it gives more insight into the crustal and mantle structures and the forces driving phenomena such as earthquakes, faulting, and mountain building in the region.

The African continent contains unique tectonic features, e.g., the African superswell in the south and the East African Rift System (EARS) in the east, which extends to the south (Figure 1.1). The African superswell is an anomalously uplifted region formed from a large buoyant plume structure between 30 and 5 million years ago and dominates Africa's southern region (Globig, Fernández, Vergés, Robert, & Faccenna, 2016). The southern Africa region is at an average of 500 m residual elevation higher than the global continental height (Brandt, Grand, Nyblade, & Dirks, 2011). The African superswell is surrounded by divergent plate boundaries, and it is beginning to break apart along the EARS, which is an important extensional tectonic feature in Africa (Hansen & Nyblade, 2013; Hansen, Nyblade, & Benoit, 2012; Ring, 2014). The EARS is an active process of continental splitting along divergent plate boundary in East Africa, which is approximately 5000 km long (Figure 1.1). The EARS comprises a series of rift basins and volcanic centres with seismicity, faulting, and volcanism (Saria, Calais, Stamps, Delvaux, & Hartnady, 2014). The EARS extends downward into the southern Africa region and is often interpreted to terminate in northern Botswana.

Botswana is an interesting area to study for tectonics and geodynamics. This is because the African superswell is at a very high elevation of about 1 km above sea level in Botswana and the southwestern tip of the EARS terminates in northern Botswana (Kinabo et al., 2007; Kinabo, Hogan, Atekwana, Abdelsalam, & Modisi, 2008b). These two tectonic features play vital roles in the tectonic history of Botswana. Botswana is a region covering transition between two major cratonic blocks: the Kalahari Craton, which comprises the Zimbabwe and Kaapvaal blocks, and the Congo Craton (Begg et al., 2009) (Figure 1.2). The deformation of the cratonic blocks through geologic history by rifting and accretion processes has shaped Botswana's crust and upper mantle. In between the bounding Kalahari and Congo cratonic blocks, the lithosphere beneath Botswana is composed of three mobile belts (Damara-Ghanzi Chobe, Kheis-Okwa-Magondi, and Limpopo Belts) and sedimentary basins (Passarge and Nosop basins), which were formed from various rifting and accretion processes (Begg et al., 2009; Haddon, 2005).

There have been many significant studies exploring the crust and upper mantle of Botswana. In the following subsection, three important tectonic domains in Botswana will be highlighted with a succinct overview of what has been found and findings still under debate.

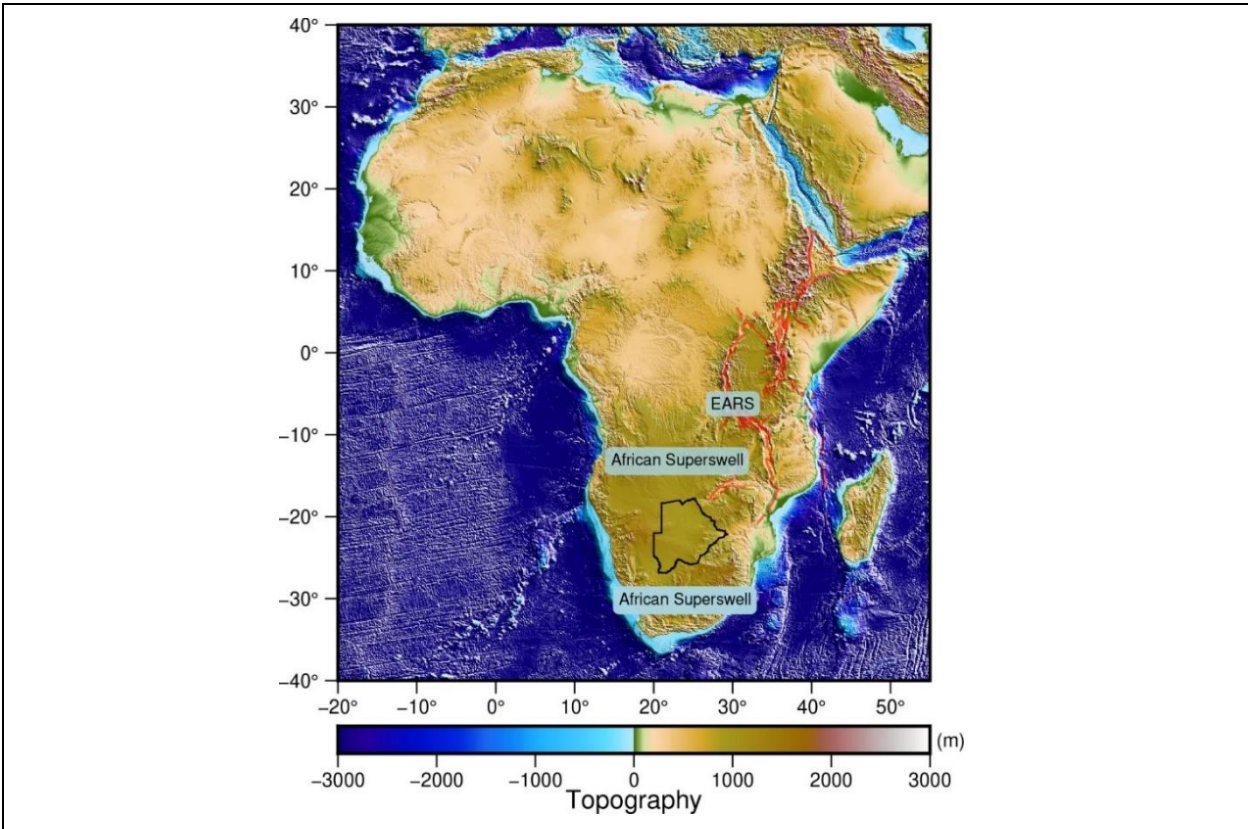


Figure 1.1: Topographic map of Africa showing Botswana in black contour, African Superswell, and the East African Rift System (EARS) rift lines in red lines.

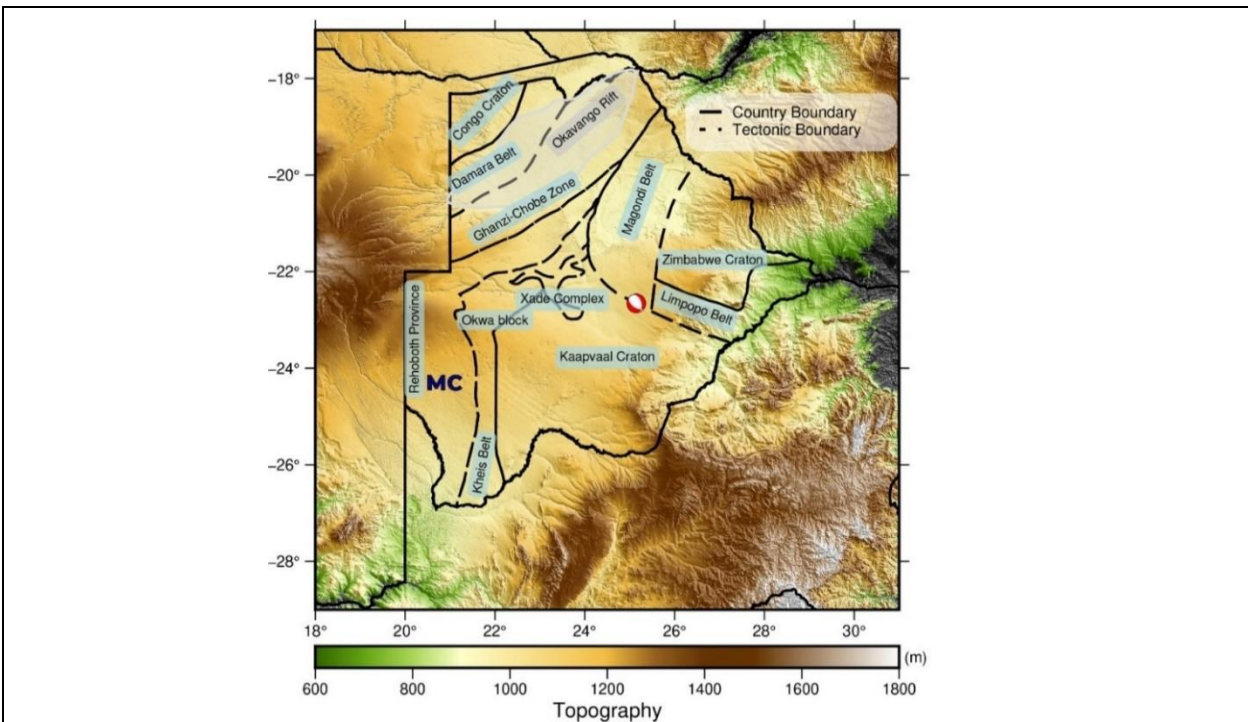


Figure 1.2: Map showing the main tectonic units in Botswana (McCourt, Armstrong, Jelsma, & Mapeo, 2013; Singletary et al., 2003). Transparent grey area = Okavango Rift Zone, MC = Suggested location of Maltahohe microcraton, and the focal mechanism represents the location and orientation of the 2017 6.5 Mw earthquake.

### 1.1.1. Some Existing Hypotheses on the Tectonics of Botswana

In the last two decades, many studies have been carried out to image the crust and upper mantle beneath Botswana compared to previous years. Nonetheless, there is a need for more exploration and clarity on current debates on some important tectonic domains that play significant roles in the geodynamic of Botswana. In this subsection, three of these tectonic domains are described, which include the existence and boundaries of a buried microcraton in southwest Botswana, the Okavango Rift Zone (ORZ), possible rifting in central Botswana, and its link to the 03 April 2017 6.5 Mw earthquake.

#### The Maltahohe Microcraton

In the southwest region of Botswana, the upper crust is formed by the Nosop basin, which is a part of the Rehoboth Province and filled with thick sediments of Nama Group up to 15 km depth (Begg et al., 2009; Pretorius, 1984; Wright & Hall, 1990). According to Begg et al. (2009), there may exist an ancient Maltahohe microcraton (MC) beneath the Rehoboth Province (Figure 1.2). In an earlier seismic study, Wright & Hall (1990) interpreted the structure beneath the Rehoboth Province as an extension of the Kaapvaal craton to the Namibian border. However, more recent seismic studies in the area (Fadel et al., 2020; Fadel, van der Meijde, & Paulssen, 2018) argued that the MC is separate from the Kaapvaal Craton, which is revealed by the observed different  $V_p/V_s$  ratios. Similarly, Chisenga, Jianguo, Fadel, Meijde, & Atekwana (2020), in a study using gravity and aeromagnetic data, supported the presence of the buried MC. However, the study argued that the location of the MC is likely south of the region suggested by Fadel et al. (2020, 2018). No previous study has been carried out using the available magnetotelluric (MT) data to investigate the suggested cratonic structure in southwest Botswana. Therefore, it is imperative to study this area further to confirm or reject the hypothesis on the existence of the MC and, if it does exist, understand its boundaries and relationship with the other cratonic blocks.

#### The Okavango Rift Zone

The EARS has been considered to have its southwestern terminus in northern Botswana (Okavango Rift Zone - ORZ) from early studies of the fault morphology and geophysical data from the area (Modisi, 2000; Modisi, Atekwana, Kampunzu, & Ngwisanyi, 2000; Scholz, Koczyński, & Hutchins, 1976). The EARS has surface expression very close to northern Botswana, evident by the rift lines (Figure 1.1). The ORZ is widely interpreted to be an incipient continental rift zone in northern Botswana (Figure 1.2), consisting of several normal to dextral strike-slip faults (Kinabo et al., 2008b; Modisi et al., 2000). However, the termination of EARS in ORZ or its further continuation in Botswana is yet to be fully understood. There are divergent views on whether the EARS terminates in northern Botswana or extends southward (Chorowicz, 2005; Kebede & Kulhánek, 1991; Kinabo et al., 2008b; Lescane et al., 2015; Pastier et al., 2017). Pastier et al. (2017) argued that there is no rifting in the Okavango area. They proposed a model of differential movement between the Congo and Kalahari cratons from their geodetic study. This argument by Pastier et al. (2017) is contrary to other studies that support rifting in ORZ. For example, Yu, Liu, Moidaki, Reed, and Gao (2015) and Yu, Liu, Reed, et al. (2015) suggest rift initiation along ancient orogenic zones in ORZ from their studies. Recently, Fadel et al. (2020) and Fadel et al. (2018) presented Botswana's first 3-D shear-wave velocity from seismological data. Their nationwide 3-D shear-wave velocity results showed a possible incipient rifting in central Botswana, evident by a thin crust (Fadel et al., 2018). The low-velocity anomaly observed in the Okavango seems to connect with the low-velocity anomaly in central Botswana Fadel et al. (2020). According to Fadel et al. (2020), these anomalies relate to possible incipient rifting in central Botswana as an extension of the EARS. These divergent views about the rifting in ORZ require further exploration and understanding from other geophysical data and models, such as the electrical conductivity model.

### **The 03 April 2017 6.5 Mw Earthquake**

There was a recent intra-plate earthquake in Botswana. On 03 April 2017, a 6.5 magnitude earthquake struck central Botswana (Figure 1.2) at an approximate depth of 29 km (Gardonio, Jolivet, Calais, & Leclère, 2018). The earthquake was the second-strongest in magnitude in the country's history and the second strongest intra-plate earthquake in the last 30 years (Gardonio et al., 2018; Midzi et al., 2018). Several studies, including the use of geophysical methods, have discussed the cause of the earthquake. Gardonio et al. (2018) suggest that the earthquake event was triggered by stress released from fluid migration from the mantle. Moorkamp et al. (2019) used surface wave and MT data to investigate the area around the earthquake location. Their results suggest that the event may be caused by weakness in the crust and upper mantle but not indicative of mantle upwelling. Their results could neither verify nor invalidate the deep mantle fluid migration source suggested by Gardonio et al. (2018). According to Fadel et al. (2020), the process that caused the earthquake suggests that it was associated with the EARS. Their result shows a connection between the low-velocity anomaly of the EARS and the low-velocity anomaly in central Botswana. Fadel et al. (2020) proposed that the EARS extends to central Botswana and that the fluids associated with the EARS triggered the 03 April 2017 earthquake in central Botswana.

On the contrary to the proposition of Fadel et al. (2020), Kolawole et al. (2017), in a combined magnetic, gravity and differential interferometric synthetic aperture radar study, argued that the earthquake event is not linked to the EARS. From their results, the orientation of the tensional stress that caused the earthquake (northeast-southwest) is different from the northwest-southeast directed tensional stress acting on the ORZ, which is an extension of the EARS. They suggest that the earthquake event was caused by extensional reactivation of a thrust splay in the crust. The limited coverage of the MT data used by Moorkamp et al. (2019) prevented the understanding of the connection between the EARS and the earthquake event from the view of the conductivity properties of the subsurface. These divergent views on the cause of the earthquake and the possible role of the EARS in the event are yet to be fully understood.

#### **1.1.2. Geophysical Investigation of the Crust and Upper Mantle**

The structure of the crust and upper can be understood from the petrological and geochemical studies of magma and xenoliths from volcanic rocks (Reilly & Griffin, 2006). However, these methods are limited because bedrock samples are not available for large areas and are scattered in space and time (Begg et al., 2009). In areas that are extensively covered by sediment, such as Botswana, it becomes impossible to collect bedrock samples to study the crust and upper mantle structure. To improve our understanding of the crust and upper mantle structure, the models from petrological and geochemical studies can be tested with appropriate geophysical data interpreted in terms of evolution and composition (Begg et al., 2009; Unsworth & Rondenay, 2012).

Geophysical methods used at the Earth's surface can measure in-situ and spatial variations of the physical properties of the subsurface. Among the various geophysical methods, seismology and electromagnetics methods are the primary geophysical methods for studying the crust and upper mantle because of the ability to image deep Earth structures (Panza, Peccerillo, Aoudia, & Farina, 2006). For studies of the crust and upper mantle structure, the MT method is the most suitable electromagnetic methods due to its ability to image great depths (Unsworth & Rondenay, 2012).

In the study of the crust and upper mantle structure, the seismological methods cannot clearly distinguish between the influence of the variations in temperature and chemical composition on the observed wave speeds, which is an important piece of information in rift zone studies (Moorkamp, Jones, & Eaton, 2007). It is therefore essential to validate interpretations from seismological methods with results from MT data. The MT data looks at different and independent geophysical information that is not accessible by

seismological methods. The MT method gives information about the electrical conductivity of the subsurface, which is the geophysical property that shows the most significant contrasts in the subsurface material (Telford, Geldart, & Sheriff, 2004). The wide variance in electrical conductivity gives a potential for producing well-constrained electrical models that can delineate variations in temperature and composition of the Earth's subsurface material. For example, Becken & Ritter (2012) and Unsworth (2010) describe how the MT method can be used to map the presence of aqueous fluids and partial melts in rocks and thermal structures. Electrical conductivity model derived from MT data can be used to image buried cratonic units, the occurrence of rifts, rift extension, and presence of fluid or melt in the crust and upper mantle. These capabilities of the MT method make it a potential method for further exploration of the existence of MC, rifting in ORZ, and an extension of the EARS to central Botswana. More discussion about the MT method and its application in the crust and upper mantle study is explained in the following subsection.

### **1.1.3. Magnetotelluric Method for Crust and Upper Mantle Imaging**

The MT is a passive and non-invasive method for imaging the electrical conductivity of the subsurface of the Earth. It is used for commercial purposes such as exploration for oil and gas, mineral and geothermal resources, and crustal and mantle studies. The MT method measures the time variations of the Earth's natural electromagnetic field from solar energy and lightning that changes due to the variation in the Earth's interior (Simpson & Bahr, 2005). The MT method can image deep depths ranging from a few meters to hundreds of kilometres in the subsurface (up to the mantle) by recording at longer periods (Simpson & Bahr, 2005). The method is sensitive to lateral and vertical variations in electrical conductivity and can differentiate geological terranes and the effects of temperature in the subsurface. Electrical conductivity is sensitive to rocks' physical and petrological properties, including conductivity of rock-forming metals and minerals like sulfide and graphite, porosity, connectivity of the pores, pore fluid content, and conductivity of the pore fluids (Kearey, Brooks, & Hill, 2002). The electrical conductivity of the Earth's crust is also affected by the geological units, fractures, fluid phases, and temperature. In the mantle region, processes like partial melting, metasomatism and hydrogen diffusion affect electrical conductivity (Unsworth & Rondenay, 2012). The electrical conductivity of Earth material has a wide variance spanning up to 14 orders magnitude and can provide a more constrained model of the Earth's subsurface that reveals the presence of aqueous fluid, partial melt and thermal structures (Simpson & Bahr, 2005; Unsworth, 2010). Hence, the electrical model from MT measurements offers a unique insight to understanding the internal structure of the crust and upper mantle and the tectonics of a dynamically complex area like Botswana (Panza et al., 2006).

The MT method is suitable for imaging different geological terranes and their boundaries using their electrical conductivity properties. Cratonic segments can be delineated from the mobile belts based on conductivity signatures (Muller et al., 2009). Older lithospheric units (Archean Craton) are more resistive and thicker than the younger lithospheric units (Proterozoic mobile belts), which are thin and have higher conductivity (Muller et al., 2009). Cratonic boundaries and tectonic transition zones are made of suture zones which are characterised by weakened crust material due to deformation processes (Türkoğlu, Unsworth, Çağlar, Tuncer, & Avşar, 2008; Unsworth & Rondenay, 2012). Tectonic transition zones are usually characterised by relatively higher electrical conductivity, which can be well mapped with the MT data. Hence, electrical conductivity models could be used to map geologic terranes like cratonic provinces, mobile belts, and suture zones. In the context of this study, the electrical conductivity model derived from MT data can be used to map major geological provinces in Botswana and give a piece of evidence to either confirm or reject the hypothesis of the existence of a buried MC in southwest Botswana.

The MT data is also sensitive to fluid content and can give a piece of evidence about melt or fluid injection in the crust (e.g., Hill et al., 2009; Le Pape, Jones, Vozar, & Wenbo, 2012). The fluid or melt content of the crust and upper mantle, which is a factor for characterizing rift systems and collision zones, affects the subsurface's electrical conductivity (Unsworth, 2010). Melt or fluid content in the crust and upper mantle have a high electrical conductivity signature and would be evident from the electrical conductivity model (Moorkamp et al., 2019). In addition to these, the subsurface electrical model can be used to highlight rifting regions. In the context of this study, the electrical conductivity model derived from MT data could give a piece of evidence about the presence of aqueous fluids and partial melts, rifting, and rift extension in the crust and upper mantle beneath Botswana. The electrical conductivity model derived from MT data could potentially test and validate existing information from previous studies about rift mechanism in ORZ, EARS' extension to central Botswana, and influence of melt or fluid injection on 03 April 2017 earthquake in central Botswana.

## **1.2. Problem Statement**

This research aims to improve understanding of Botswana's crust and upper mantle structure by explaining the tectonic features and geodynamic processes in the crust and upper mantle using a 3-D geoelectric model derived from MT data. There exist unclear and debated hypotheses about some important tectonic features and the geodynamics of Botswana described previously (subsection 1.1.1). There are open debates on the existence of a buried MC in the southwest region, the termination of EARS in ORZ, the extension of the EARS to central Botswana, and its influence on the 03 April 2017 earthquake in central Botswana. The new 3-D geoelectric model developed offers new insight into understanding the tectonics of Botswana and would complement what is already known from other geophysical investigations.

A few small-scale studies have been conducted to image the crust and upper mantle beneath Botswana with MT data. However, studies so far are too fragmented and hardly overlap. Also, these previous MT studies did not coincide spatially with some of the important features of the tectonics of Botswana, like the ORZ and suggested MC in southwest Botswana. Hence, these are not fit to investigate the crust and upper mantle beneath Botswana wholly, resolving the tectonic boundaries on a national scale and providing insights about hypotheses on some important tectonic features from this perspective of MT data.

In this research, a 3-D nationwide electrical conductivity model of Botswana is derived from MT data to image the crust and upper mantle structure. The new information from the electrical conductivity model adds value to existing geophysical datasets in Botswana and brings new insight into the three tectonic domains highlighted previously (subsection 1.1.1). In this study, Botswana's crust and upper mantle are investigated to define the tectonic units and confirm or reject existing hypothesis about the buried MC, rifting in ORZ, and rift extension to central Botswana. Further exploration of the crust and upper beneath Botswana in these three highlighted tectonic domains above would fundamentally improve our understanding of the features in relation to the initiation and development of the two main features of the south African lithosphere, the African superswell and the EARS. Besides understanding these features, this study helps to improve the understanding of the current tectonic settings of Botswana, the deformation history, and the general African geodynamics. These improvements in understanding these important tectonic features of Botswana will be significant contributions to the scientific community.

### **1.3. Research Objectives**

#### **1.3.1. Main Objective**

The main objective of this research is to image the 3-D electrical structure of the crust and upper mantle of Botswana using MT data to highlight, confirm or reject existing hypotheses about the tectonics and geodynamics of Botswana.

#### **1.3.2. Sub-objectives**

To achieve the main objective of the proposed research, the following sub-objectives will be addressed:

1. to improve the understanding of the major geological provinces in Botswana with constraints from MT data;
2. to confirm or reject the hypothesis of the existence of buried Maltahohe microcraton in southwest Botswana, and if it exists, define the possible links with the Kaapvaal Craton;
3. to confirm or reject the hypothesis of rifting in the central part of Botswana from the interpretation of MT data with constraints from existing seismic models; and
4. if the EARS' extension to central Botswana is confirmed, understand its link with the mechanism that caused the 6.5 Mw earthquake in central Botswana.

### **1.4. Research Questions**

1. What improvements does the nationwide 3-D electrical conductivity model derived from MT data add to the understanding of the geological provinces in Botswana?
2. Are there electrical structures that suggest the existence of the buried MC in southwest Botswana?
3. If the presence of cratonic electrical structure is confirmed in southwest Botswana which suggests the existence of the buried MC, does it occur as a separate craton or as an extension of Kaapvaal Craton?
4. Can the MT data with constraints from the available seismic models confirm or reject the hypothesis of rifting along the Okavango zone?
5. Can the MT data, with constraints from the available seismic models, confirm or reject the hypothesis of rifting in central Botswana?
6. What is the role of the EARS in the 6.5Mw earthquake in central Botswana?

### **1.5. Thesis Structure**

Chapter 1: includes background, a brief description of the research problem, research objectives, research questions, and a brief description of the research methodology.

Chapter 2: includes a detailed description of the study area and previous studies.

Chapter 3: includes a detailed explanation of the dataset and the methodology.

Chapter 4: includes the results from the data analysis and the 3-D geoelectric model developed in this study with discussions of the results.

Chapter 5: includes the conclusion, limitations, and recommendations for future research.

## 2. STUDY AREA AND GEOPHYSICAL STUDIES

The first two sections (2.1 and 2.2) of this chapter describe the study area, Botswana, and gives an overview of the main geological provinces and the tectonic evolution of the region. After that, a concise overview of previous geophysical studies done within or covering parts of Botswana is explained (section 2.3).

### 2.1. Study Area

The study area covers Botswana (Figure 2.1). Botswana is an area covering two stable cratonic blocks; the Congo Craton and the Kalahari Craton (Zimbabwe and Kaapvaal blocks) (Begg et al., 2009) (Figure 2.1a).. Through several processes of accretion and rifting, mobile belts and sedimentary basins (Figure 2.1b) were formed in between the stable cratonic blocks (Haddon, 2005). An overview of the main tectonic events that formed the geologic terranes of Botswana is given in (Figure 2.2) and explained in the next section.

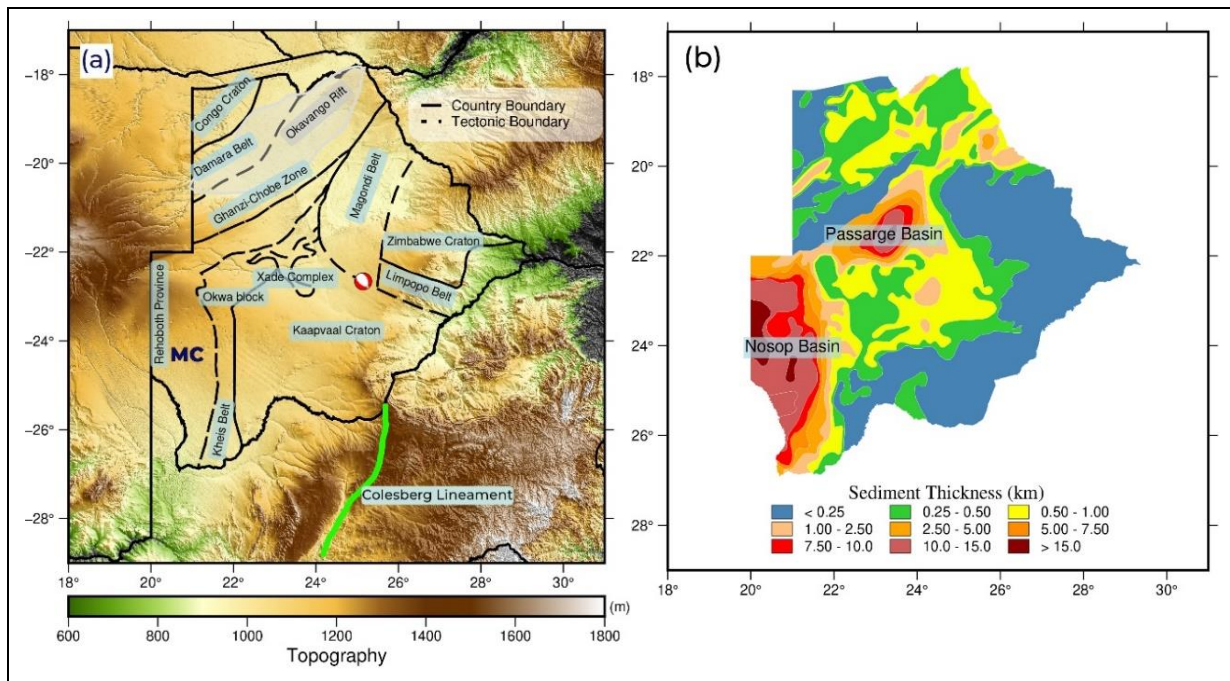


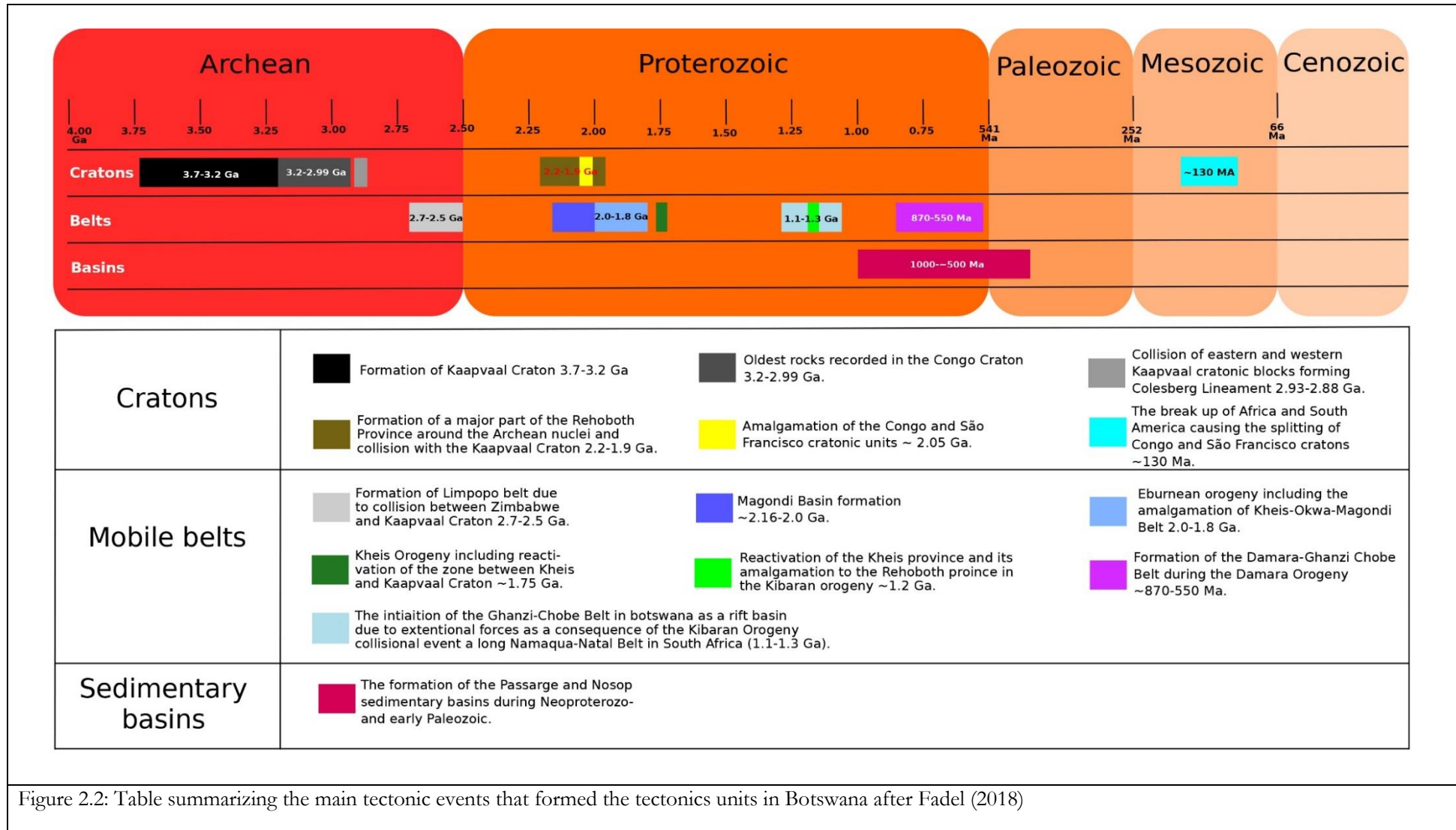
Figure 2.1: (a) Map showing the main tectonic units in Botswana from McCourt et al. (2013) and Singletary et al. (2003). (b) Sedimentary thickness map derived from aeromagnetic data (Pretorius 1984). Transparent grey area = Okavango Rift Zone, MC = Suggested location of Maltahohe microcraton, and the focal mechanism represents the location and orientation of the 2017 6.5 Mw earthquake.

### 2.2. Geological Terranes of Botswana

#### 2.2.1. Cratons

##### 2.2.1.1. Kalahari Craton

The Archean Kalahari Craton is made up of two cratonic blocks; the Zimbabwe block in the east and the Kaapvaal block in the southeast of Botswana (Begg et al., 2009) (Figure 2.1a). In between Zimbabwe and Kaapvaal cratonic blocks is the Limpopo mobile Belt. Limpopo Belt is a zone of weakness separating these two cratons. The Zimbabwe cratonic block consists of tonalite-trondhjemite-granodiorite gneiss complex formed around 3.5 – 2.8 Ga, which is unconformably overlain by flood basalt, komatites and sediments (Begg et al., 2009). The Kaapvaal cratonic block was formed between 3.7 – 3.2 Ga (Figure 2.2), and it is composed mostly of gneisses, granitoids and narrow greenstone Belts (Haddon, 2005).



### 2.2.1.2. Congo Craton

The larger parts of the Congo craton are located in Namibia and Angola. However, the southeastern border of the craton extends into the northwest Botswana and is poorly exposed due to sediments overlay (Fadel et al., 2018; Key & Ayres, 2000; Khoza et al., 2013). The Congo Craton is separated from the Zimbabwe and Kaapvaal cratonic blocks by Neoproterozoic Damara and Ghanzi-Chobe mobile belts (Figure 2.1a). The Congo Craton consists of various Archean and Paleoproterozoic units (Figure 2.2). In its southeastern border, which extends into Botswana, the Congo Craton consists of gneisses and granulite complex which are cut by younger granite plutons (Begg et al., 2009).

### 2.2.1.3. Rehoboth Province

The Rehoboth Province is a region that extends from eastern Namibia to southwest Botswana and is composed of aggregated mobile Belts during the Paleoproterozoic around an Archean nucleus (Van Schijndel, Cornell, Frei, Simonsen, & Whitehouse, 2014; Van Schijndel, Cornell, Hoffmann, & Frei, 2011). The main part of the Rehoboth Province was formed in the Proterozoic between 2.2 – 1.9 Ga around the Archean nuclei (Van Schijndel et al., 2011) and which later collided with the Kaapvaal Craton around 1.9 Ga (Luchs, Brey, Gerdes, & Höfer, 2013) (Figure 2.2). In the Rehoboth Province, there may exist an enigmatic ancient buried MC (Begg et al., 2009; Fadel et al., 2020), which was also interpreted by Wright and Hall (1990) as a deep extension of the Kaapvaal Craton.

## 2.2.2. Mobile Belts

### 2.2.2.1. Limpopo Belt

The Limpopo Belt separates the Zimbabwe and Kaapvaal cratonic blocks (Figure 2.1a). The Limpopo Belt is an Archean mobile belt formed from the collision between the Zimbabwe and Kaapvaal Cratons around 2.7 – 2.5 Ga (Begg et al., 2009) (Figure 2.2). The Limpopo Belt consists of rock units including migmatite, porphyritic granite, gneissic granite, metasedimentary rocks and meta-intrusive rocks (Key & Ayres, 2000). The Limpopo Belt is highly deformed and was affected by granulite-facies metamorphism, with the peak of the metamorphism process around 2.56 Ga in the northern zone and 2.7 Ga in the southern part (Begg et al., 2009). The Limpopo Belt appears to have been reactivated around 2.0 Ga as a result of the events in Kheis-Okwa-Magondi Belt (discussed next) and the emplacement of the Bushveld Complex, which is located in north-central part of the Kaapvaal Craton and is the largest mafic intrusion into the crust in the world (Begg et al., 2009; Haddon, 2005).

### 2.2.2.2. Kheis-Okwa-Magondi Belt

The Kheis-Okwa-Magondi composite, which is a Paleoproterozoic belt, covers the central part of Botswana in the northeast-southwest direction along the western boundary of Kaapvaal Craton (Figure 2.1). The Kheis located in the western margin of the Kaapvaal Craton is comprised of low to medium grade metamorphic rocks. The Archean rocks of the western margin of the Kaapvaal craton were also deformed and metamorphosed during the Kheis Orogeny around 1.75 Ga (Thomas, von Veh, & McCourt, 1993). The Okwa block consists of metamorphic rocks of 2.1 Ga and is believed to have been accreted to the Kaapvaal Craton around 1.8 Ga after its emplacement (Begg et al., 2009; Haddon, 2005) (Figure 2.2). The Magondi basin is composed of sediments sequence and volcanic rocks metamorphosed around 2.1 – 1.96 Ga (granulite grade) and intruded by granitoids. The Magondi basin was accreted with the Okwa-Kheis Belt during the Eburnean Orogeny, which was an episode of plutonic and metamorphic events around 2.0 – 1.8 Ga (Thomas et al., 1993) (Figure 2.2). The epicentre of the 03 April 2017 earthquake in central Botswana is located in the southeast boundary of the Magondi Belt (Figure 2.1).

### 2.2.2.3. Damara-Ghanzi-Chobe Belt

The Damara-Ghanzi-Chobe Belt (DGC) is located between the Congo Craton in its northwest and the Kalahari Craton in its southeast. The DGC was formed by the Damara Orogeny around 870 – 550 Ma, which was the start of the Neoproterozoic Pan-African event due to the collision between the Kaapvaal and Congo cratonic blocks (Haddon, 2005) (Figure 2.2). The Okavango Rift Zone (ORZ), an incipient rift zone, which is considered as the southwestern terminus of the EARS, is located within the Damara-Ghanzi-Chobe Belt (Kinabo, Hogan, Atekwana, Abdelsalam, & Modisi, 2008a; Modisi et al., 2000) (Figure 2.1a).

### 2.2.3. Passarge and Nosop Basins

There are two major sedimentary basins in Botswana which are caught between the Kheis-Okwa-Magondi and Damara-Ghanzi-Chobe mobile Belts (Figure 2.1b). The Passarge basin is located in central Botswana (Figure 2.1b), between the Ghanzi-Chobe Belt in northwestern Botswana and the Kaapvaal Craton. The Passarge basin is filled with thick and weakly folded sediments up to 15km from the Ghanzi Group sediments, which is composed of siliciclastic and carbonates sedimentary rocks (Key & Ayres, 2000; Pretorius, 1984) (Figure 2.2). In the southwest region of Botswana, the upper crust is formed by Nosop basin, which is a part of the Rehoboth Province (Figure 2.1b). The Nosop basin is filled with thick sediments up to 15 km depth formed from the deposition of the Nama Group sediments, which is composed of marine carbonates and siliciclastic rocks, and underlain by the Ghanzi Group sediments (Begg et al., 2009; Pretorius, 1984; Wright & Hall, 1990) (Figure 2.2).

## 2.3. Previous Geophysical Studies

The Botswana Geoscience Institute holds a compilation gravity dataset from multiple nationwide surveys and other gravity station from the private sector and research and educational projects which covers Botswana. Figure A1(a) (in Appendix 1) shows the coverage of the aeromagnetic data cover in southern Africa. Figure 2.3 shows the regional tectonic map and the distribution of seismic and MT data over the southern Africa region. A brief description of previous geophysical studies done within or covering parts of Botswana is explained in this subsection. These works include the use of gravity, magnetic, seismological, seismic, and MT dataset.

### 2.3.1.1. Gravity and Magnetic Studies

Gravity and magnetic data provided some of the earliest understanding of the geological provinces in Botswana due to the obscuring of the Precambrian geology by thick overburden formed from Kalahari group sediment (e.g., Hutchins & Reeves, 1980). The works of Hutchins and Reeves (1980) and Reeves and Hutchins (1982) formed the fundamental understanding of the different geological provinces in Botswana from magnetic and gravity mapping. Kinabo et al. (2007), in a detailed gravity and magnetic investigation, examined the processes of the early stage of the incipient continental rifting in ORZ. Their results show a strong correlation between the orientation of the pre-existing structures and fabrics (fold axes and foliation) in the basement and the rift induced faults. With this observation, they inferred that the pre-existing basement structure has a significant influence on the early development of the rift faults in ORZ. Leseane et al. (2015) investigated the thermal and Moho depth structure beneath the ORZ using gravity and magnetic data. Their results show shallow Curie Point Depths, thin-crust, and high heat flow from upward movement of mantle fluid to the lithosphere through weak lithospheric zones beneath the ORZ. On the contrary to Kinabo et al. (2007), Leseane et al. (2015) suggest a fluid influenced weakening of the lithosphere as the process facilitating the incipient rifting in ORZ. The electrical conductivity model is suitable for further investigation of this elevated heat regime and fluid weakening process beneath the ORZ.

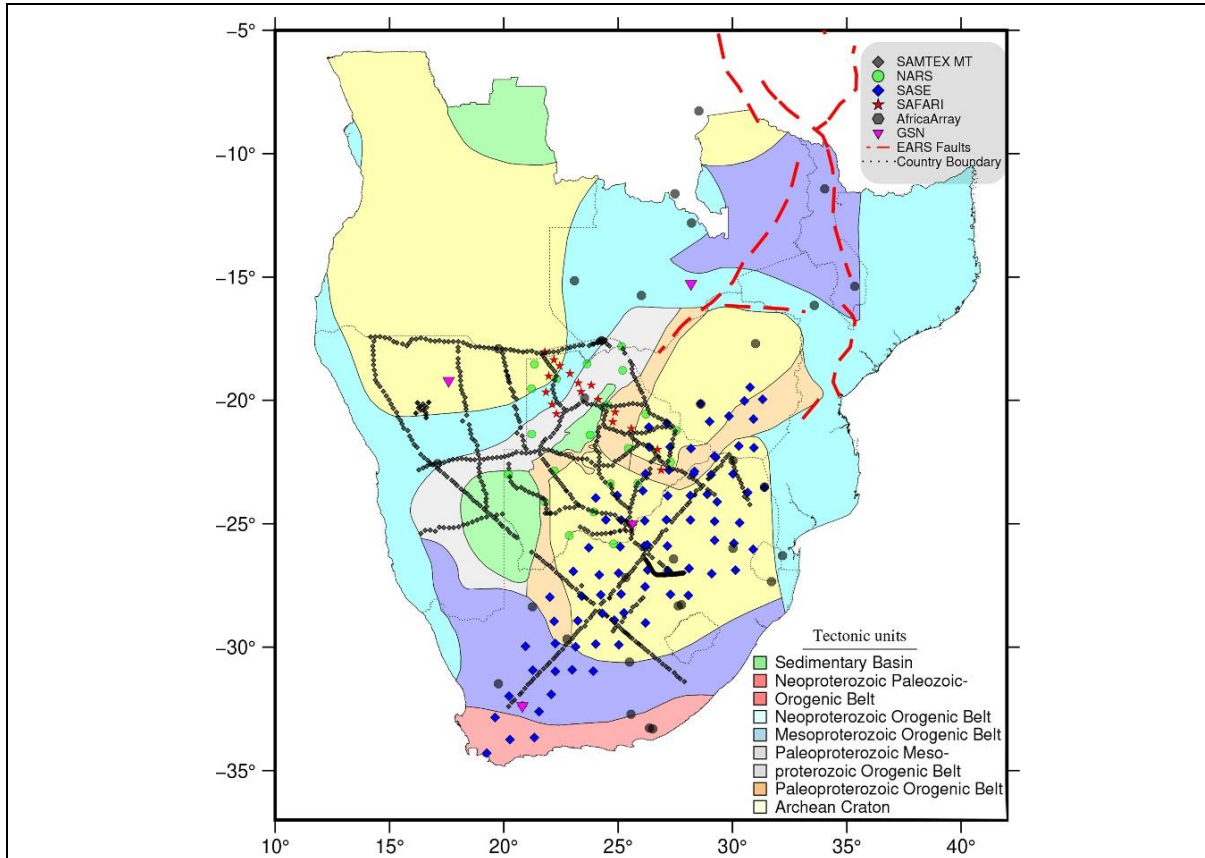


Figure 2.3: Regional tectonic map of southern Africa showing the distribution of seismic and MT data in the region. SAMTEX = Southern Africa Magnetotelluric Experiment (Jones et al., 2009), NARS = Network of Autonomously Recording Seismographs (NARS-Botswana) (Fadel et al., 2018), SASE = Southern Africa Seismic Experiment, SAFARI = Seismic Arrays for African Rift Initiation (Carlson et al., 1996), AfricaArray = Africa Array Initiative (Nyblade et al., 2008), GSN = Global Seismological Network.

In a more recent study, Chisenga, Jianguo, et al. (2020) integrated gravity and aeromagnetic data to investigate the crustal units and update the tectonic boundaries of Botswana. Their results confirmed the extension of the Congo Craton to northwestern Botswana as suggested by seismic and MT studies (e.g., Yu et al., (2017) and Khoza et al., (2013), which are described in the two subsequent subsections). In another recent study, Chisenga, Van der Meijde, et al. (2020) modelled the crustal thickness of the crustal structure beneath Botswana using gravity data. From their results, the crust beneath the epicentre of the 03 April earthquake in central Botswana is relatively thinner with an approximate thickness of 40 km compared to 43 km and 46 km thicknesses in adjacent Kaapvaal Craton and central part of Limpopo Belt, respectively. Their result suggested that the thinning of the crust beneath the earthquake epicentre was caused by migrating thermal fluids from the EARS, eroding the lower crust structure. They propose that the combination of migrating thermal fluids from EARS, high heat flow, thin-crust and local stress in the crust contributed to the 03 April earthquake occurrence. This proposition by Chisenga, Van der Meijde, et al. (2020) strongly support the role of the EARS, fluid migration, and elevated heat regime as part of the cause of the 03 April 2017 earthquake in Botswana, which the electrical conductivity modelling is suitable to test.

### 2.3.2. Seismological and Seismic Studies

Several seismological studies have been done to understand the tectonics of Botswana. One of the earliest seismological studies was done by Reeves (1972), which focused on the ORZ. This study reported a high level of seismicity and was the first to suggest an extension of the EARS to northern Botswana, causing

rift in the ORZ. Many years later, several other seismological studies covering the eastern and southeast Botswana (Kalahari Craton and Limpopo Belt areas) were done using the data from the temporary network of the Southern Africa Seismic Experiment (SASE) (Carlson et al., 1996) and the Africa Array Initiative (Nyblade et al., 2008) (Figure 2.3). These studies (e.g., Delph & Porter, 2015) allowed high-resolution imaging of the crustal and upper mantle structure in southeast Botswana.

Between 2013 – 2015, the Seismic Arrays for African Rift Initiation (SAFARI) was deployed across the ORZ (Gao et al., 2013) (Figure 2.3). The SAFARI project brought new understanding to the incipient rifting and crustal and upper mantle structure of the ORZ (Yu, Liu, Reed, et al., 2015; Yu, Gao, Moidaki, et al., 2015; Yu, Liu, Moidaki, Reed, & Gao, 2015). Yu, Gao, Moidaki, et al. (2015) conducted the first shear-wave splitting investigation of the ORZ. Their result show mantle anisotropy predominantly in the northeast-southwest direction with no evidence of horizontal component of a flowing mantle magma system. This result supports a differential basal drag model between the Congo Craton, Kalahari Craton, and the Damara-Ghanzi Chobe orogenic Belt in-between them, leading to intra-plate movements and passive rifting, rather than an active mantle plume source explanation for the rift incipient rifting in ORZ. Yu, Liu, Moidaki, et al. (2015) observed no thermal anomalies beneath the ORZ given the normal thickness of the mantle transition zone in their results, which also support the passive rifting process model for the ORZ.

Yu, Liu, Reed, et al. (2015) conducted a joint receiver function and gravity study of the crust beneath the ORZ. The result shows a possible discontinuity in the crust beneath ORZ. This observation needs to be confirmed by other studies with active source seismic or MT data to confirm a possible magma intrusion into the crust. Their result also shows a thinned crust by 4-5 km beneath ORZ and infilled low-density materials from the mantle due to decompression melting caused by the lithospheric thinning process.

A later study by Yu et al. (2017) shows a deep root of the Congo Craton in the southwestern edge of the ORZ and a low-velocity anomaly in the upper asthenosphere beneath ORZ, which is also interpreted to be due to decompression melting. These pieces of evidence supporting the passive rifting model in ORZ from the SAFARI seismological data are also supported by an earlier geodetic study by (Malservisi, Hugentobler, Wonnacott, & Hackl, 2013). However, Yu, Liu, Moidaki, et al. (2015) observed an anomalous thickness in the mantle transition zone which corresponds to a positive thermal anomaly in central-west Botswana, which is at the edge of their model. The limited coverage of the SAFARI seismological stations around this observed anomaly hindered its further investigation. This anomaly, if confirmed by other studies, could suggest a possible heat transfer that may be related to heat from the confined African superplume in the lower mantle to the upper mantle beneath the southern African region (Gao, Silver, Liu, & Group, 2002).

All the above-mentioned seismological networks cover Botswana partially. A seismological project, Network of Autonomously Recording Seismographs (NARS-Botswana) (Figure 2.3), covering the whole of Botswana, was conducted between 2013-2018 to image the crustal and upper mantle structure. Fadel et al. (2018) and Fadel et al. (2020) presented the first 3-D shear-wave velocity of crust and upper mantle beneath Botswana from the NARS-Botswana seismological data. Their nationwide 3-D shear-wave velocity results confirm incipient rifting in the ORZ, evident by a thin crust. The low-velocity anomaly observed in Okavango seems to connect to the low-velocity anomaly in central Botswana. According to Fadel et al. (2020), this anomaly relates to incipient rifting in central Botswana, which is an extension of the EARS, as against the commonly interpreted termination of the EARS in ORZ. The location of this low-velocity anomaly also coincides with that of the 2017 6.5 Mw earthquake in central Botswana. However, the studies have a very coarse resolution of about 1 degree, and the nature of the interpreted low-velocity anomaly remains unclear. Understanding their model from other types of data, for example, the conductivity model from the MT method would help validate the interpretations.

All the previously mentioned seismic wave velocity studies covering Botswana are based on low frequency passive seismological data. There is only one known active seismic investigation of the crust in Botswana. Wright and Hall (1990) investigated the Rehoboth Province using active deep seismic profiling covering the southwest Botswana. Their study shows that the Nosop basin (above Rehoboth Province) is deep and has a sedimentary thickness of up to 15 km. Also, Wright and Hall (1990) suggested an extension of Kaapvaal Craton to southwest Botswana from high-velocity signature in the result as discussed in the previous chapter (subsection 1.1.1). However, other more recent seismological studies by Fadel et al. (2018) and Fadel et al. (2020) suggest a preferred interpretation of a buried MC beneath the Rehoboth Province.

### 2.3.3. Magnetotelluric Studies

The Southern African Magnetotelluric Experiment (SAMTEX) was conducted to image the electrical structure of the crust and upper mantle beneath the southern African region (Jones et al., 2009) (Figure 2.3). The data from the experiment complemented available data from xenolith studies, seismological studies, and other geophysical data in the region. Jones et al. (2009) presented preliminary regional electrical conductivity and electrical anisotropy maps of the southern African region at depths of 100 km and 200 km from the MT data. Their results showed the cratonic blocks (Angola, Kaapvaal, and Zimbabwe cratons) to be resistive, and the conductive regions are associated spatially with the mobile belts. The resistivity image maps from their preliminary study correlated spatially with previous seismic velocity models for southern Africa, with regions of high resistivities having high velocities and conductive regions having low velocities. Aside from this preliminary regional interpretation of the SAMTEX data, a few other smaller-scale studies have been conducted to image the crust and upper mantle beneath Botswana. However, these MT studies so far in Botswana are too fragmented spatially and hardly overlap. Figure 2.4 shows the spatial distribution of all known previous MT studies covering parts of Botswana.

A two-dimensional (2-D) MT data inversion results from a profile across Kaapvaal Craton, Rehoboth Province and Ghanzi-Chobe/Damara Belt in southwest Botswana was presented by Muller et al. (2009) (Figure 2.4a). The MT profile data, which are characteristically closer to 3-D data due to the presence of multiple geoelectric strike directions, were inverted independently in two geoelectric strike directions of 25° and 45° (Figure 2.5). Their model showed significant variation in the electrical conductivity of the lithosphere laterally. The results show that the section of Kaapvaal Craton imaged is very resistive and has a high thickness of about 190 km, extending into the asthenosphere. The structure of the Kheis Belt and Rehoboth Province is less resistive and thinner (about 180 km). In contrast, the Ghanzi-Chobe/Damara Belt is conductive and of a lower thickness (about 160 km) along the profile. Their results show the first geophysical interpretation of the deep structure beneath the Rehoboth Province, which had not been previously studied using geophysical methods at that time. However, this study did not include the interpretation of the possible existence of buried MC in southwest Botswana (e.g., Begg et al., 2009).

In northeast Botswana, Miensopust et al. (2011) carried out 2-D imaging of the electrical structure of the lithosphere from a MT data profile across Zimbabwe Craton, Magondi mobile Belt, and Ghanzi-Chobe Belt (Figure 2.4b). The results show a highly resistive lithosphere of about 220 km thickness for the Zimbabwe Craton, which is similar to estimates from geochemical and geothermal studies (Miensopust et al., 2011). The study shows a resistive and relatively thin lithosphere for Ghanzi-Chobe Belt of about 180 km thickness and two conductors in the middle to lower crustal part of Magondi Belt. The interpretations of these conductors are uncertain; however, they favoured graphite and/or sulfide as the cause of the conducting bodies. Also, their results revealed a highly resistive crustal structure in the Okavango Dyke Swarm within the Limpopo Belt. However, the results of their MT study did not include the interpretation of possible extension of the EARS in the northeastern tip of Botswana, as suggested by Fadel et al. (2020). A further study into the evolutionary model of the Limpopo Belt was carried out by Khoza et al. (2012) using 2-D

MT data inversion and metamorphic data (Figure 2.4c). The result of their model shows the relationship between the Kaapvaal Craton, Zimbabwe Craton, Limpopo Belt, and the shear zone in-between these geologic terranes as revealed in the LIM-SSO-KAP profile shown in Figure 2.6. Their study proposed an evolutionary model involving the collisional suture between the Zimbabwe and Kaapvaal Cratons for the formation of the Limpopo Belt.

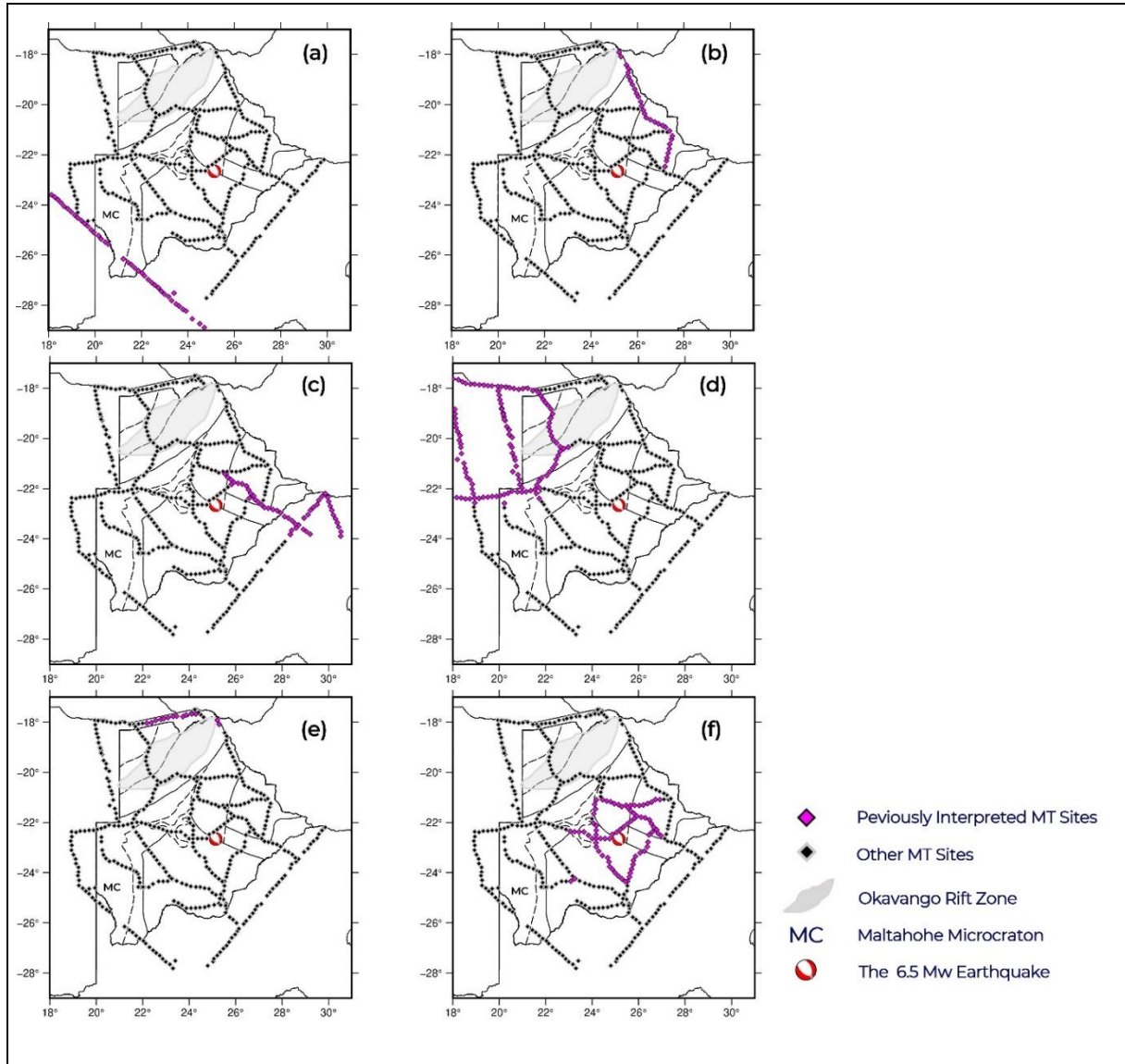


Figure 2.4: Location of SAMTEX sites across Botswana showing previously interpreted sites in magenta squares: (a) Muller et al., (2009) (b) Miensopust et al., (2011) (c) Khoza et al., (2012) (d) Khoza et al., (2013) (e) Evans et al., (2019) (f) Moorkamp et al., (2019). Other MT sites are shown in black squares. Transparent grey area = Okavango Rift Zone, MC = Suggested location of Maltahohe microcraton, and the focal mechanism represents the location and orientation of the 2017 6.5 Mw earthquake.

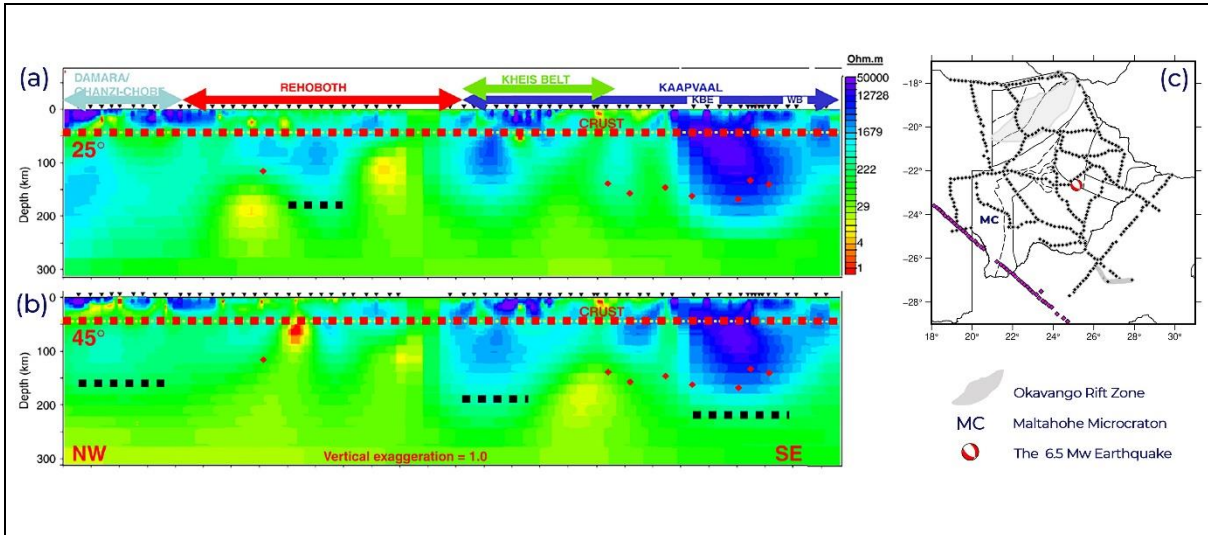


Figure 2.5: Electrical conductivity models derived from 2-D smooth inversion of decomposed MT station responses by Muller et al. (2009) for (a). 25° E of N strike azimuth and (b). 45° E of N azimuth (c) Map of MT stations covering Botswana. The magenta squares show the MT sites profile published by Muller et al. (2009).

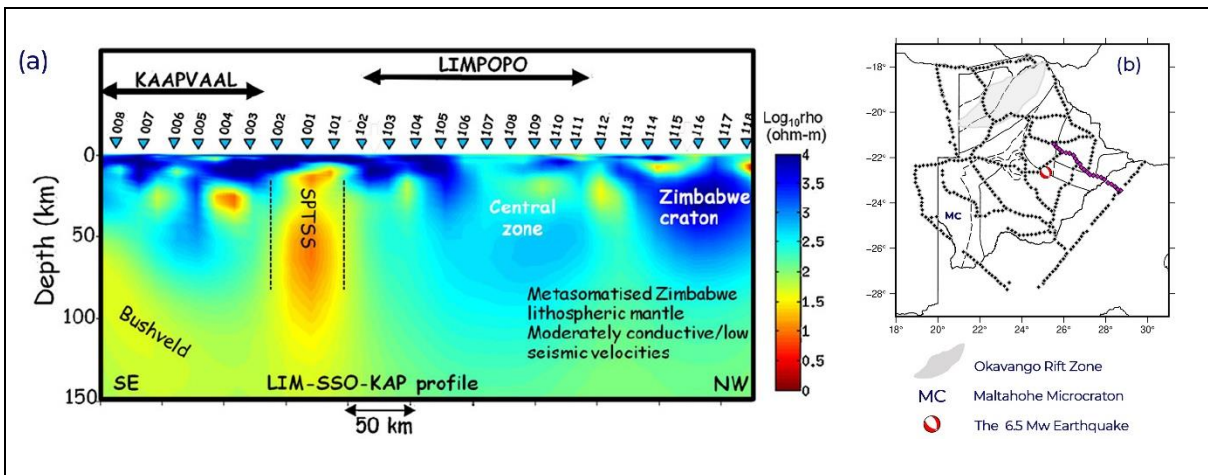
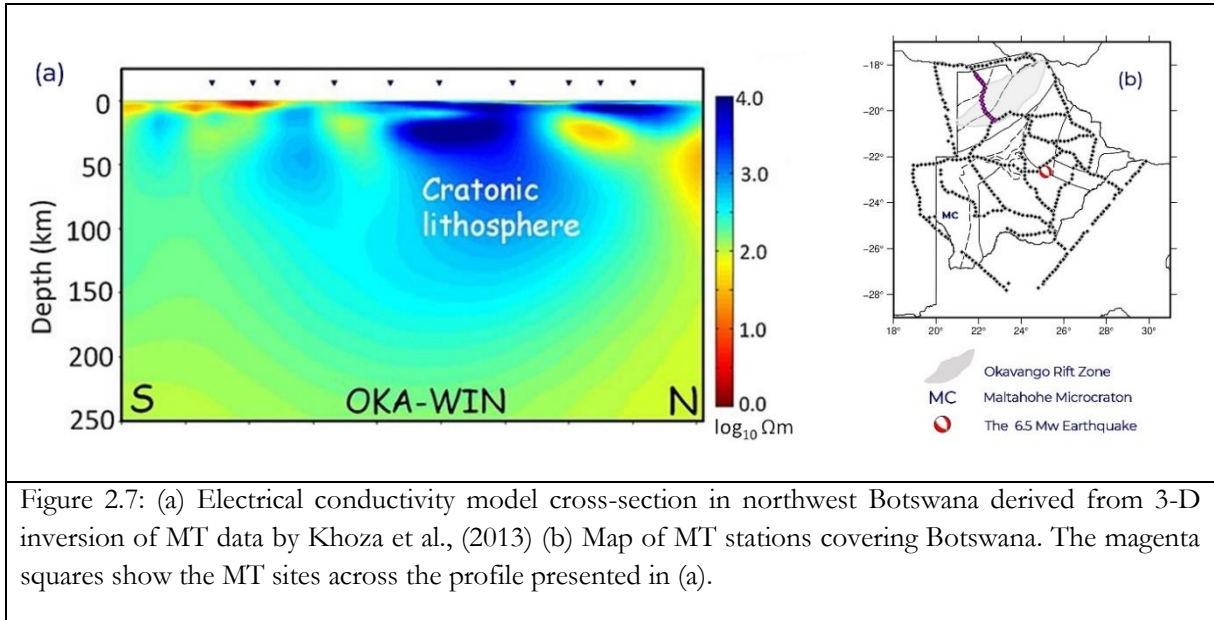


Figure 2.6: (a) Electrical conductivity model cross-section across Limpopo Belt-Kaapvaal Craton and Zimbabwe Craton in Botswana derived from 3-D inversion of MT data by Khoza et al., (2012) (b) Map of MT stations covering Botswana. The magenta squares show the MT sites across the profile presented in (a). SPTSS=Sunnyside-Palala-Tshipise Shear System.

Khoza et al. (2013) carried out a 2-D and 3-D MT inversion to image the lithosphere across Kalahari Craton, Damara-Ghanzi-Chobe Belts, and Congo Craton, covering northeast Namibia and a small area of northwest Botswana (Figure 2.4d). The electrical conductivity model shows a significant lateral variation in the resistivity across the section imaged. The Congo Craton, which extends to northwest Botswana, is highly resistive and has thick lithosphere to the depths of 250 km. OKA-WIN profile in Figure 2.7 presented by Khoza et al. (2013) shows the Congo Craton’s extension to northwest Botswana. Similarly, Evans et al. (2019) studied the lithosphere beneath Barotse Basin in western Zambia, also covering some parts of northern Botswana using MT data. The MT data used in the 3-D included the SAMTEX data profile along northern Botswana (Figure 2.4e) as well as other MT broadband data acquired around the Barotse Basin. From their model, the lithosphere beneath Barotse Basin is substantially thinned and is underlain by melt

from the African superplume, which is evidenced by high conductivity structures in the upper mantle. Their results suggest continental rifting beneath the Barotse basin, which connects with parts of the more mature EARS in the Okavango Rift Zone. However, their interpretation does not include the east-west (EW) electrical conductivity model across the SAMTEX profile in northern Botswana, which could provide more information about the development of the ORZ in Botswana and its relationship with the EARS.



Moorkamp et al. (2019) investigated the 3 April 2017 6.5 Mw earthquake in central Botswana using surface wave and MT data (Figure 2.4f). From their resistivity models, two displaced conductive structures are revealed and interpreted as fluid/melt (Figure A2 in Appendix 2). Their results suggest the reactivation of the old fault zone by the injection of melt from the mantle as the cause of the earthquake. Also, Moorkamp et al. (2019) suggest that the earthquake reactivated existing fault from the deformation process of the collision between Kaapvaal and Zimbabwe cratonic blocks. However, the limited coverage of their study did not allow for further investigation of the possible association of the melt/fluid with the EARS.

#### 2.3.4. Joint Velocity-Conductivity Inversion and Interpretation Efforts

The efforts to perform joint inversion or joint interpretation of seismological and MT data to investigate the crust and upper mantle structure of the southern African region have been restricted to only two known case studies. Hamilton et al. (2006) conducted a study on the crust and upper mantle of the northern part of South Africa using the joint interpretation of electrical anisotropy derived MT data and seismic anisotropy derived from shear-wave splitting. This study does not cover any part of Botswana. A joint velocity-conductivity interpretation study in southern Africa was done by Jones et al. (2013). Jones et al. (2013) carried out a joint interpretation of the 3-D shear wave tomography model from seismic data and conductivity model from MT data to study the lithosphere beneath the southern Africa region. This study shows the linear relationship between conductivity and shear wave velocity structure at 100 km depth beneath southern Africa. Their velocity-conductivity model also shows a very wet and depleted lithosphere in central Botswana at depth of 100 km. A high-resolution joint inversion and interpretation would give a better understanding of the tectonic units and geodynamic processes in Botswana.

### 3. DATASET AND METHODOLOGY

The first section (3.1) gives a succinct description of the MT method, explaining the theoretical basis of the methodological steps used in this research. The description of the data used for the study is given in the second section (3.2). Finally, the methodology workflow and how it was applied are provided in the last section of this chapter (3.3).

#### 3.1. The Magnetotelluric Method

##### 3.1.1. Overview

The MT is a passive geophysical method that uses the natural Earth's electromagnetic field to infer the distribution of electrical conductivity of the Earth's subsurface up to hundreds of kilometers depth (up to the Earth's mantle) (Cagniard, 1953; Tikhonov, 1950). The electromagnetic source field penetrating the subsurface induces electrical currents (also called telluric), which generate secondary magnetic fields. In the MT method, the induced time-varying Earth's electric (E) and magnetic (B) fields are simultaneously measured from the Earth's surface. Later in this chapter, the processing, analysis, and inversion techniques of the MT data are described with the aim to image the subsurface electrical conductivity.

##### 3.1.2. Basic Theoretical Concepts of Electromagnetics

The earliest works on the fundamental theory of the MT method were by Rikitake (1946) and Tikhonov (1950), who proposed that the relationship between the electric and magnetic field can be used to determine the electrical characteristics of the Earth's subsurface. In more detail, Cagniard (1953) described a practical application of the MT method in a study over sedimentary basins. Over time, the theory and practical application of the MT methods have developed in the last decades (e.g., Becken et al., 2008; Jones et al., 2009; Meqbel et al., 2014)

The time variations in the natural electromagnetic field of the Earth are utilized in MT investigations. The electromagnetic field of the Earth is generated mainly by the magneto-hydrodynamic process of the Earth's outer core (McPherron, 2005). Whilst the magneto-hydrodynamic process generates the greater part of the Earth's time-varying magnetic field; the MT method makes use of the low-amplitude and transient variations in the external geomagnetic fields. The small-amplitude fluctuating signals with periods between  $10^3$ -  $10^5$  seconds (corresponding to frequencies between  $10^3$ - $10^5$  Hertz) are used in the MT method (Vozoff, 1991). Electromagnetic fields with periods below 1s are generated from lightning (spherics), while long-period signals are generated from the interaction of the solar wind with the Earth's magnetic field and ionosphere (Parker, 1958). There exist an MT signal dead-band between frequencies 0.5 – 5 Hz, where the intensities of the electromagnetic fluctuation is low, which give rise to reduced MT data quality within this frequency range.

The electromagnetic field of the Earth used in MT measurements propagates diffusely, which yields volumetric soundings (volumetric bulk property), and the energy decays exponentially as it travels through the Earth. The propagation and induction of the electrical and magnetic fields in a medium as used in the MT method are well described by Maxwell's equations:

$$\text{Gauss' Law for magnetic field} \quad \nabla \times E = -\frac{\partial B}{\partial t} \quad \text{Equation 3.1}$$

$$\text{Gauss's Law for electric field} \quad \nabla \times H = j_f + \frac{\partial D}{\partial t} \quad \text{Equation 3.2}$$

$$\text{Faraday's Law} \quad \nabla \cdot B = 0 \quad \text{Equation 3.3}$$

Ampere's Law with Maxwell's Term

$$\nabla \cdot D = \eta_f$$

Equation 3.4

where  $E$  is the electric field in volt per meter ( $\text{Vm}^{-1}$ ),  $B$  is the magnetic induction in tesla (T),  $H$  is the magnetic intensity in ampere per meter ( $\text{Am}^{-1}$ ),  $D$  is the electric displacement in coulomb per square meter ( $\text{Cm}^{-2}$ ),  $j_f$  is the electric current density in ampere per square meter ( $\text{Am}^{-2}$ ), and  $\eta_f$ , the electric charge density in coulomb per cubic meter ( $\text{Cm}^{-3}$ ).

In a uniform isotropic medium, Maxwell's equations can be expressed by following constitutive relationships given in the equations below (3.5, 3.6, and 3.7). In the case of isotropic medium, the magnitudes of the electrical conductivity ( $\sigma$ ) and electrical permittivity ( $\epsilon$ ) are scalars and a free space magnetic permeability ( $\mu_0$ ) is assumed, while they take tensorial form in an anisotropic medium.

$$j_f = \sigma E \quad \text{Equation 3.5}$$

$$D = \epsilon E \quad \text{Equation 3.6}$$

$$B = \mu H \quad \text{Equation 3.7}$$

Where  $\sigma$  is the electrical conductivity in siemens per metre ( $\text{Sm}^{-1}$ ),  $\epsilon$  is the electrical permittivity in farads per meter ( $\text{Fm}^{-1}$ ), and  $\mu$  is the magnetic permeability in henry per meter ( $\text{Hm}^{-1}$ ).

The measured time-domain variation in the electric and magnetic fields MT data is generally analysed in the frequency domain. The depth of penetration of the electromagnetic wave is dependent on the resistivity of the medium and oscillation frequency of the signal. The higher the resistivity of the medium, the higher the depth of penetration and the lower the frequency of measurement, the higher the penetration depth. Electromagnetic skin depth is a measure of the depth of the maximum sensitivity of the measured field. The skin depth is the distance in the subsurface at which the amplitude of the propagating electromagnetic wave attenuates to  $\sim 37\%$  of its surface value. Skin depth depends on the square root of the product of the resistivity of the medium and the period of the signal (Simpson & Bahr, 2005). Long period (low frequency) MT data can be used to image greater depth in the subsurface (up to the mantle). This is because long period electromagnetic waves attenuate slower than short period waves; hence the former penetrates deeper into the Earth.

$$\text{Skin depth } (\delta) = 503\sqrt{\rho T} \quad \text{Equation 3.8}$$

where  $\rho$  = resistivity of medium and  $T$  = period of the MT measured signal

The simultaneous measurement of the electric and magnetic field time variations in orthogonal directions at the Earth's surface, including two horizontal electric components ( $E_x$ ,  $E_y$ ), two horizontal magnetic components ( $H_x$ ,  $H_y$ ), and one vertical magnetic component ( $H_z$ ), generates the time series MT data. The measured time series data is then processed by transforming the data from the time domain to the frequency domain. Also, complex transfer function ratios (impedances and vertical magnetic field) that describe the penetration of the electromagnetic field in the subsurface, apparent resistivity and phase parameters can be derived from the MT data (Simpson & Bahr, 2005).

### 3.1.3. Transfer Functions of Magnetotelluric Response

To obtain conductivity information from the MT method, the measured time-series data of the electric and magnetic field must be processed into MT response data (transfer function). A transfer function can be defined as a function that linearly relates the measured electric and magnetic field components to the properties of the subsurface materials at a given frequency. The natural sources used in the MT method are

of variable and unknown intensities; hence the transfer functions must be independent of the signal source (Booker, 2014). Therefore, the transfer function depends only on the electrical properties of the medium, and they can be used to infer the conductivity distribution of the subsurface materials from the measured data. Examples of transfer functions are impedance tensor, MT tensor and vertical magnetic transfer function. Various methods of processing MT time series data into MT response functions, including the remote-reference and robust time series processing methods, are described in details by Jones, Chave, Egbert, and Auld (1989).

The impedance tensor ( $Z$ ) is a complex second-rank frequency-dependent tensor. Impedance tensor shows the relationship between the horizontal components of the electric and magnetic fields at a particular frequency. The MT tensor is like the impedance tensor but uses magnetic induction ( $B$ ) instead of the horizontal components to express the relationship between the field components (Weaver, Agarwal, & Lilley, 2000). The impedance tensor ( $Z$ ) is given by:

$$Z = \frac{E}{H} \quad \text{or} \quad \begin{bmatrix} E_x \\ E_y \end{bmatrix} = \begin{bmatrix} Z_{xx} & Z_{xy} \\ Z_{yx} & Z_{yy} \end{bmatrix} \begin{bmatrix} H_x \\ H_y \end{bmatrix} \quad \text{Equation 3.9}$$

where  $Z_{xx}$  and  $Z_{yy}$  are the principal diagonal impedances and  $Z_{xy}$  and  $Z_{yx}$  are the principal off-diagonal impedances.

The impedance tensor is composed of the real and imaginary part. The magnitude of the impedance tensor is used to derive the apparent resistivity. Apparent resistivity ( $\rho_a$ ) represents the volumetric average resistivity value of the subsurface. Also, the phase parameters can be extracted from the impedance tensor. Impedance phase ( $\Phi$ ) is given by the inverse tangent of the ratio of the real and imaginary parts of the impedance tensor. The impedance phase gives additional information about the conductivity of the subsurface structures (Simpson & Bahr, 2005). Impedance phase above  $45^\circ$  is diagnostic of increase in conductivity with depth (also evident in apparent resistivity curve), impedance phase below  $45^\circ$  is diagnostic of decrease in substrata conductivity with depth. If the impedance phase is  $45^\circ$ , it is diagnostic of no change in the substrata conductivity (Meqbel et al., 2014; Simpson & Bahr, 2005). These two parameters, apparent resistivity and phase, are the most frequently used parameters for visualizing MT data and are plotted against period (Campany et al., 2016; Robertson et al., 2020).

$$\rho_{a,ij} = \frac{1}{\mu_0 \omega} |Z_{ij}(\omega)|^2 \quad \text{Equation 3.10}$$

$$\Phi_{ij} = \tan^{-1} \left( \frac{\text{Im}\{Z_{ij}\}}{\text{Re}\{Z_{ij}\}} \right) \quad \text{Equation 3.11}$$

where  $\omega$  is the angular velocity (period,  $T = 2\pi / \omega$ ) and  $\mu_0$  is magnetic permeability of free space.

The vertical magnetic transfer function (VTFs) is a dimensionless complex induction vector that shows the relation between the horizontal and vertical components of the magnetic field. It is also referred to as the tipper vector and is represented by:

$$H_z = T_{zx}H_x + T_{zy}H_y \quad \text{Equation 3.12}$$

where  $T_{zx}$  and  $T_{zy}$  are the induction VTFs components.

The vertical component of the magnetic field is created by lateral conductivity variation. In a case where the conductivity of the subsurface only varies with depth, that is, one-dimensional (1-D), the vertical component of the magnetic field is zero.

### 3.1.4. Dimensionality Distortion of Magnetotelluric Data

Dimensionality analysis of MT data is an essential step to ensure that the subsurface structure has the same dimensionality as the modelling approach used for the data. In a case where the dimensionality of the MT data is higher than the dimension in which the data is modelled or interpreted (e.g., a 1-D interpretation of a 2-D or 3-D structure), dimensionality distortion occurs in the model, causing inaccurate and erroneous interpretation (Ledo, 2005; Ledo et al., 2002). There are different methods for assessing the dimensionality of MT data, including rotational invariants, induction arrows, Groom and Bailey distortion parameters, and dimensionality indicators (e.g., Groom & Bailey, 1991; Ledo et al., 2002; McNeice & Jones, 2001; Ritter & Banks, 1998; Smith, 1995 and references therein). Aside from the methods above, the impedance tensor holds essential information about the dimensionality of the MT data. In a 1-D Earth, lateral conductivity variation is zero as conductivity varies only with depth. Hence, the diagonal components of the impedance tensor are zero, and the off-diagonal components are equal in magnitude but of opposite signs:

$$\begin{aligned} Z_{xx} = Z_{yy} &= 0 \\ Z_{xy} &= -Z_{yx} \end{aligned} \quad \text{Equation 3.13}$$

For a 2-D Earth model, conductivity varies with depth as well as along horizontal direction; hence the diagonal components of the impedance tensor are equal in magnitude but of opposite signs, and the off-diagonal components differ and are non-zero:

$$\begin{aligned} Z_{xx} &= -Z_{yy} \\ Z_{xy} &\neq -Z_{yx} \end{aligned} \quad \text{Equation 3.14}$$

For a 3-D Earth, conductivity varies in all directions, and all the components of the impedance tensor are independent of each other. The dimensionality of the MT data is dependent on the scale of the structure. For MT data with short periods, the electromagnetic skin depths are small relative to the dimension of the anomalous structure, and only 1-D information can be retrieved. With increasing period of MT sounding, the depth to which the data is sensitive increases and sufficient to cover at least one edge of the anomalous structure and 2-D information can be retrieved from the data. As the MT sounding period increases further, the electromagnetic skin depth increases sufficiently to encompass the dimensions of the anomalous structure. However, the non-inductive response generated by near-surface 3-D conductive bodies persists and cause a frequency-independent distortion in the MT data. The effects of these distortions of MT data and how to correct them are described next.

### 3.1.5. Distortion of the Magnetotelluric Data

The time series MT data collected is often affected by distortions in the electromagnetic field. The distortions in the MT data (galvanic distortion) are caused by the disturbance of the current that generates the electrical field. Galvanic distortions are non-inductive frequency-independent responses caused by the scattering of regional MT response by accumulated charge distribution on small-scale shallow bodies or inhomogeneity in local geologic structures (Chave & Jones, 2012). Multidimensional conductivity contrasts at depths shallower than the penetration depth of the electromagnetic field cause galvanic distortion in the amplitudes of the electric field, hence, affecting the magnitudes of impedance tensor. This distortion causes obscuring of the geoelectric strike, phase mixing, masking of properties of regional structures, and static shift of the apparent resistivity. At long periods, the magnitude of the inductive response decreases; however, non-inductive response persists, which makes galvanic distortion removal important in MT data analysis.

The inherent distortion in the MT data has informed the need to extract undistorted data from the measured data for the purpose of modelling the deep subsurface. There are several approaches discussed by several authors on reducing the effects of the galvanic distortion on MT response to improve the certainty of the interpretation of the data. The foremost and most common methods used for galvanic distortion removal are the decomposition methods of Groom and Bailey (1989, 1991) and Smith (1995). However, both methods assume that regional structures are 2-D to determine the appropriate strike of the regional structure. Hence, the methods pre-condition MT data survey to 2-D interpretations. An alternative method for galvanic distortion removal is that of Bahr (1988,1991), which is aimed at determining the dimension of the regional MT response and strike direction. However, in some cases, more than one strike direction exist in MT response at different depths due to continual changes in the Earth's structure by geologic processes. This makes the galvanic distortion removal process more complex, and assumptions of average strike direction would result in 2-D models that contain extraneous structures due to displacement of other structures from the assumed strike direction (Simpson & Bahr, 2005). Examples of good in-depth descriptions of the other galvanic distortion removal approaches can be found in McNeice and Jones (2001) and Ritter and Banks (1998). More recently, there are newer approaches that explore the recovery of the regional MT response with the use of phase parameters of the MT response, which are undistorted by galvanic distortion (e.g., Becken & Burkhardt, 2004; Bibby, Caldwell, & Brown, 2005).

According to Caldwell, Bibby, & Brown (2004), the heterogeneity in the near-surface causes distortion to the electric field; however, the phase relationship between the magnetic field and electric field remains unaffected and can be used to retrieve the regional impedance tensor. On this basis, Bibby, Caldwell, and Brown (2005) described an approach of galvanic distortion removal in MT response using the phase tensor, which provides maximum information about the dimensionality of the regional impedance tensor with the minimum assumptions about the data and provides a solution to the challenge of strike directions. This has been used as a better approach for galvanic distortion removal in several studies (e.g., Dehkordi, Ferguson, Jones, Ledo, & Wennberg, 2019; Xue et al., 2019). However, there are other arguments that there would be no need to perform galvanic distortion if the MT response can be modelled directly in 3-D interpretation (Chave & Jones, 2012). According to Meqbel et al. (2014), the scattering effects of small-scale local structures with dimensions or spatial scales larger than the MT site spacing can be modelled in 3-D inversion, and the regional MT response can be reliably recovered. However, when MT site spacings are very large and cannot recover details of scattering effects of small-scale local structures, the need to correct for galvanic distortion in the MT response remains essential.

The static shift is a subclass of local galvanic distortion in MT response. The static shift is a frequency-independent shift in the apparent resistivity curve by a factor (Chave & Jones, 2012; Simpson & Bahr, 2005). In 1-D modelling, static shift causes a shift in the depth to a conductive body and error in the modelled resistivity values. In 2-D and 3-D cases, static shift, if not corrected, may cause artefacts (extraneous structures) in the model (Simpson & Bahr, 2005). There are several approaches to correcting static shift effects in MT response. Simpson & Bahr (2005) described three broad methods for static shift correction, which are:

- (i) short period correction based on data from active electromagnetic method,
- (ii) spatial averaging method (statistical), and
- (iii) long-period corrections.

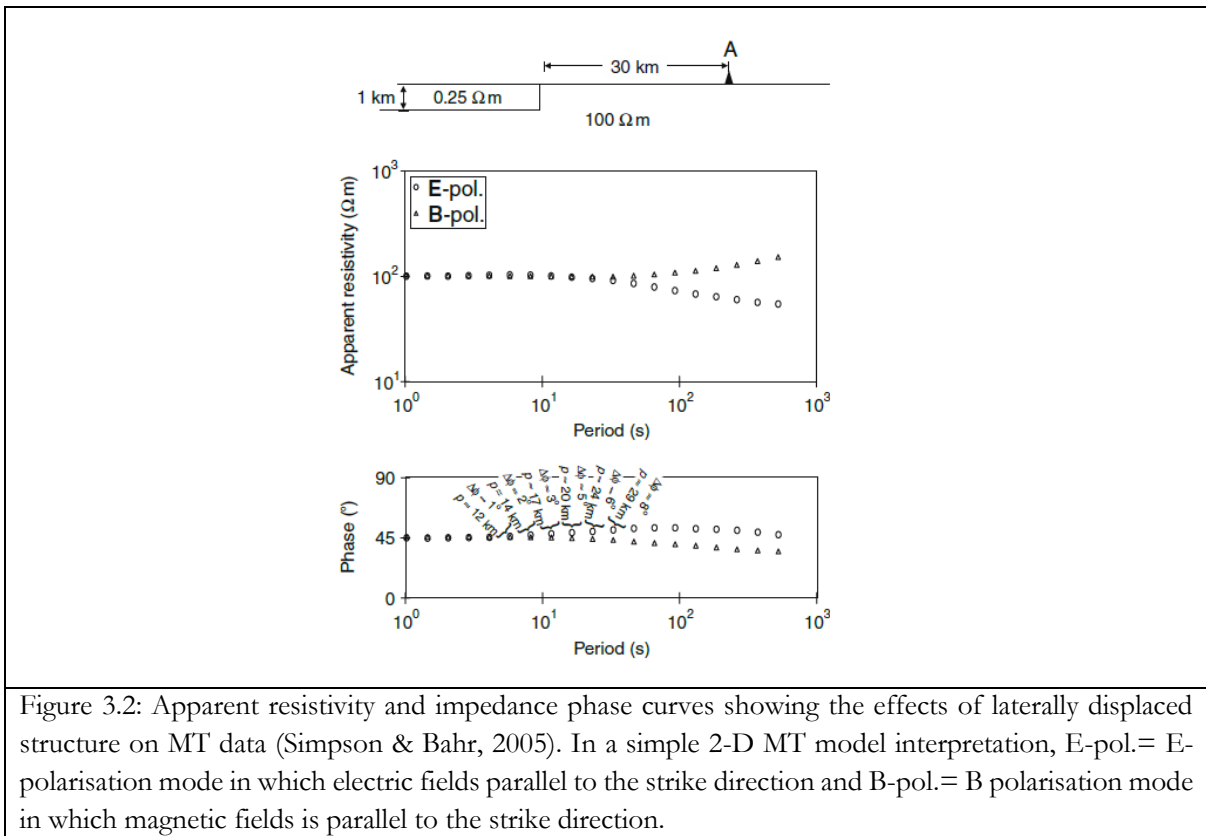
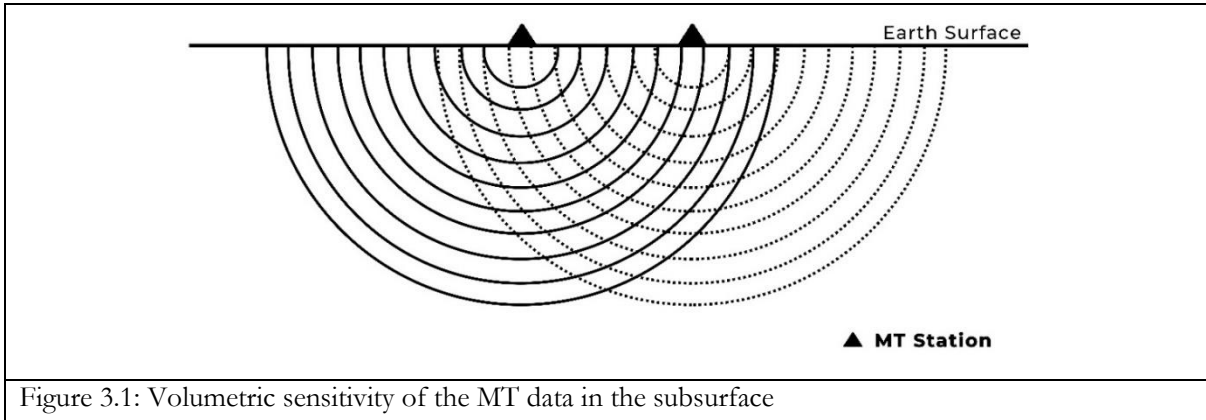
The first technique is based on active electromagnetic data recorded at locations close to the MT sites. The active electromagnetic data is not affected by static shift (Simpson & Bahr, 2005); hence, it can be used to correct static shift rising from near-surface effects in MT data. The second technique, which is the spatial averaging method, gives a relative static shift correction factor based on other MT sites rather than an

absolute correction factor. As the spatial coverage of the area to be imaged increases, the inaccuracies of the depth estimates and resistivity values in the resultant model based on spatial averaging corrected static shift reduces (Simpson & Bahr, 2005). Lastly, static shift corrections based on long-period depends on assumed deep structures (up to mid mantle depth) and required MT data with periods up to 100,000 seconds (Simpson & Bahr, 2005). When possible, the short period correction based on data from an active electromagnetic method is preferred, as it gives absolute values of static shift factor (Simpson & Bahr, 2005).

### 3.1.6. What can the Magnetotelluric Method Image?

The MT method images the electrical conductivity property of the subsurface, which defines the ability of Earth materials to carry electric current. The electrical conductivity of Earth materials has a wide variance spanning up to 14 orders of magnitude, as dry crystalline rocks (igneous and metamorphic) can have resistivity above  $10^6 \Omega m$ , while rocks bearing graphite can have resistivity values below  $0.01 \Omega m$  (Simpson & Bahr, 2005). Factors affecting the conductivity of rocks and minerals include temperature, permeability, porosity, physical and chemical state, and pressure. Since MT yields volumetric bulk conductivity of the medium and is less sensitive to the electrical conductivity of the host rock, it is generally not possible to link electrical conductivity to lithology. Sedimentary rocks generally have high porosity and typically contain fluids, which make them more conductive than igneous and metamorphic rocks. However, highly fractured igneous and metamorphic rocks would have relatively high porosity and permeability, hence have a high conductivity signature. Other factors that affect the bulk conductivity of Earth materials are the presence of highly conductive minerals (such as ore minerals and graphite), aqueous fluid, and partial melt. For example, long-period MT sounding shows that the anomalous high conductivity of the deep-crust and upper mantle (asthenosphere) is generally due to partial melting materials present in the tectonically active crust and volcanic areas (Unsworth & Rondenay, 2012; Wei et al., 2001).

The MT method is capable of imaging great depths (up to the upper mantle) significantly more than other active source electromagnetic methods. As described earlier (subsection 3.1.2), the depth of penetration of the MT method is dependent on the resistivity of the medium and the period of sounding. With an assumed average resistivity of the crust and upper mantle and data recording at long-period fluctuations of the Earth's electromagnetic field, a depth of penetration greater than 500 km might be possible with the MT method. The electromagnetic waves have a diffusive nature; hence the MT images volumetric property of the Earth and not only depths beneath the stations as shown in Figure 3.1. The MT data is sensitive to changes in the electrical conductivity of the Earth in-depth as well as in the horizontal directions (Meqbel, Weckmann, Muñoz, & Ritter, 2016). Structures that are laterally displaced from MT stations could influence the MT data. The lateral distance to which the MT data is sensitive is referred to as horizontal adjustment length, which must be considered alongside the depth of penetration when quantifying the sensitivity of MT data. "Penetration depths and horizontal adjustment lengths are not equivalent. In fact, conductivity anomalies laterally displaced by 2–3 times the penetration depth may affect the MT transfer functions." (Simpson & Bahr, 2005, p. 31). An example by Simpson and Bahr (2005) shows that a conductive structure that is located 30 km away from an MT site A (Figure 3.2) begins to affect the MT transfer function as the period of measurement increases. The resistivity of the layer beneath the MT site A is  $100 \Omega m$ , and at 10 second period, the depth of penetration is  $\sim 16$  km when calculated using Equation 8. As shown in Figure 3.2, the impedance phase response at about 10 seconds begins to deviate from the expected response from a  $100 \Omega m$  half-space that is beneath the MT site. For example, the impedance phase begins to split at a period of  $\sim 8$  s by up to  $2^\circ$  and up to  $8^\circ$  divergence at 50 seconds. Hence, the horizontal adjustment length is approximately twice the depth of penetration at period of 10 seconds, which demonstrates the possibility that horizontal adjustment can vary from the depth of penetration depending on the subsurface resistivity structure.

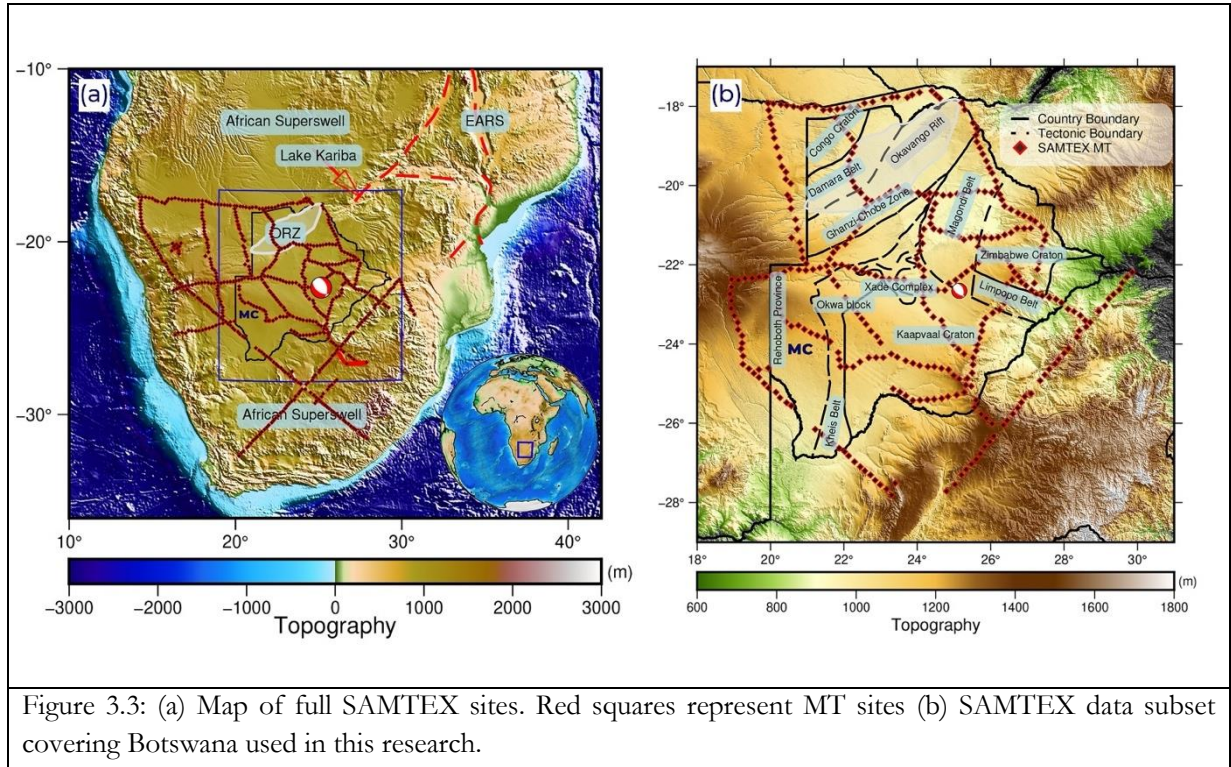


### 3.2. Dataset

For this study, the Southern African Magnetotelluric Experiment (SAMTEX) data was used (Figure 3.3a). The SAMTEX was conducted to image the electrical structure of the crust and upper mantle beneath the southern African region comprising of Botswana, Namibia, and South Africa (Jones et al., 2009). The data consist mainly of broadband MT sites (up to 1000s period), and some sites with long-period MT (up to 10,000 s period) and audio MT recordings (up to  $\sim 0.1$  second). Figure A4 (in Appendix 4) shows the maximum periods available in SAMTEX data sites in Botswana. The average intervals between the MT sites are approximately 20 km. The recorded time series of the fluctuations of the electric and magnetic field were processed into MT response function using the robust processing methods described in Jones et al. (1989). The SAMTEX data is generally of high quality in Botswana and Namibia but poor in some locations in South Africa due to cultural noise from DC power supply to railway lines and mines. A subset of the data covering Botswana and its boundaries was used for this study (Figure 3.3b).

### 3.3. Methodology

The methodology used for this study is divided into three main stages: data correction and preparation, data analysis, and data inversion. Figure 3.4 summarizes the main steps of the methodology workflow used. In this section, the description of the codes used, the different methodology steps, and outputs are explained.



#### 3.3.1. Codes

The MT method is a relatively new geophysical method; hence the software available for the data analysis and interpretation are still limited compare to the other methods (Kirkby, Zhang, Peacock, Hassan, & Duan, 2019). For this study, the MTPy, which is a Python toolbox for MT (Kirkby et al., 2019; Krieger & Peacock, 2014) and ModEM inversion codes (Kelbert, Meqbel, Egbert, & Tandon, 2014) were used for the data preparation, analysis, and inversion. These codes allow for various processing steps in one framework, including processing, analysis, modelling, and visualization (Kelbert et al., 2014; Krieger & Peacock, 2014). The MTPy package can also handle common file handling operations, coordinate transformation, and conversion from impedance tensor to phase and apparent resistivity. For the visualization of the results, figures and illustrations the MTPy, Matplotlib and the Generic Mapping Tools (GMT) (Wessel et al., 2019) were used.

#### 3.3.2. Data Correction and Preparation

The full impedance tensor and the VTF were jointly used for modelling the electrical structure in this study (Becken et al., 2008; Campany et al., 2016). To achieve more accurate inversion results, the MT data were corrected for distortions and errors. The data correction processes that included galvanic distortion removal, static shift removal, and data smoothening were done on all the impedance tensor and VTF components. Figure 3.5 shows examples of outputs of data correction on the MT data for two MT sites.

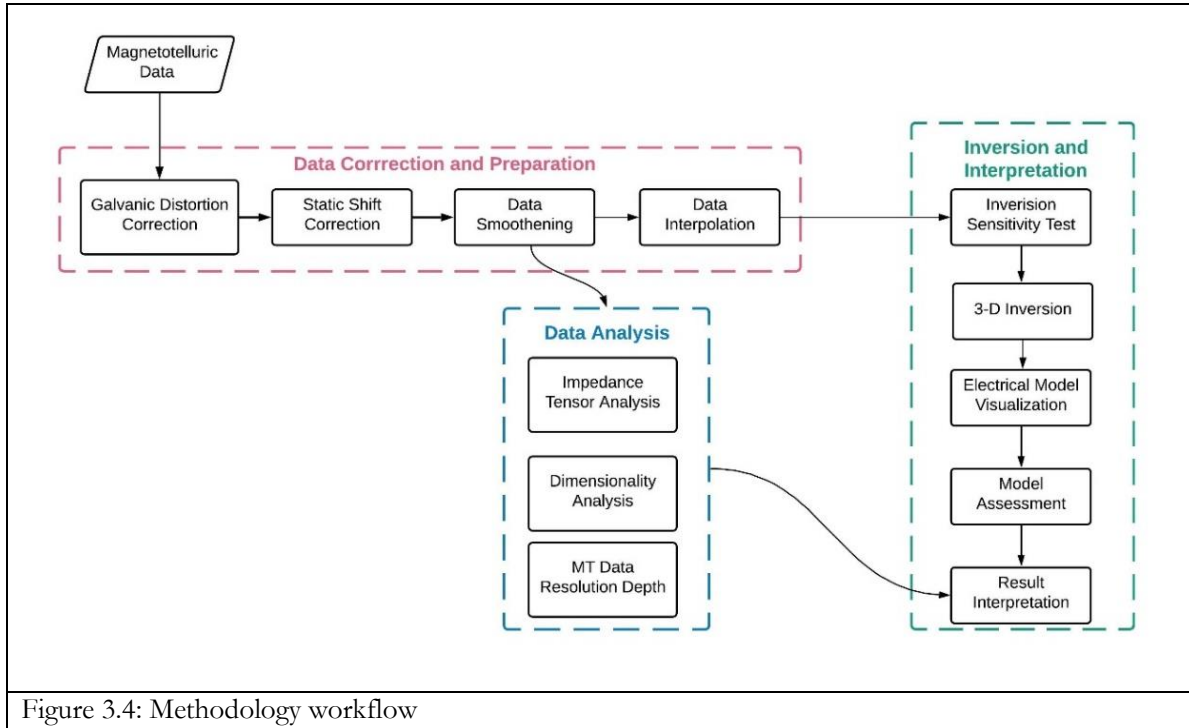


Figure 3.4: Methodology workflow

### 3.3.2.1. Galvanic Distortion Correction

The galvanic distortion correction was done to remove the effects of near-surface conductive heterogeneity from the MT response. The galvanic distortion correction was necessary for this dataset because of the high spatial aliasing between the MT site profiles (Figure 3.3b). The dataset would not be able to recover details of scattering effects of small-scale local structures, hence the galvanic distortion correction (Meqbel et al., 2014). The galvanic distortion was done following Bibby et al., (2005) approach, which makes use of phase tensor parameters and implements minimum explicit assumptions about the data parameters as describes earlier. This processing step removes galvanic distortion from the MT response and writes new data files. The outputs of the process are galvanic distortion corrected MT responses.

### 3.3.2.2. Static Shift Correction

The purpose of this processing step was to correct for the frequency-independent shift in the apparent resistivity curve so that they can correctly represent the subsurface resistivity structure. The static shift correction process will ensure that extraneous structures because of static shift error are removed from the data and consequently produces more accurate models. Static shift factors are generally undeterminable from the MT data itself. Addition measurements such as audio-magnetotelluric data or time-domain electromagnetic data are more suitable for estimating the static shift correction factor. In the absence of such additional data, the statistical averaging method was used to estimate the relative static shift correction factor for each MT station from other stations in the radius of 30 km (Simpson & Bahr, 2005). The outputs of the process are static shift corrected MT responses.

### 3.3.2.3. Data Smoothing

The MT data were smoothed to improve the quality of the MT response, remove outliers in the data and improve the convergence of the data inversion process. To ensure minimum errors in the data, period data points with error bars of the impedance tensor data above 5% were removed from the data. This maximum error threshold of 5% was also used as the inversion Egbert error floor value for the impedance data. From data examination, high error values were observed at long periods in the data. The removal of data points

with high errors meant a trade-off of long period part of the data for high-quality inversion data input. This trade-off helps to improve the convergence of the inversion process and produce more accurate electrical models. The maximum period in the MT data after the smoothing process was 10,000 seconds. Figure A4 (in Appendix 4) shows the range of maximum periods available in MT data before and after the data smoothing process was done. Alongside the removal of data with high errors, all the MT sites data were examined visually to verify the data quality and smoothness. The curve smoothness was examined on the criteria that the variation in MT apparent resistivity curve from period to period should not be more than  $45^\circ$  on a logarithm versus logarithm scale plot. Periods with anomalous data were removed to improve the smoothness of the MT response curve. The outputs of the process are smooth MT responses.

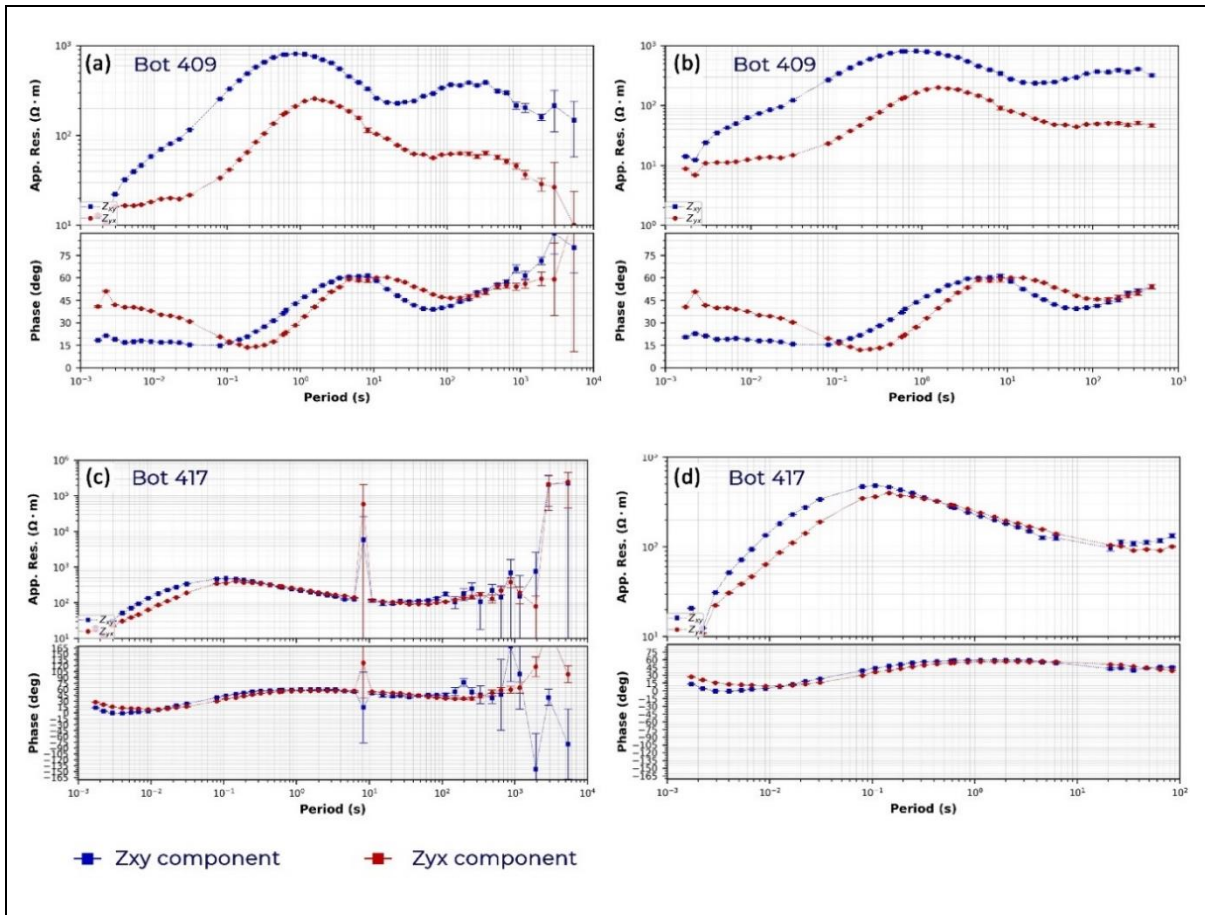


Figure 3.5: Examples of data correction of MT data through the galvanic distortion removal, static shift correction and data smoothing processing steps. Products are plotted as apparent resistivity and impedance phases against period (in logarithm scale). (a) Raw MT response from station Bot 409 (b) Corrected Bot 409 MT data after galvanic distortion, static shift correction and data smoothing. (c) Raw MT response from station Bot 417. (d) Corrected Bot 417 MT data (similar to (b)).

### 3.3.3. Data Analysis

Analysis of the MT data that involved dimensionality analysis, impedance component analysis and depth sensitivity were done. The descriptions of data analysis processes are discussed next.

#### 3.3.3.1. Dimensionality and Impedance Data Analysis

The purpose of this process is to analyse the dimensionality captured in the MT data. The dimensionality analysis was done based on the phase tensor, which is not affected by galvanic distortion as described by Bibby et al. (2005), Booker (2014) and Caldwell et al. (2004). The skew value and ellipticity parameters of

the phase tensor were used to analyse the dimensionality. The skew value is a ratio of the amplitudes of the sum of diagonal components to the sum of the off-diagonal components of the impedance tensor. High skew values of the phase tensor greater than  $6^\circ$  indicate 3-D effects, skew values of  $0^\circ$  indicate 2-D data, and lower skew values indicate 1-D subsurface structure (Cherevatova et al., 2015; Comeau et al., 2020). The ellipticity of the phase tensor is defined by the ratio of the amplitudes of the sum of diagonal components to the sum of the off-diagonal components of the impedance phase. When the phase tensor is a circle, it indicates 1-D subsurface, while the elliptical phase tensor represents 2-D or 3-D effects in the conductivity distribution (Becken & Burkhardt, 2004; Bibby et al., 2005). Figure A3 (in Appendix 3) shows the graphical description of the phase tensor parameters. A more in-depth description of the parameters of the impedance tensor can be found in Bibby et al. (2005) and Booker (2014).

The analysis of the apparent resistivity of the MT site was done. The outputs of the process are apparent resistivity derived from the off-diagonal components of the MT data at representative periods (100, 250, 500, and 1000 seconds) and are described in subsection 4.1.2.

### 3.3.3.2. Penetration Depth and Horizontal Adjustment Length

The purpose of this step is to examine the depth of penetration and estimate the horizontal distance to which the MT response is sensitive. The depths of penetration were calculated using the Niblett-Bostick transformation (Niblett & Sayn-wittgenstein, 1960) to account for variation in depth of penetration for MT sites at similar frequencies. The outputs of this process are penetration depths of the MT data at representative periods (100, 250, 500, and 1000 seconds). From the estimated penetration depths at various periods, the horizontal adjustment was estimated to be equal to the penetration depth at the minimum or up to two times the penetration depth as described by Simpson and Bahr (2005). The result of the depth sensitivity analysis is described in subsection 4.1.1.

### 3.3.4. 3-D Inversion

Iterated and linearized inversion algorithms have been the standard method for solving nonlinear geophysical inverse problems. These iterated linearized inversion methods require large computation power, taking several hours on modern workstations, and are impractical to compute as complexities increase from 2-D to 3-D. To solve the challenge of large demand of computing resources and minimize the misfit in data and model norms in solving the inverse problem in electromagnetics, several algorithms, including the Newton method, Gauss-Newton method (Mackie, Madden, & Wannamaker, 1993), and gradient-based minimization methods (Newman & Alumbaugh, 2000; Rodi & Mackie, 2001) have been used. Examples of good in-depth descriptions of the different algorithms to solve the inverse problem with particular focus on the use for MT data can be found in Rodi & Mackie (2001) and Egbert & Kelbert (2012). Of particular interest to discuss in this report is the non-linear conjugate gradient (NLCG) technique for solving the inverse problem in MT, which is an example of gradient-based minimization schemes. The NLCG algorithm uses non-linear optimization, which deviates from the traditional geophysical techniques of linearized solutions for the nonlinear inverse problem. The NLCG applies nonlinear optimization for minimizing the objective function of the nonlinear inverse problem, which includes data misfit and model norm (Avdeev, 2005). The NLCG method is generally accepted in the electromagnetics community due to its relative simplicity in solving large inverse problems compared to the other techniques. The NLCG method is efficient because it requires lesser processing units (CPU and memory) as inversion model grids and data increases compared to other techniques.

For this study, the MT data were inverted in 3-D to image the crust and upper mantle structure beneath Botswana. In a 3-D inversion, no assumption about the dimensionality of the data is required, and it also accounts for conductivity variations in all directions, hence making the subsurface structure interpretation

more straightforward. Imaging the crust and upper mantle structure in 3-D gives the opportunity for precise geological interpretation of the nature of the structures. The Modular system for Electromagnetic Inversion (ModEM) code was used for the inversion of the MT data (Egbert & Kelbert, 2012; Kelbert et al., 2014). The ModEM utilizes the finite difference approach for forward calculations and NLCG to solve the inverse problem. In the MT academia community, the ModEM code is the most widely used 3-D code. This is because the ModEM is the only codes with both serial and parallel versions available for non-commercial academic use. ModEM code is very robust and also take relatively shorter computation time (Miensopust et al., 2013). Kelbert et al. (2014) gives a detailed description of the ModEM codes for inversion of MT data.

The ModEM codes allow the user to control the inversion process with the initial damping parameter and inversion computation stopping criterion (Kelbert et al., 2014). The damping parameter controls how the model fits the data progressively in the inversion process (Robertson et al., 2020). As part of this study, a sensitivity test was carried out to investigate how the initial damping parameter affects the resultant model. The description of these tests is given in subsection 3.3.4.4.

For the 3-D electrical modelling of this study, the full impedance ( $Z$ ) and the VTF were jointly inverted. Incorporating the VTF into the inversion complements the model development by improving the resolution of high resistivity anomalies and 3-D structures than inversion with standard impedance tensor ( $Z$ ) only (Becken et al., 2008; Campany et al., 2016). Several parameters were set to build the starting model grid for the MT inversion. Figure A5 (in Appendix 5) shows an illustration of how the model grid was developed and an example of the starting model grid. Topography data was incorporated into the 3-D model grid to account for topographic variations of the MT sites in the model. The minimum interstation spacing in the MT dataset used was 10 km. The minimum interstation spacing could already inform the suitable grid resolution for the electrical modelling. A choice of 10 km grid resolution will not only recover finer resolution model but also ensure that the MT sites are approximately positioned at the centre of the grid cells as required by ModEM codes (Meqbel et al., 2014). However, a test on sensitivity of the inversion result to the model grid resolution was carried out to understand how it influences the resultant model. Another parameter that affects model development is covariance. The covariance controls how the norm of the model behaves. The covariance parameter has possible values between 0 – 1. Large covariance values result in smoother models, while small covariance values result in less smooth models (Robertson et al., 2020).

For this study, an inversion of the MT data covering Botswana was done to derive a nationwide 3-D electrical conductivity model of Botswana. Multiple inversions were done to assess the sensitivity of the model to inversion parameters, data, and model grid properties (Figure A6 in Appendix 6). For the MT data and inversion parameter sensitivity tests, smaller datasets were used to ensure that the computational time required are shorter and feasible within the time frame of this research. The details of the data used for the various inversions are given below. For the inversion computation, two Intel Xeon computing facilities (with CPU @ 3.20GHz and @ 2.60GHz) of the Faculty ITC, University of Twente, were used. The Dutch National Supercomputing Facilities, Cartesius (Grant Number: EINF-1468), which has higher computing power, was also used to accelerate the computation of the 3-D electrical conductivity models.

#### **3.3.4.1. Nationwide 3-D Electrical Conductivity Model of Botswana**

The SAMTEX sites comprising of 355 stations covering Botswana were inverted to create the nationwide electrical conductivity model of Botswana. The location of the MT data is shown in Figure 3.6. The MT data covers 31 periods from 0.1 – 10,000 seconds. In this inversion, a fine 10 km × 10 km grid resolution was used, which was chosen based on the minimum MT site spacing in the data (10 km) and results of the grid resolution sensitivity test. A first layer thickness of 10 m was used in the starting model, and the

subsequent layers' thicknesses increase by a factor of 1.1 logarithmically. The choice of first-layer thickness of 10 m was based on the tenth of the skin depth in the most conductive surface layer at the shortest period in the data and a need to recover high resolution in the vertical gridding (Meqbel et al., 2016). Topography data was incorporated into the inversion process to compensate for site elevation difference in the model. With the incorporation of the topography data, areas between the MT sites that are not on the topography are masked with highly resistive air column. To compensate for the effect of the highly resistive air in the model, ten air layers were added to the starting model to pad the Earth model. Starting resistivity of  $100 \Omega\text{m}$  was used for the prior model. Also, for this inversion, error floor ( $\sqrt{|Z_{xy}Z_{yx}|}$ ) of 5% was used for the  $Z_{xy}$  and  $Z_{yx}$  impedance data, ( $\sqrt{|Z_{xx}Z_{yy}|}$ ) of 5% was used for the  $Z_{xx}$  and  $Z_{yy}$  impedance data, and 0.03 for the VTFs. These error floor values were chosen to account for numerical and systematic limitations of the model (Kelbert et al., 2014; Robertson et al., 2020). An initial damping parameter of 10 was used based on the model space exploration results (subsection 4.2.4). A covariance value of 0.4 was used in inversion to better resolve features in the model (less smooth) (Robertson et al., 2020).

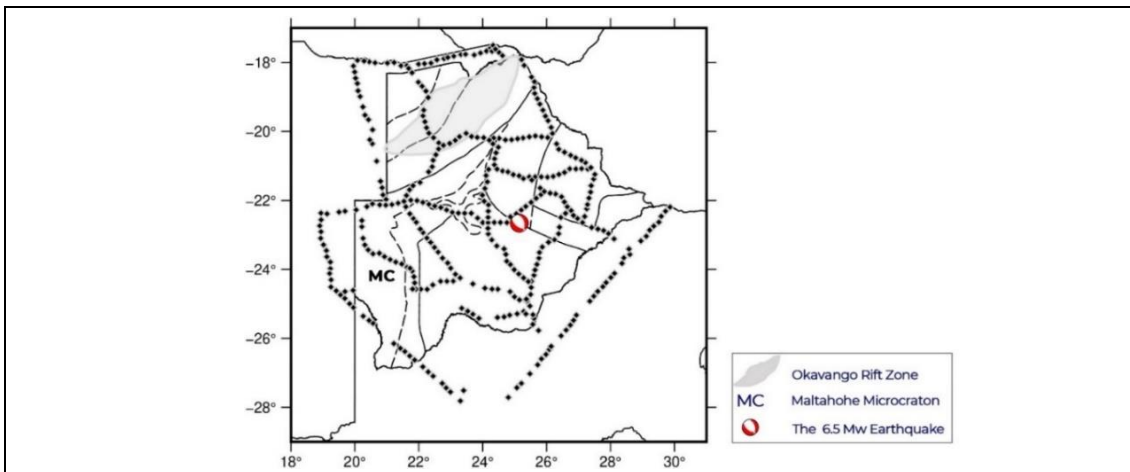


Figure 3.6: Map of SAMTEX data covering 355 stations in Botswana used for the nationwide 3-D electrical conductivity modelling (MT station represented with black squares).

#### 3.3.4.2. Data Period Resolution Test and Effect of Short Period Data

To test how the resolution of the data in period domain affects the inversion model, MT data from 127 sites covering central and northeastern Botswana were used (Figure 3.7a). This subset was chosen because the MT data arrays are more closely spaced. The dataset was prepared in four different ways with all other data and inversion parameters constant (subsection 3.3.4.1), except for the period resolution of the data. The first dataset was prepared with data at 3 periods per decade of the period (in logarithm scale), with a total of 16 periods from 0.1 – 10,000 seconds. The second dataset was prepared with data at 6 periods per decade of the period (in logarithm scale), with a total of 31 periods from 0.1 – 10,000 seconds. The third dataset was prepared with data at 10 periods per decade of the period, with a total of 51 periods from 0.1 – 10,000 seconds. Finally, the last dataset has data points at 15 periods per decade of period (in logarithm scale), which total to 76 periods from 0.1 – 10,000 seconds. The results from the test and the discussion are provided in subsection 4.2.1.

Other inversions were done with this dataset to verify the influence of short-period data (high frequency) on the inversion process and the output model. The test matrix includes dataset with periods covering 0.0001 - 10,000 seconds, 0.001 – 10,000 seconds, 0.01 – 10,000, 0.1 – 10,000 seconds and 1 – 10,000 seconds. In this test, only the period coverage of the data was varied, while keeping other data and inversion

parameters fixed. The results and discussion on the test with short period data on the inversion are provided in the next chapter (subsection 4.2.2).

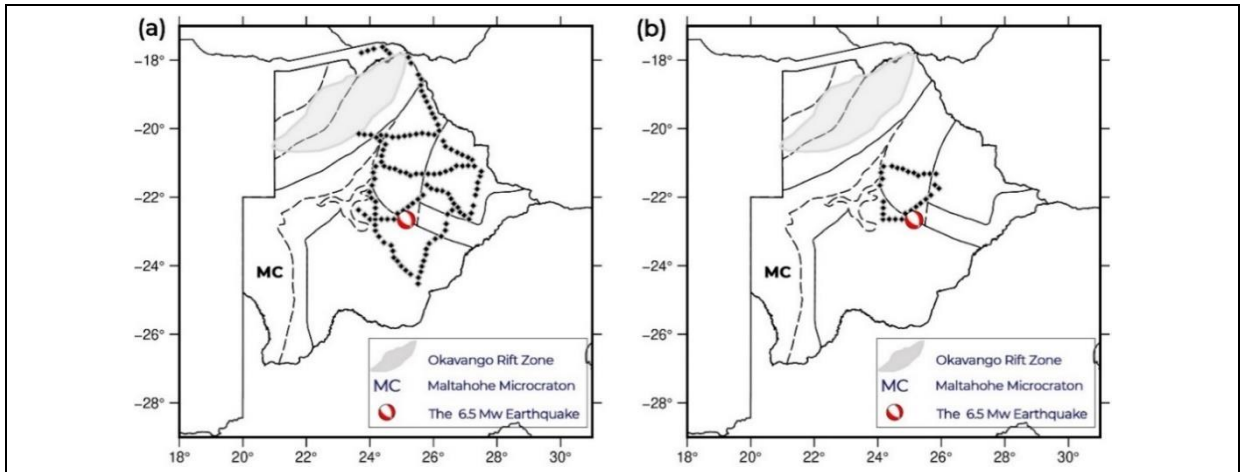


Figure 3.7: (a) Map of SAMTEX data covering 127 stations used for data period and model grid resolution sensitivity tests (b) Map of SAMTEX data covering 28 stations used for ModEM inversion damping parameter sensitivity test (MT station represented with black squares).

### 3.3.4.3. Model Grid Resolution Test

Model grid resolution determination is an important step in 3-D MT inversion. The decision of the size of the model grid is usually based on two factors; the need to recover fine model details by using a higher-resolution grid (smaller grid dimension) and minimization of the computation time and resources required by using coarser grid resolution. In this study, the sensitivity of the inversion result to the resolution of the model grid was tested using a dataset covering central and northeast Botswana (Figure 3.7a). This test was done using a coarse grid of 30 km, an intermediate grid of 15 km and a fine 10 km grid resolutions, while other data and inversion parameters remain constant (subsection 3.3.4.1). The results and discussion on the grid resolution test are provided in subsection 4.2.3.

### 3.3.4.4. ModEM Inversion Damping Parameter Sensitivity

To understand how the initial damping parameter affects the output model and the final data misfit. A sensitivity test was done on a smaller data subset covering 28 stations in central Botswana (Figure 3.7b). Initial damping parameters of 1, 10, 100 and 1,000 were tested while keeping other inversion parameters constant (subsection 3.3.4.1). The data were interpolated to six periods per decade of the period, with a total of 31 periods from 0.1 - 10,000 seconds. The results from the test and the discussion are provided in subsection 4.2.4.

### 3.3.5. Model Visualization and Assessment

The geoelectric models were visualized using MTPy, Matplotlib, and GMT. The models were visualized using plan view depth sections and vertical cross-sections to answer the defined research questions. Misfit analysis of the results of the inversion and the measured data was done using the normalized root-mean-square (nRMS) analysis. The nRMS describes how the model fits the data, and this measure is ubiquitously used for electrical model assessment in the MT community (e.g., Meqbel et al., 2014; Marion et al., 2013; Robertson et al., 2020).

## 4. RESULTS AND DISCUSSION

The result and discussions on the analysis of the MT dataset used for the nationwide conductivity modelling are provided in the first section (4.1). In section 4.2, the results and the discussion on the sensitivity tests on the inversion and data parameters are provided. The results and discussion on the new 3-D nationwide electrical conductivity model of Botswana are provided in section 4.3. Finally, a velocity-conductivity interpretation of the crust and upper mantle structure beneath Botswana is discussed in the last section (4.4).

### 4.1. Magnetotelluric Data Analysis

The results of resolution depth analysis, apparent resistivity analysis, and dimensionality of the MT dataset in Botswana are given and discussed.

#### 4.1.1. Resolution Depth and Horizontal Adjustment Length

The results of the depth of penetration estimates of the MT data coverage in Botswana for representative periods of 100, 250, 500, and 1,000 seconds are shown in Figure 4.1. The red colour indicate high depth of penetration of the MT data (between 200 km – 250 km), while the blue colour shows shallower depth of penetration (< 120 km). There is a general increase in the depth of penetration of the MT sites as the period increases, which is evident by more MT sites with high depth of penetration at periods of 500 seconds and 1,000 seconds. At the period of 100 seconds, there are some missing MT sites in the result, whose shortest periods are greater than 100 seconds. The disappearance of some MT sites in the result at longer periods of 500 seconds and 1,000 seconds is due to the lack of long-period data at those sites.

The depth of penetration of the MT data is dependent on the period of recording the MT data and the bulk resistivity of the Earth medium. High bulk resistivity in the subsurface allows for a high depth of penetration of the MT data. Spatially, MT sites that have a relatively higher depth of penetration correspond to stations above cratonic provinces, which have high bulk resistivity values as revealed in the electrical conductivity model discussed in section 4.3. For example, at the period of 250 seconds, higher depth up to 250 km depth is sensed by MT stations above the Congo Craton, Zimbabwe Craton, Rehoboth Province, and Kaapvaal Craton in the northwest, east, west, and south of Botswana, respectively. From the results, the MT data cover in Botswana used in this study can image up to 200 - 250 km depth in the subsurface, with 68% of the MT sites having periods above 1,000 seconds.

As the depth of penetration of the MT data becomes higher, the horizontal adjustment length, which is the lateral distance that the MT data is sensitive to increases. At the various depth of penetration of the MT data, the horizontal adjustment length is approximately 2 – 3 times the value of the penetration depth (Simpson & Bahr, 2005). It is then possible to image any subsurface structure that is off the MT data site within the horizontal adjustment length range at a given depth. The results of the 3D nationwide model of this study are discussed along profiles on top or in the near proximity of the MT stations to address the shortcoming of the small horizontal adjustment distance at short periods.

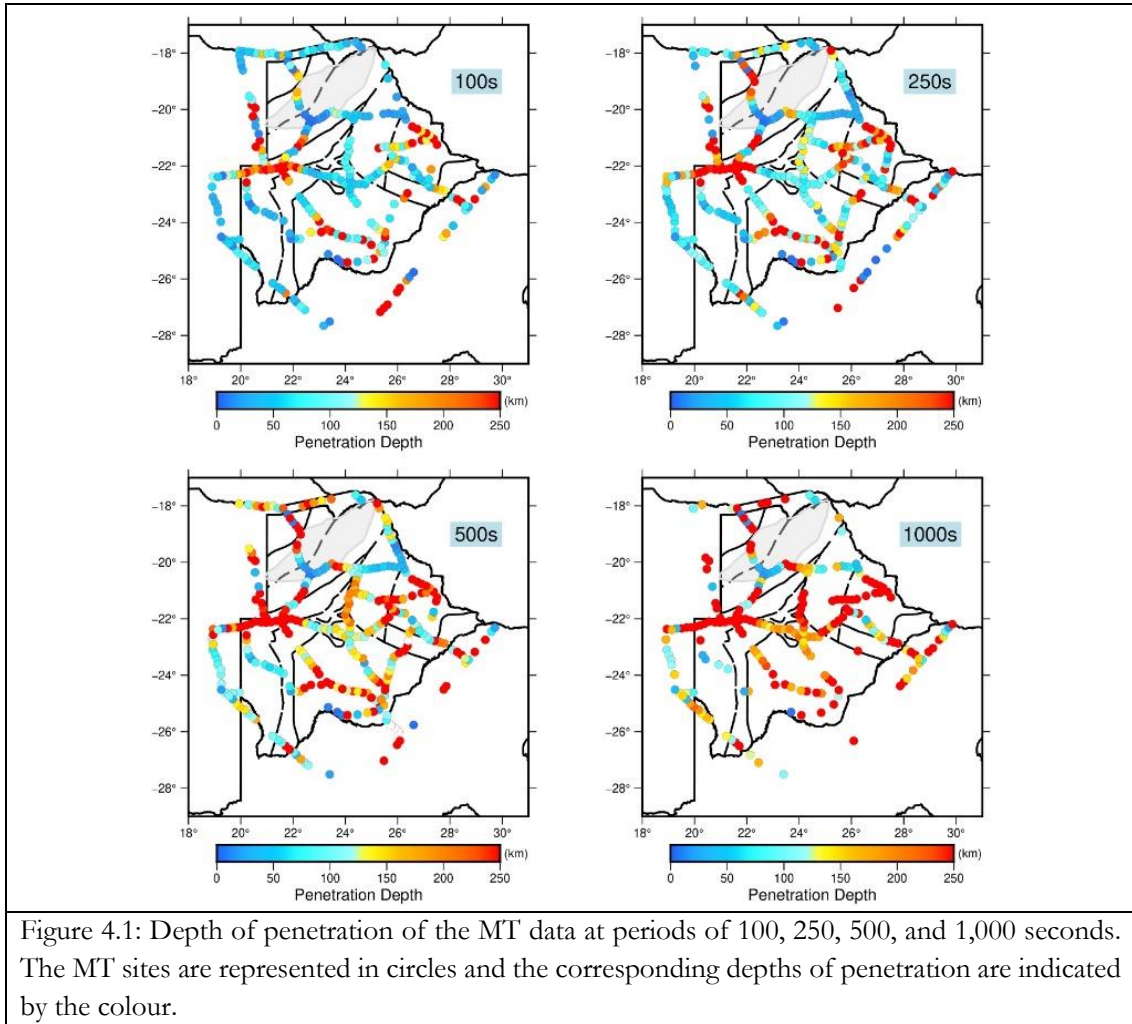


Figure 4.1: Depth of penetration of the MT data at periods of 100, 250, 500, and 1,000 seconds. The MT sites are represented in circles and the corresponding depths of penetration are indicated by the colour.

#### 4.1.2. Apparent Resistivity

The apparent resistivity maps for the off-diagonal components of the impedance ( $\rho_{xy}$  and  $\rho_{yx}$ ) are plotted as a function of the MT station at representative periods of 100, 250, 500 and 1,000 seconds (Figure 4.2). The blue colour represents high apparent resistivity values, while the yellow-red colours show low apparent resistivity values. One of the most prominent features in the apparent resistivity map (Figure 4.2) is the very low apparent resistivity values ( $< 5 \Omega\text{m}$ ) at MT sites located within the ORZ. This anomaly occurs at periods of 100, 250, 500, and 1,000 seconds. This feature indicates the presence of a conductive structure in the subsurface. Similarly, there is an observed low apparent resistivity anomaly ( $< 10 \Omega\text{m}$ ) at MT sites located in northeast Botswana. Another conductivity anomaly of note is the high conductivity feature ( $< 5 \Omega\text{m}$ ) in the southern part of Botswana. This anomaly is consistent in both the  $\rho_{xy}$  and  $\rho_{yx}$  components. The anomaly corresponds spatially with some parts of the Kaapvaal Craton region. The preliminary interpretation of this high conductivity feature is that it is due to the Bushveld Complex. The three distinctive high conductivity anomalous features observed in the apparent resistivity maps correspond to high conductivity structures in the crust and upper mantle from the new nationwide 3-D electrical conductivity model, which is discussed in detail later in this chapter (section 4.3).

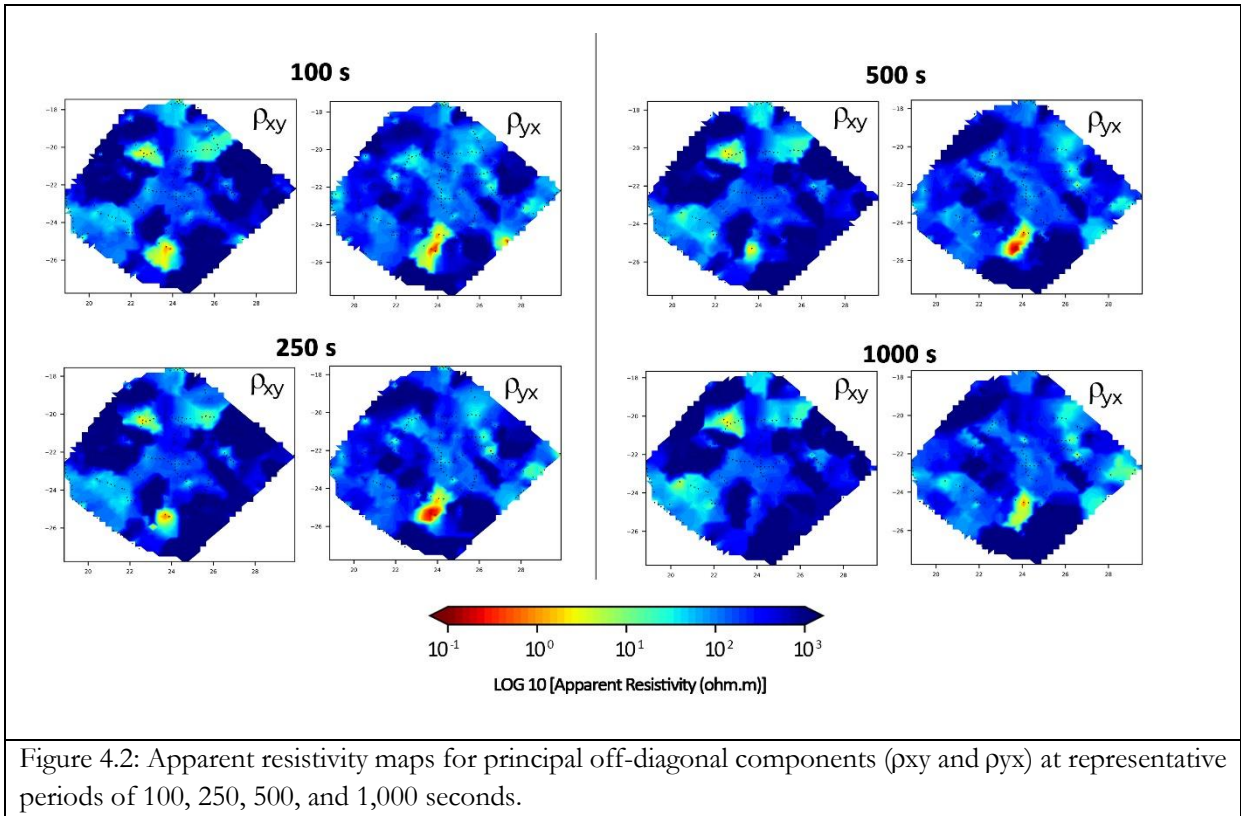


Figure 4.2: Apparent resistivity maps for principal off-diagonal components ( $\rho_{xy}$  and  $\rho_{yx}$ ) at representative periods of 100, 250, 500, and 1,000 seconds.

#### 4.1.3. Dimensionality of the Magnetotelluric Data

The results of the phase tensor dimensionality analysis for three representative profiles from major geological provinces in Botswana are presented as pseudo section plots in Figure 4.3. The results for three other representative profiles are given in Figure A7 (in Appendix 7). The pseudo sections are plotted as circles and ellipses, while the colour indicates the skew value of the phase tensor. High skew values greater than  $6^\circ$ , which are shown in light to dark brown colour, indicate 3-D effects in the data. Also, when the phase tensor's shape is circular, it indicates a 1-D structure, while elliptical phase tensors show 2-D or 3-D effects in the data. More explanation on the phase tensor skew, the skew threshold of  $6^\circ$  for 3-D signature and ellipticity of the phase tensor is given in subsection 3.3.3.1.

The previous MT studies done in Botswana using the SAMTEX data (e.g., Miensopest et al., (2011), Muller et al., (2009), and Khoza et al., (2012)) confirmed the presence of 3-D components in the MT data. There exist multiple principal geoelectric strike directions in the MT data, which is indicative of 3-D structure (e.g., Miensopest et al., (2011), Muller et al., (2009), and Khoza et al., (2012)). The results of the phase tensor analysis (Figure 4.3) shows the presences of 3-D components in the MT data. There is 3-D resistivity structure in most of the MT data sites, which is evident by the high skew values ( $> 6^\circ$ ) and elliptical nature of the phase tensor for many of the MT sites, hence the need to model the data in 3-D. The result of this analysis confirms the 3-D nature of the terrane beneath Botswana as reflected in the MT data. The MT data for this study were inverted in 3-D without need for assumption of geoelectric strike directions, which is required for 2-D modelling.

#### 4.2. Results and Discussion on Sensitivity Tests

To explore the influence of the various inversion parameters, data resolution, and model grid properties on the 3-D resultant model, several sensitivity tests were carried out. The results of these tests and discussions on them are explained in this section.

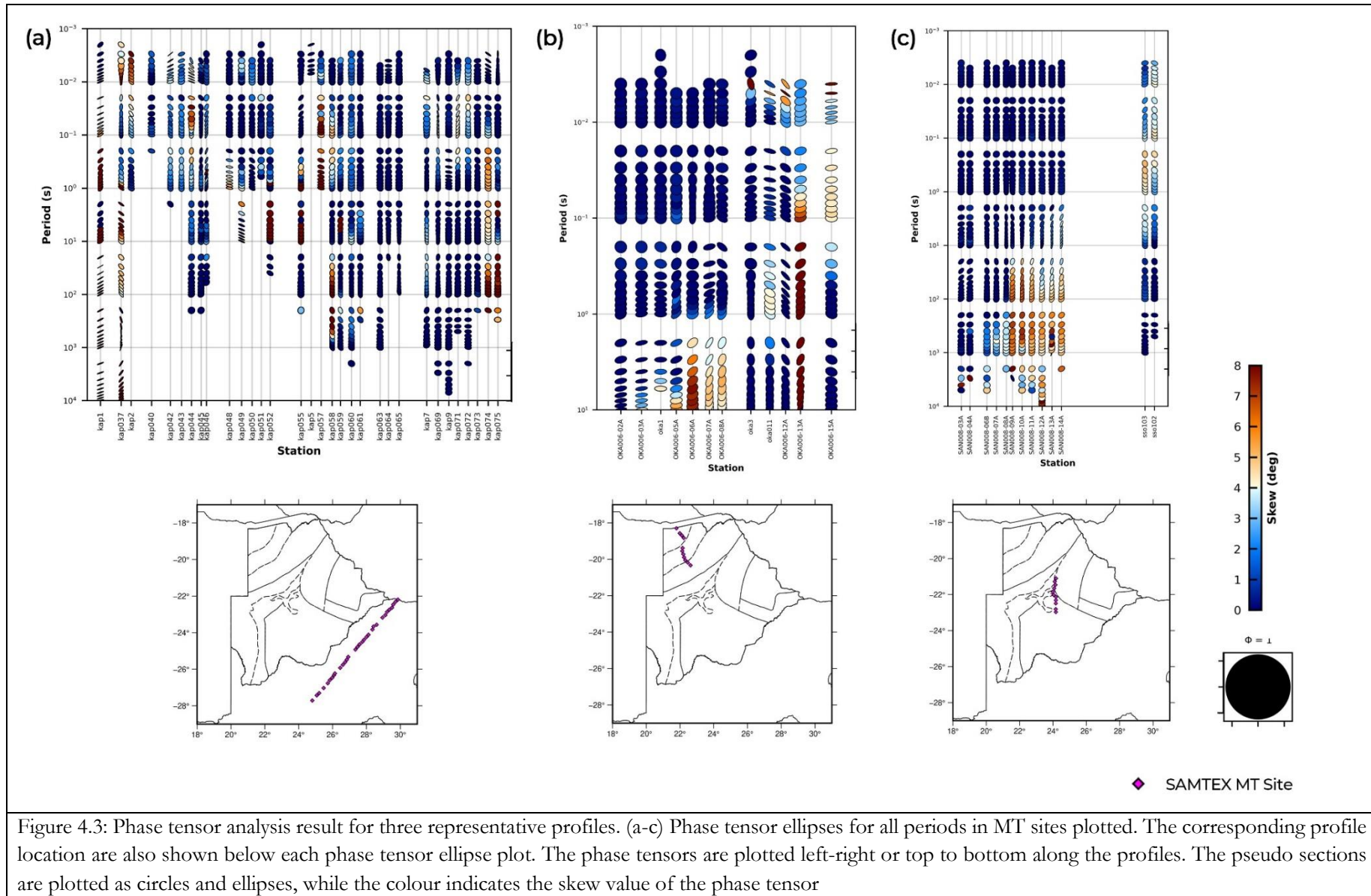


Figure 4.3: Phase tensor analysis result for three representative profiles. (a-c) Phase tensor ellipses for all periods in MT sites plotted. The corresponding profile location are also shown below each phase tensor ellipse plot. The phase tensors are plotted left-right or top to bottom along the profiles. The pseudo sections are plotted as circles and ellipses, while the colour indicates the skew value of the phase tensor

#### 4.2.1. Data Period Resolution

Table 4.1 shows how the nRMS of the four models created with varying data period resolutions and the number of NLCG iterations completed before the convergence of the inversions compare. The results show similar overall nRMS values for the four models. To gain insight from this test, misfit analysis of the data components for the four resultant models was done. Figure A10 (in Appendix 10) shows how the MT site nRMS values for the impedance and VTFs components of the data compare. From the results, the nRMS values per MT sites are similar for the four models.

Table 4.1: Summary of the nRMS for the Data Period Sensitivity Test

Data Period Resolution	Overall nRMS	Number of NLCG Iteration
16 periods	3.150337	81
31 periods	3.115478	82
51 periods	3.120504	83
76 periods	2.977310	82

From the results, the overall nRMS values of the four models have no significant differences, which implies that increasing the period resolution of the data does not significantly improve the nRMS of the model. Although increasing the period resolution of the data from 16 periods to 31 periods did improve the data fit, the decrease in nRMS is not very significant (Table 4.1). On the other hand, there was an increase in the nRMS when the data period resolution was increased from 31 to 51 periods, although not very significant also (Table 4.1). There is an observed slight decrease in the nRMS value from the 76 periods data inversion. However, this change is not very significant. Also, the number of NLCG iterations required for the four different inversions to converge are similar. No change is observable in the nRMS values per site of the four different models with data of varying period resolution (Figure A10 in Appendix 10). Generally, from the visual comparison of the resultant models from these four different models (Figure A6 in Appendix 6), there is no significant changes in the resolved features.

It is expected that MT data with lower period resolution will have smoother impedance data curves than data with higher period resolution. This smoothness property of the data makes it easy for the inversion process to fit the electrical conductivity model to the data better. The data used in this study were smoothed as part of the data preparation, which improved the data curve smoothness and reduced error points in the data. Hence, the differences observed in the results of the inversion of MT data with the different period resolution is quite negligible. It can be inferred that once the MT data sufficiently represent the behaviour of the impedance curve, it can be used to model the subsurface electrical structure effectively. The penalty for increased period resolution in the data is the higher computational resources and time required for the inversion process. For the 3-D nationwide electrical conductivity modelling of Botswana, MT data with 6 periods per decade of period (in total 31 periods) were used to reduce the computation time while still retaining the properties of the impedance curve of the data.

#### 4.2.2. Effects of Short Period Data in Inversion Process

The SAMTEX data includes high-quality MT data at short period range up to 0.0001 seconds. Multiple inversions were done, which include various levels of the short period data. While including short period (high frequency) data in the inversion resolves the near-surface structures in high detail, it does not allow for quick development of deeper structures in the model. From the several inversions done, the inversions of the MT data that include periods lower than 0.1 seconds took longer time, up to 12 hours per NLCG

iteration for the nationwide 3-D electrical conductivity model. Also, those inversions with short period data restrict the model development to only topmost 300 m depth even after 40 NLCCG iterations (Figure A6 in Appendix 6). The high variability in the short period data dominated the misfit function of the inversion and therefore made the inversion busy instead of resolving the smaller variability in the long period data. This was not efficient, as the inversion process spends a lot of time in resolving the near-surface features in the model. In the context of this study, the structures of interest are in the crust and upper mantle and not the overburden layers. Therefore, a choice of 0.1 seconds as the shortest period to include in the inversion data was made for subsequent inversions. This helps to resolve the deeper structures in the model and reduce computation time without compromise on the shallow structures in the subsurface.

#### 4.2.3. Model Grid Resolution

To investigate the influence of the model grid resolution on the resultant electrical model, test was done to compare the results from three model grids with resolutions of 10 km, 15 km, and 30 km. Table 4.2 shows how the overall nRMS of the three models compare and the number of NLCCG iterations completed before the convergence of the inversions. The overall nRMS decreases with increasing grid resolution. Increasing the resolution of the grid from 30 km to twice as fine resolution of 15 km has a considerable improvement on the nRMS. Similarly, a further increase in the grid resolution of the model from 15 km to 10 km significantly improved the data fit, which is evident in the reduced nRMS.

Table 4.2: Summary of the nRMS for the Model Grid Resolution Sensitivity Test

Model Grid Resolution	Overall nRMS	Number of NLCCG Iteration
10 km × 10 km	2.392333	98
15 km × 15 km	3.115478	82
30 km × 30 km	4.067719	74

Figure 4.4 shows how the MT site nRMS values for all the components of the data (Z and T) compare for the three models per MT sites. The nRMS per site generally decreases with increasing model grid resolution (Figure 4.4). A closer examination of the nRMS per site revealed that the tipper components have a higher data fit (low nRMS) than the impedance component (Figure 4.4). However, there are some other local areas with poor data fit (high nRMS) for all the data components. These results reveal that finer grid model resolution inversion aids better data fit and increase the confidence in the recovered model. However, extremely fine grid resolution could lead to artefacts in the model and a higher weight of model norm over the data misfit norm (Meqbel et al., 2014; Marion et al., 2013).

To further gain insight from how the electrical structures develop in the three different models, depth sections at representative depths in the subsurface were examined. A plan view of the depth sections at 19 km and 49 km from the three models are given in Figure 4.5 and Figure 4.6, respectively. From the results of the 19 km depth section, it is revealed that the electrical structures are narrower and less connected in the fine grid model of 10 km (Figure 4.5). As the model grid resolution becomes coarser (15 km and 30 km), the electrical structures become wider and more connected spatially. Deeper electrical structures are also affected by the reduction of the model grid resolution in similar ways, as shown in the depth sections from 49 km in Figure 4.6. Also, the finer model shows fine and smooth boundaries of the electrical structures. It is observed that conductive structures are more distinctive at deeper depth in the finer grid model (Figure 4.6.). From these results, it is revealed that finer grid resolution aid the recovery of high-resolution electrical structure with smooth boundaries.

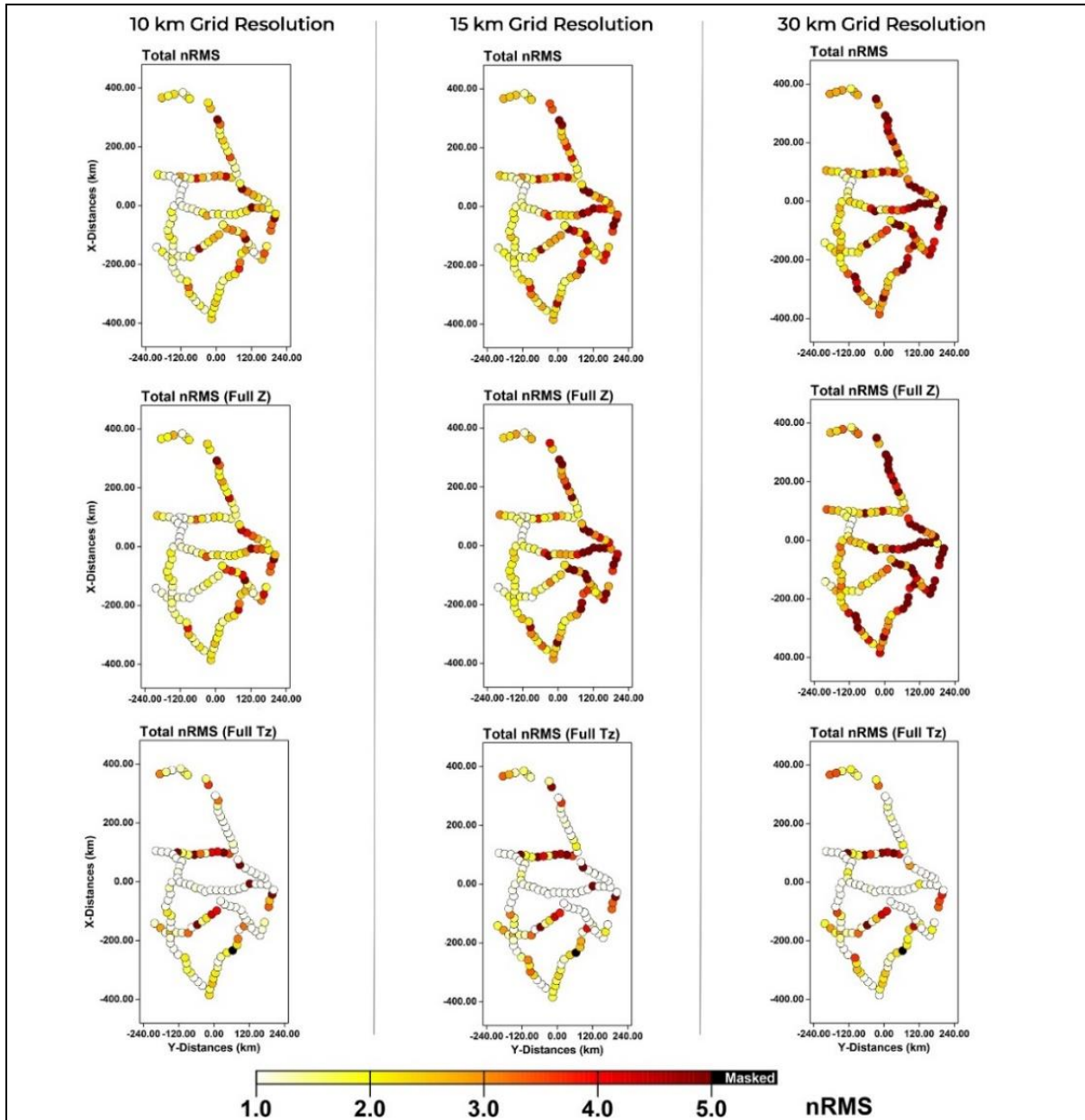


Figure 4.4: nRMS plot per station for impedance tensor and tipper data components derived for 10 km, 15 km, and 30 km model grid resolutions. The MT sites are represented in circles and the corresponding nRMS are indicated by the colour. Masked sites (shown in black colour) =no data.

In terms of computation time required, the 10 km grid model took 4.5 hours per NLCG iteration, the 15 km grid model took 3 hours, and the 30 km grid model took 1 hour. From the results of this sensitivity test, a choice of 10 km grid was made for the new nationwide 3-D electrical conductivity modelling in Botswana to recover a finer model and more realistic model with better data fit. This helps to increase the confidence in the recovered model, which has better data fit and fine spatial resolution. The choice of 10 km, which is the minimum interstation spacing in the dataset, is also supported by the need to centre the MT stations in the grid cells. However, the nationwide model comprising of 355 MT sites took a longer time per NLCG iteration compared to the sensitivity test runs, which has 127 MT sites.

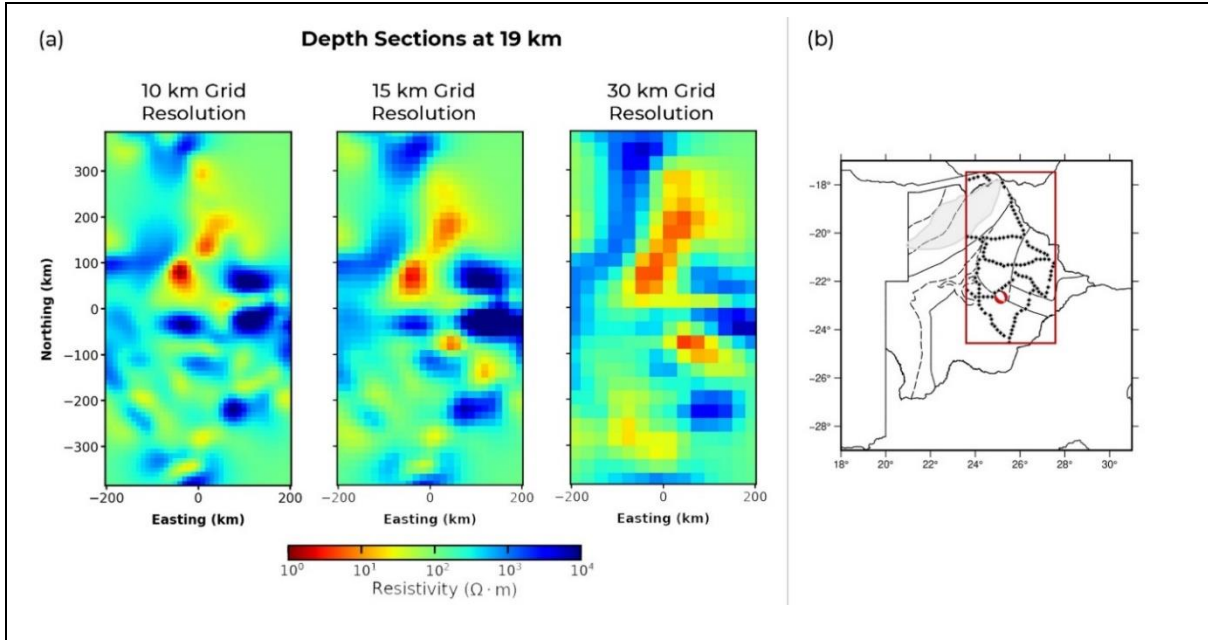


Figure 4.5: (a) Plan view of electrical conductivity model depth slices at 19 km derived for 10 km, 15 km, and 30 km grid resolution (b) Location Map. Red bounding box = location of models presented in (a).

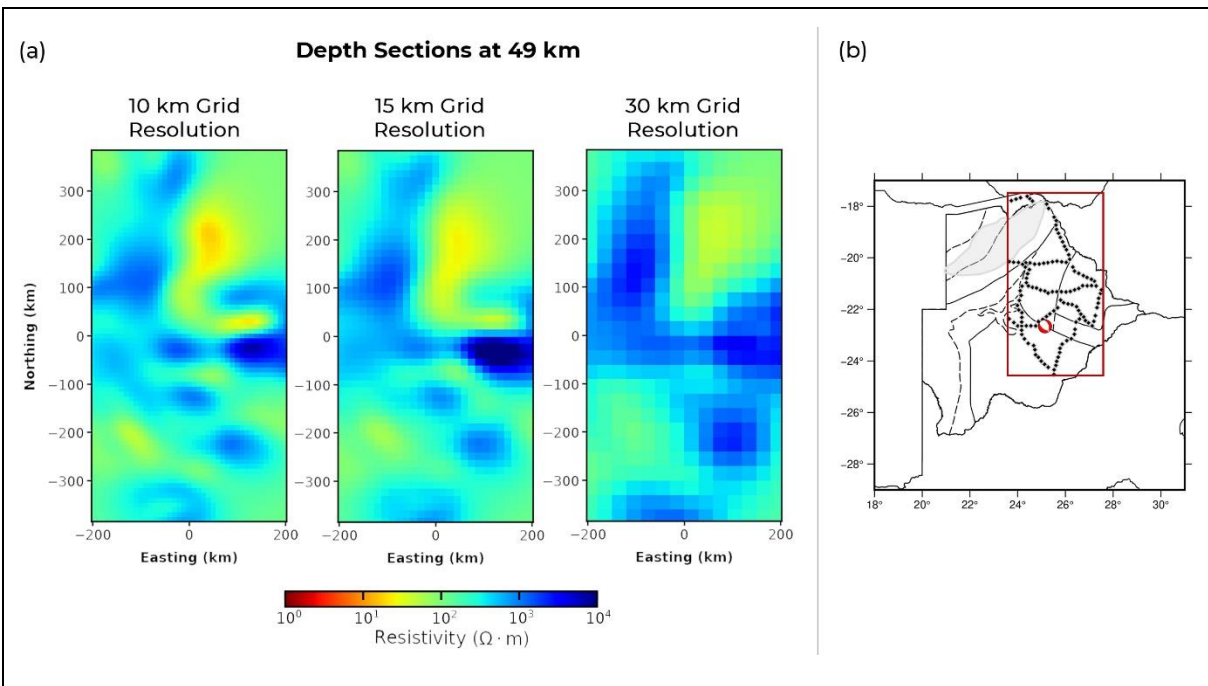


Figure 4.6: (a) Plan view of electrical conductivity model depth slices at 49 km derived for 10 km, 15 km, and 30 km grid resolution (b) Location Map. Red bounding box = location of models presented in (a).

#### 4.2.4. ModEM Inversion Damping Parameter

The inversion initial damping parameters (described in subsection 3.3.4) of 1, 10, 100, and 1,000 were used to test the sensitivity of the model space to this parameter. The summary of the results of the misfit analysis of the tests is present in Table 4.3. From the results, the nRMS values for the four models are similar. To further gain insight into the resultant models, depth sections corresponding to 7 km, 31 km, and 49 km for the four different models are presented in Figure 4.7. Visually, the plan view of depth sections when compared for the four models look similar (Figure 4.7). However, there is a difference in the number of

NLCG iterations required for the model to converge for the different initial damping parameters used. Higher initial damping parameters of 100 and 1,000 took longer NLCG iterations and computation time to achieve convergence of the inversion. The choice of the initial damping parameter has little influence on the resultant model and data misfit. The observations from this sensitivity test are consistent with the results from model space exploration with the Australian Lithospheric Architecture Magnetotelluric Project data using the ModEM codes done by Robertson et al. (2020). For the Botswana 3-D national electrical conductivity modelling, an initial damping parameter of 10 was used to reduce the computing time.

Table 4.3: Summary of the nRMS for Initial Damping Parameter Sensitivity Test

Initial Damping Parameter	Overall nRMS	Number of NLCG Iteration
1	2.044264	81
10	2.101267	80
100	2.085736	110
1000	2.069875	122

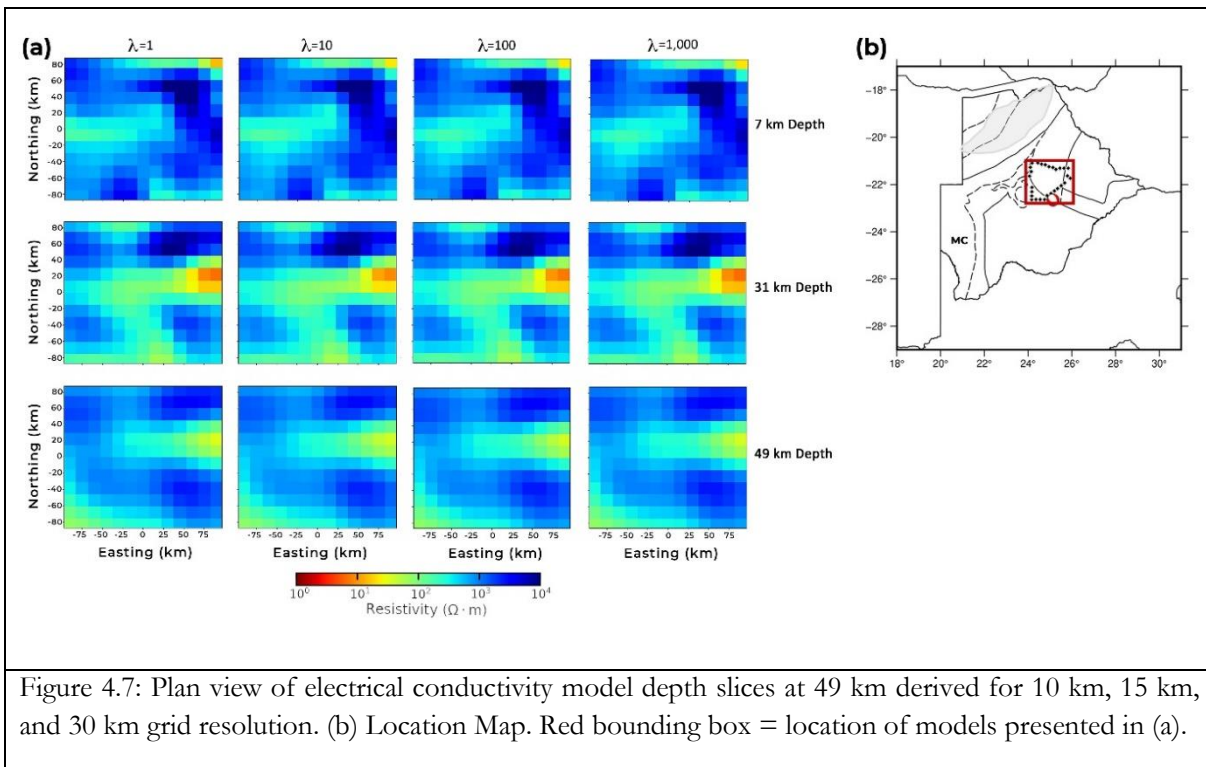


Figure 4.7: Plan view of electrical conductivity model depth slices at 49 km derived for 10 km, 15 km, and 30 km grid resolution. (b) Location Map. Red bounding box = location of models presented in (a).

### 4.3. Nationwide 3-D Electrical Conductivity Model of Botswana

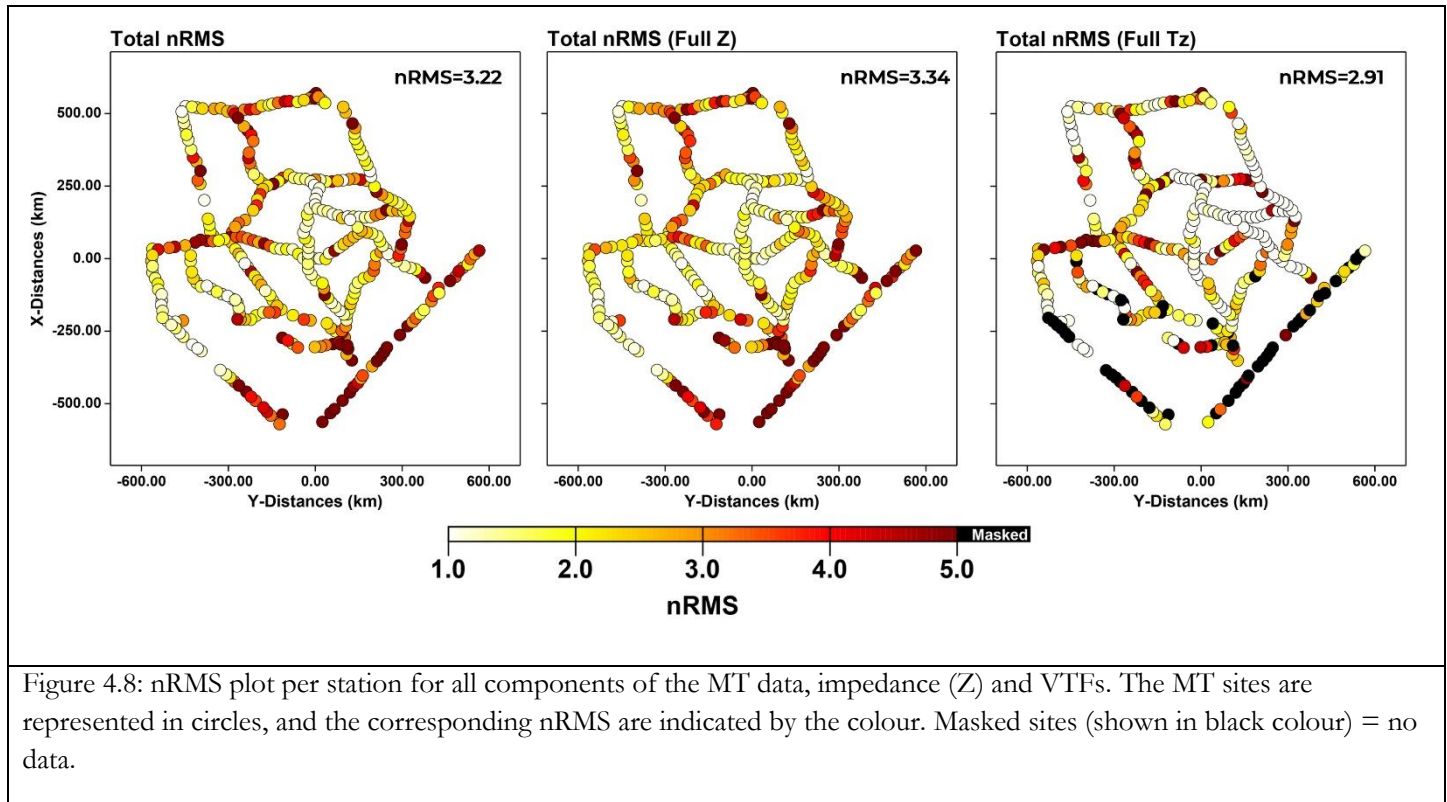
An evaluation of the 3-D nationwide electrical conductivity model of Botswana was done and presented in this section. The result of the new nationwide 3-D electrical conductivity model of Botswana are presented in various representative plan view maps and cross-sections to show the crust and upper mantle electrical structures (Figures 4.10 – 4.14). Based on the results presented, geological and tectonic interpretation of the electrical structures are discussed.

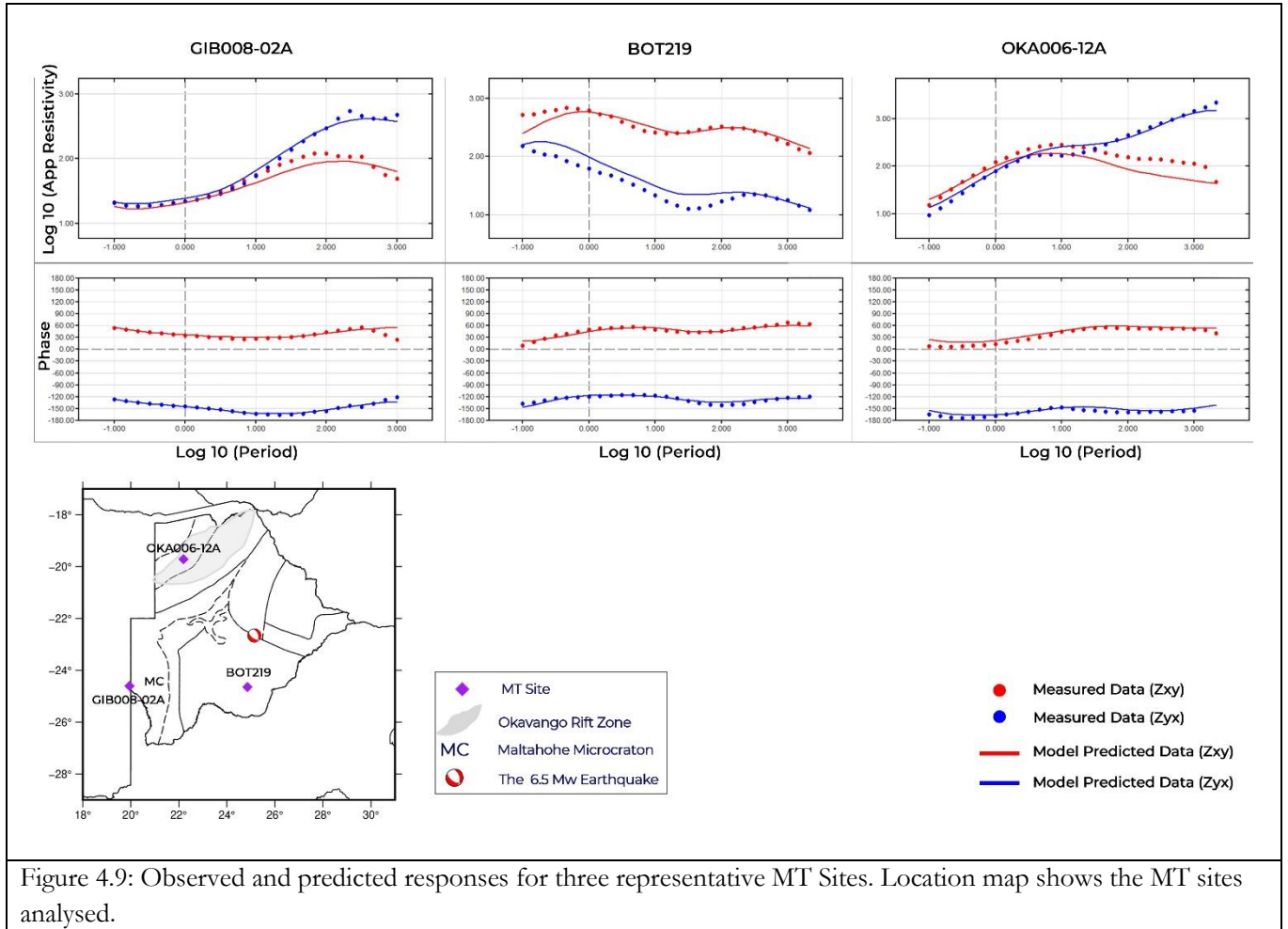
#### 4.3.1. Evaluation of Data Fit of the 3-D Nationwide Electrical Conductivity Model

To evaluate the result of the nationwide electrical conductivity model, nRMS analysis of the model was done to examine how it fits the measured MT data. Figure 4.8 shows the nRMS analysis between the measured MT data and the model-predicted data from the inversion as a function of the MT station for impedance tensor ( $Z$ ) components, the VTFs components and all the components together. Figure A8 (in Appendix 8) shows nRMS plot per station for each component of the impedance tensor and VTFs. From an examination of the nRMS for the components of the data used, the impedance tensor components have poorer nRMS (3.34) than the VTFs components (2.91). However, there are some sites with poor data fit across the whole dataset for both the impedance tensor and VTFs components, as shown in the total nRMS plots per site (Figure 4.8 and Figure A8).

Figure 4.9 shows the plot of measured and model-predicted responses for three representative MT sites that are in close proximity to some of the major tectonic domains. The measured and model-predicted responses plots for six others MT sites are given in Figure A9 (in Appendix 9). The result shows a good fit between the measured and model-predicted data across the whole periods for these representative sites.

From the inversion, the overall nRMS of the nationwide electrical conductivity model is 3.22 after 126 NLCCG iterations. The overall nRMS is below the set error floors of 5% used in the inversion process, which is considered good for the model. This error is considered good for a comprehensive dataset in terms of spatial coverage and range of period as this.





#### 4.3.2. Overview of the Electrical Structure of the Crust and Upper Mantle

To image the electrical structure of the crust and upper mantle beneath Botswana, depth sections from representative depths in the subsurface are presented. Figure 4.10 shows a plan view of the depth sections of the electrical conductivity structures of the crust and upper mantle corresponding to depths of 13 km, 20 km, 32 km, 50 km, 92 km, 120 km, 186 km, and 222 km in the subsurface.

From the 3-D electrical conductivity model, there exist some significant electrical structures in the tectonic domains investigated. The main results of the electrical conductivity model and the geologic interpretations are discussed in the coming subsections. However, this subsection discusses an overview of the electrical structures imaged in the middle-lower crust and upper mantle beneath Botswana.

In depths that correspond to the crust (Figure 4.10), there exist spatial aliasing of the imaged electrical structures. This is as a result of the low spatial coverage and density of the MT sites in Botswana, leaving large distances between data profiles. At shallow depths, the horizontal adjustment length to which the MT data is sensitive is small. For example, at a depth of 13km (Figure 4.10), the MT data is not sensitive enough to resolve structures at locations that are spatially off the MT data stations. The background resistivity used for the 3-D inversion is  $100 \Omega\text{m}$ , and at locations that cannot be resolved by the MT data, the model retains the background resistivity value. Hence, structures that are far from the MT profile are not reliably recovered at such shallow depth, and  $100 \Omega\text{m}$  is retained at those locations. However, as the depth of penetration of the MT data increases, the lateral distance to which the MT data is sensitive increases, and the structures recovered are more regional. For example, at depths of 92 km and 119 km (Figure 4.10), horizontal

adjustment is much higher, and at the minimum, it is equal to the depths of penetration. The structures recovered at locations that are spatially off the MT data profiles at such depths are more regional and are reliably interpreted (Figure 4.10).

From the results of the depth sections (Figure 4.10), there are distinctive high conductive structure spread across the study area, both in the crust and upper mantle regions. In the middle and lower crust (12 km, 20 km, and 32 km), there are several local anomalous conductive structures that are mainly in the northeast and northwest of Botswana. Also, in the mantle, there are some distinctive conductive structures in southern Botswana. Several factors can contribute to the high conductivity in the mid-lower crust and upper mantle, as discussed next.

Anomalous conductive structures in the lower crust can be interpreted as the presence of graphite or aqueous fluids (Jones, Ledo, & Ferguson, 2005). In some areas, sulfides and other metalliferous ore deposits or partial melt contribute to high conductivity in the lower crust (Wannamaker et al., 2008). The areas that are spatially close to suture zones or fault zones also have high conductivity features due to the weakening of the crust (Jones, Ledo, & Ferguson, 2005). In the mantle, high conductivity anomalies can be due to high temperatures, partial melting, or hydration (Evans et al., 2019). In the context of this study area, the proximity to some regional features such as the EARS, African superplume, Bushveld Complex, and orogenic Belt from past tectonic activities play significant roles in the electrical structures in the crust and upper mantle beneath Botswana. Results and interpretations focused on the main tectonic domains of interest to this study, and their conductivity structures are given in the subsequent subsections.

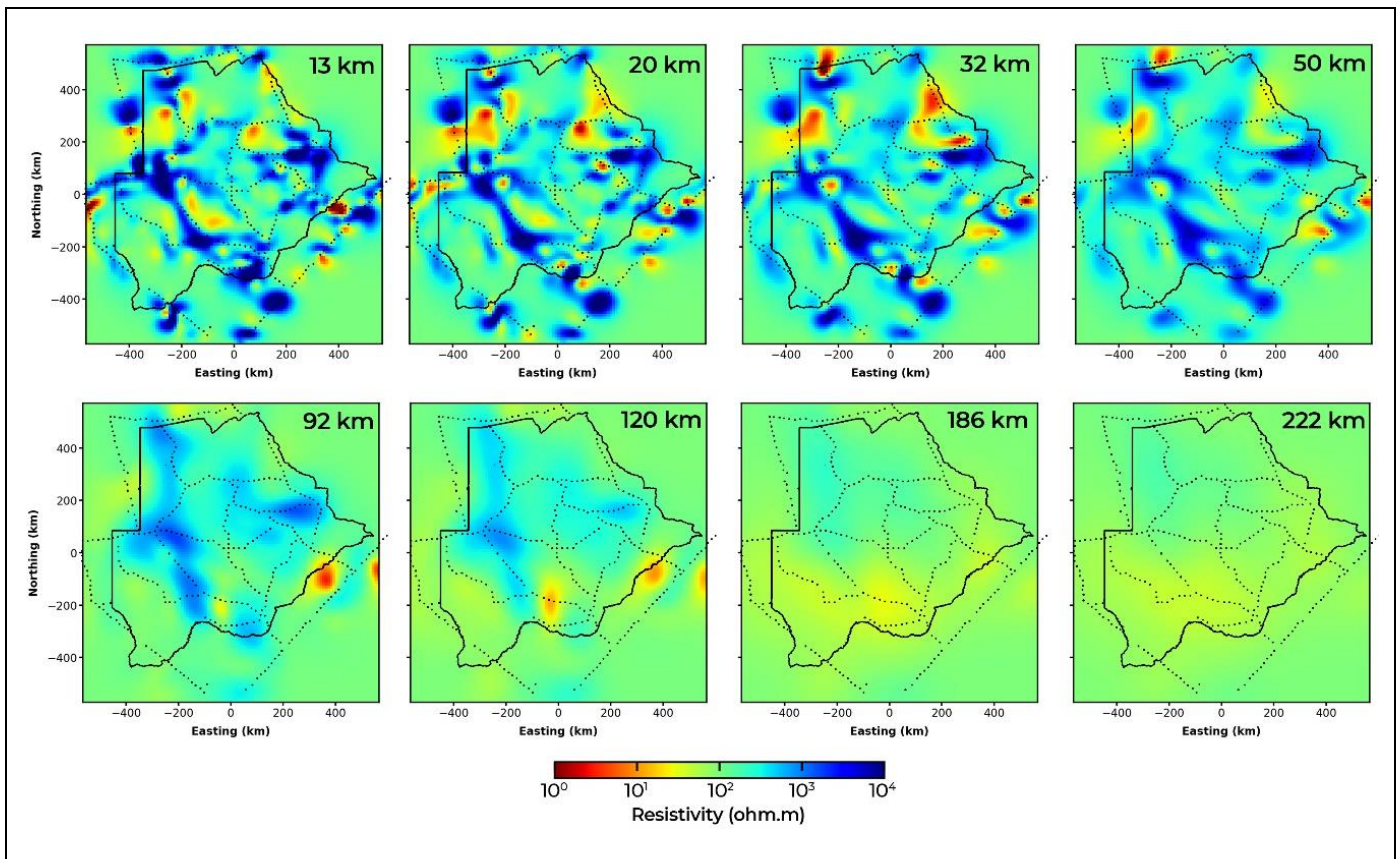


Figure 4.10: Plan view of electrical conductivity model depth slices at 13 km, 20 km, 32 km, 50 km, 92 km, 120 km, 186 km, and 222 km depths. MT sites are represented in black dots.

### 4.3.3. Imaging the Geological Provinces of Botswana

To map the geological provinces of Botswana, vertical cross-sections along or in close proximity to MT data profiles were taken to address the shortcoming of small horizontal adjustment length and make the geologic interpretations reliable. These results provide images of the variation of the electrical structures of the crust and upper mantle along the profiles with depth. The choices of the cross-section locations were defined to address the first research question of this study. In southwest Botswana, Figure 4.11 shows cross-sections A-A', B-B', and C-C' of the electrical structure across the Rehoboth Province-Kheis Belt-Okwa Block-Kaapvaal Craton. In northwest Botswana, Figure 4.12 shows cross-sections D-D' and E-E' through the Congo Craton-Damara-Ghanzi-Chobe Belt. Cross-sections F-F' and G-G' across the Magondi Belt, Zimbabwe Craton and Limpopo Belt are shown in Figure 4.13.

#### Rehoboth Province-Kheis Belt-Okwa Block-Kaapvaal Craton

Figure 4.11 shows the 2-D cross-section across the Rehoboth Province to the Kaapvaal Craton in the southwestern part of Botswana. In the northwestern part of the cross-section A-A', the Rehoboth Province is imaged as a resistive structure. The Kaapvaal Craton is imaged in the cross-sections as a highly resistive and very thick lithosphere. Between the Kaapvaal Craton and Rehoboth Province is the Kheis Belt, which is imaged as a less resistive and very thin lithosphere relative to the adjacent Kaapvaal Craton. In the cross-section, the Kheis Belt shows the thinnest and most conductive lithospheric structure.

The Archean Kaapvaal Craton was formed between 3.7 – 3.2 Ga (Figure 2.2) and has a resistive structure as revealed by the 3-D conductivity model. The structure of the Kaapvaal craton as imaged in this electrical conductivity model compares well with high-velocity anomaly associated with the Craton from previous studies that used seismic data (e.g., Fadel et al., 2020; Ortiz et al., 2019). However, the transition from the highly resistive cratonic root of the Kaapvaal Craton into the asthenosphere is poorly resolved by the MT data. One other significant feature that is revealed in the Kaapvaal Craton from the electrical conductivity model is the conductive Colesberg Magnetic Lineament (Figure 4.11, cross-section A-A'), which is a suture zone separating the eastern Witwatersrand and western Kimberly blocks of the Kaapvaal Craton (Figure 2.1a). The Colesberg Lineament represents the zone along which the two blocks of the Kaapvaal Craton were accreted from 2.93 – 2.88 Ga (Eglington & Armstrong, 2004). The Colesberg Lineament, which is a magnetic anomaly, is confirmed by previous gravity and magnetic studies that cover the Kaapvaal Craton (Corner, Durrheim, & Nicolaysen, 1990), geochronological data (Eglington & Armstrong, 2004; Schmitz, Bowring, de Wit, & Gartz, 2004), and rheological modelling (Kgaswane, Rathod, & Saunders, 2018).

The part of the Rehoboth Province imaged (Figure 4.11, cross-section A-A') has a similar cratonic electrical structure as the Kaapvaal Craton, although it is of relatively lower resistivity. This observation is confirmed by the high-velocity anomaly beneath the Rehoboth Province from the shear wave velocity study (Fadel et al., 2020) and high P and S wave velocity anomalies (Ortiz et al., 2019). More discussion on the electrical structure beneath the Rehoboth Province as it relates to the hypothesis of the presence of MC in southwest Botswana is explained in subsection 4.3.4.1

The Kheis Belt was formed between the western margin of the Kaapvaal Craton and the Rehoboth Province. The Kheis Belt has been significantly deformed by series of orogenesis, reactivation, and amalgamation processes (Figure 2.2). The weakness of this zone is evident by its relatively lower resistivity signature compared to the Kaapvaal Craton (Figure 4.11, cross-sections A-A' and B-B'). This observation is confirmed by the shear wave velocity observed beneath Kheis Belt, which is relatively lower than that of the adjacent Kaapvaal Craton (Fadel et al., 2020). Similarly, the low negative P and S wave velocity anomaly in the western end of the Kaapvaal Craton presented by Youssof et al. (2015) is related to the Kheis Belt.

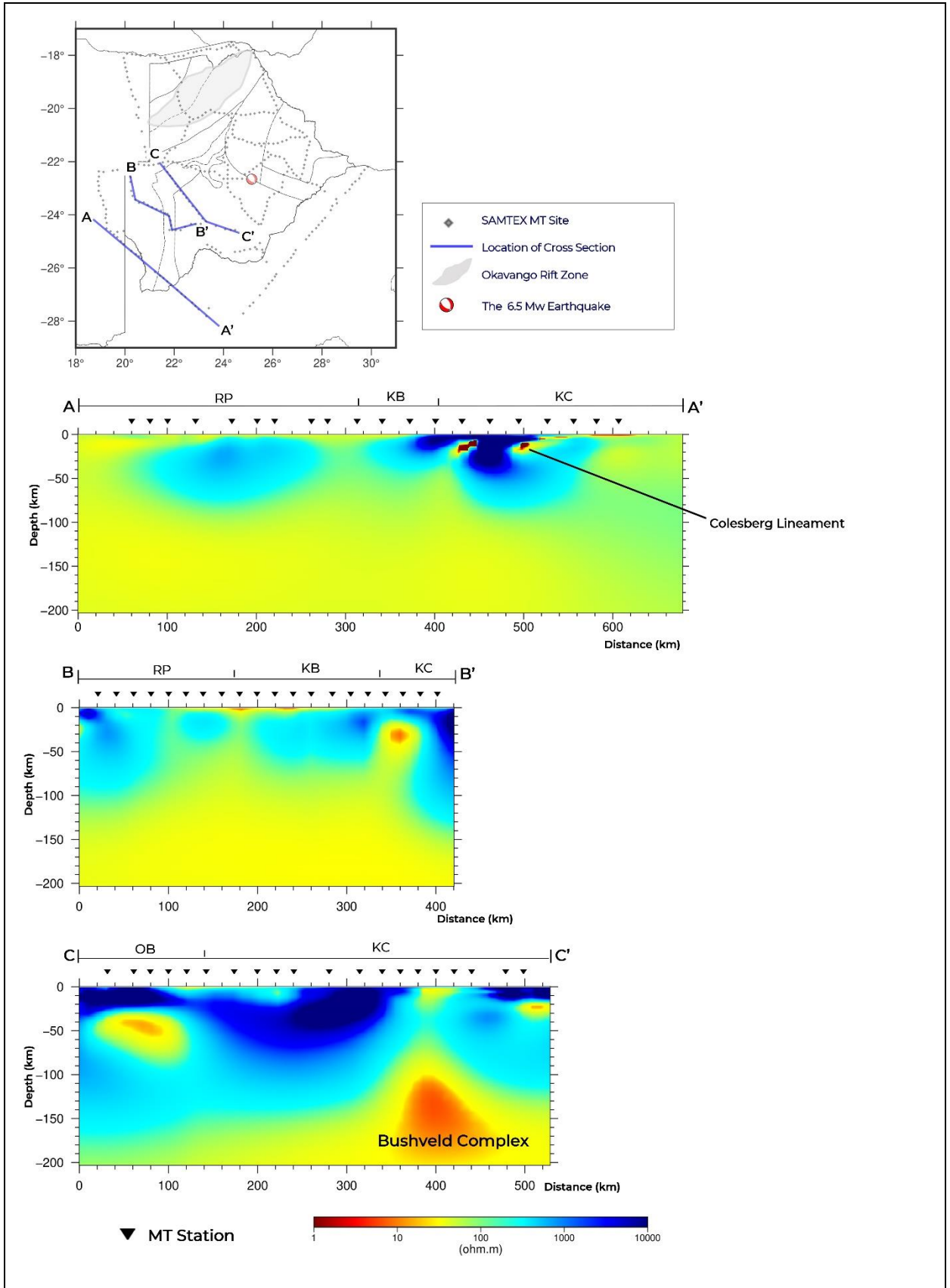


Figure 4.11: Nationwide electrical conductivity model vertical profiles across the Rehoboth Province - Kheis Belt - Okwa Block - Kaapvaal Craton in southwest Botswana. KC=Kaapvaal Craton, KB=Kheis Belt, OB=Okwa Block, and RP=Rehoboth Province.

From the result of the electrical conductivity model (Figure 4.11, cross-section A-A'), there is a variation in the thickness and resistivity values across this terrane laterally. The Kaapvaal block has average resistivity of approximately 10,000  $\Omega\text{m}$ , the Rehoboth Province has an average resistivity of approximately 1,000  $\Omega\text{m}$ , while the Kheis Belt has an average resistivity of approximately 500  $\Omega\text{m}$ . According to Jones et al. (2009), at depths that correspond to mantle structure, variation in the electrical conductivity of the Earth is more sensitive to temperature changes than it is to variation in composition. Therefore, the lateral variation observed in the resistivity across the Rehoboth Province-Kheis Belt-Kaapvaal Craton can be explained by changes in the lithospheric geothermal gradient (Muller et al., 2009). The Kheis Belt has the lowest bulk electrical resistivity, which corresponds to high geotherm, while the Kaapvaal Craton has the highest bulk electrical resistivity, which corresponds to lower geotherm. The observed lateral variation across the Rehoboth Province-Kheis Belt-Kaapvaal Craton is confirmed by the previous shear wave velocity model by (Fadel et al., 2020). The Kheis Belt has low shear wave velocity, the Rehoboth has intermediate shear wave velocity, while the Kaapvaal Craton has high shear velocity.

The delineation of the terranes from the results of this cross-section (Figure 4.11, cross-section A-A') is quite similar to the results published by Muller et al. (2009) from the same profile (Figure 2.4). However, there exist some differences. Muller et al. (2009) carried out the electrical conductivity modelling of this profile in 2-D. Their data decomposition analysis showed the presence of multiple strike directions, which confirms the 3-D nature of the structure captured in the data. The challenge with multiple geoelectric strike directions and the uncertainty based on the assumptions required for the 2-D inversion can be overcome by modelling the data in 3-D. In this study, the data was inverted in 3-D and the result presented shows better recovery of the electrical conductivity structures along this profile. The results from Muller et al. (2009) could not recover the structure of the Rehoboth Province effectively. From their results (Figure 2.4), the 2-D model with an assigned strike direction of 25° seemed to image the Rehoboth Province better in terms of positioning of the structure and the resistivity value when compared with the model with assigned 45° strike direction. However, the model from both the 25° and 45° strike direction interpretations are not consistent with the velocity models of Fadel et al. (2020) and Ortiz et al. (2019). Due to the robustness of 3-D inversion and no directionality assumptions required to model the electrical structure of the subsurface, the interpretation from this 3-D electrical conductivity model is preferred in this scenario.

Another major difference between the 2-D conductivity models of Muller et al. (2009) and the new 3-D electrical model is the small low resistivity blobs in the 2-D models beneath the Rehoboth Province. The blobs occur in dissimilar forms and at different depths in the 2-D model with an assigned strike direction of 25° and the model with an assigned strike direction of 45°. The low resistivity blobs could be because of dimensionality distortion in the 2-D interpretations with different assumptions on the geoelectric strike directions. In the 3-D electrical conductivity model (Figure 4.11, cross-section A-A'), the Rehoboth Province is more reliably defined as a resistive structure (approximately 1,000  $\Omega\text{m}$ ) with a lateral extent of about 120 km compared to Muller et al. (2009). This again validates the need to avoid dimensionality distortion in MT data modelling (discussed in subsection 3.1.4) by ensuring that the modelling approach has the same dimensionality as the dimensionality captured in the MT data. For example, 2-D interpretation of a 3-D structure would cause erroneous interpretations (Ledo, 2005; Ledo et al., 2002).

### **Okwa Block-Kaapvaal Craton-The Bushveld Complex**

To further image the terranes in southwest Botswana, another cross-section C-C' across Okwa Block and the Kaapvaal Craton is shown in Figure 4.11. From the result, the lithosphere beneath the Okwa Block (northwest of the cross-section C-C') is moderately resistive with an approximate resistivity of 1,000  $\Omega\text{m}$ . There is also a conductive structure beneath the Okwa Block. The Okwa Block is a zone of weakness that

has experienced significant deformation, such as accretion and reworking (Begg et al., 2009). The weakness in this zone explains the observed intermediate resistivity from the electrical conductivity model. The Okwa-Kheis Belt was affected by metamorphism between 2.0 - 2.06 Ga (Begg et al., 2009). The time correlation between this event and the emplacement of the Bushveld complex (2.06-2.05 Ga) suggests a possibility that the two events are linked together.

The Kaapvaal Craton is imaged in the southeast of the profile as a very resistive structure ( $\sim 10,000 \Omega\text{m}$ ). Another major feature imaged in the cross-section C-C' (Figure 4.11) is a highly conductive structure beneath the southeast end of the cross-section. The possible interpretation of this high conductivity structure is the Bushveld Complex magmatic intrusion into the Kaapvaal Craton.

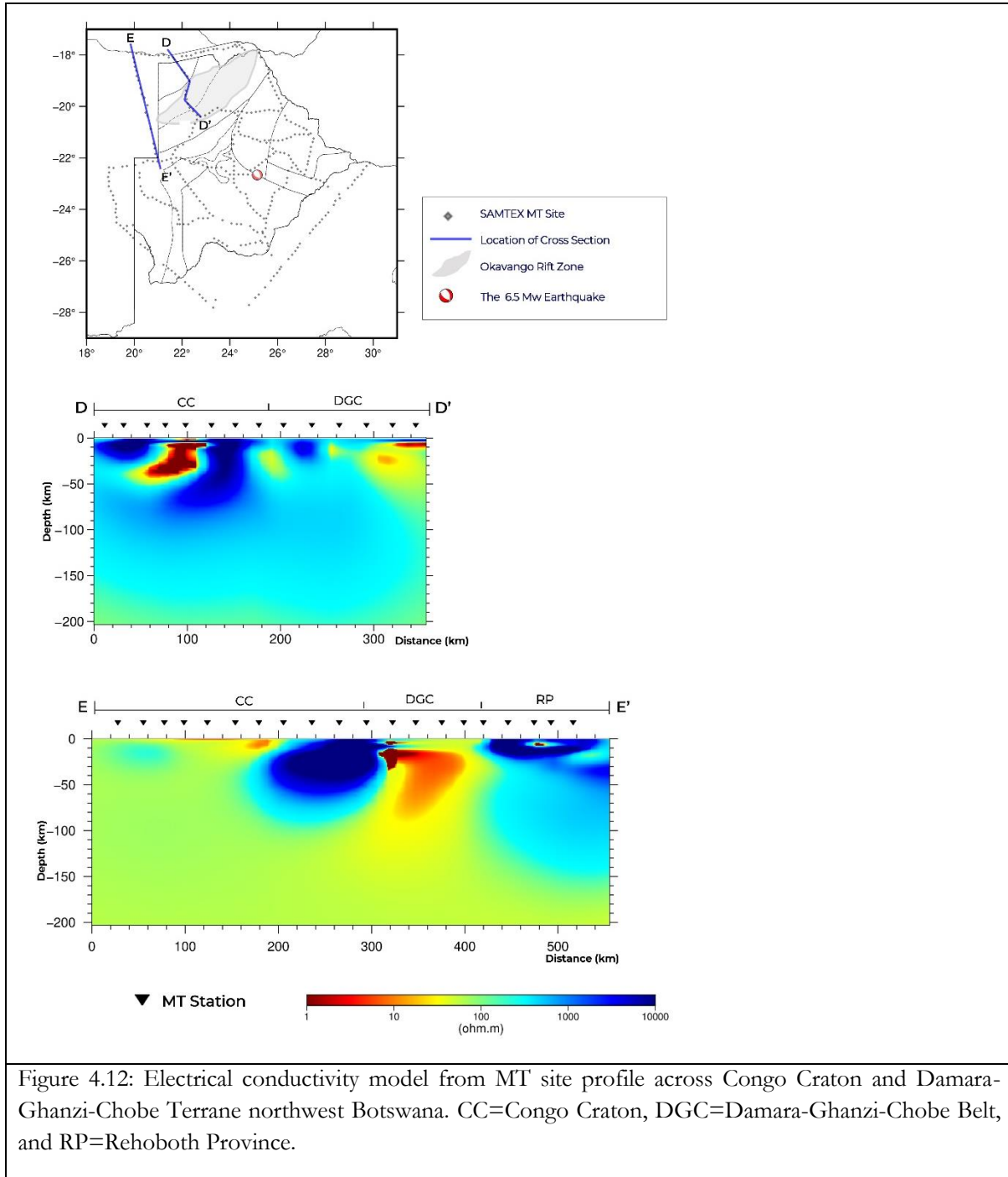
The Bushveld Complex is the most extensive layered mafic intrusion into the crust in the world (Begg et al., 2009). The emplacement of the Bushveld Complex in the north-central part of the Kaapvaal Craton took place between 2.06-2.05 Ga (Begg et al., 2009; Haddon, 2005). Fouch et al. (2004), in a seismic study, observed low seismic wave velocities in the Bushveld Complex and linked it to compositional changes in the mantle due to iron enrichment from the formation of the Bushveld Complex. Similarly, other seismic investigations, including the P and S wave velocity study by Ortiz et al. (2019) and the shear-wave velocity study by White-Gaynor et al. (2021), revealed a region of low velocities beneath the Bushveld Complex in the Kaapvaal Craton. Ortiz et al. (2019), supporting Fouch et al. (2004), argued that the low velocities anomalies observed beneath the Okwa Block, Magondi Belt and Limpopo Belt, which are extensions of the Bushveld Complex, are results of the modification of the composition of the mantle material from the magmatic event. Ortiz et al. (2019) ruled out the possibilities of thermal anomalies as the explanation of these low-velocity anomalies since no tectonic event affected these terranes in the Phanerozoic age.

In a previous MT study across the Kaapvaal Craton, Evans et al. (2011) found an extremely high electrical conductivity structure in the Bushveld Complex (Figure A1 in Appendix 1). From their MT study, Evans et al. (2011) suggest that connected metallic sulphides, iron-rich garnets, and other economic minerals form the network of conductors within the Bushveld Complex. This is similar to the proposition of Jones and Garcia (2006) for the high conductivity anomalies beneath the Yellowknife River Fault zone in the Slave Craton in northern Canada.

At the depth in the upper mantle ( $\sim 70 \text{ km}$ ) where the conductive structure occurs in the electrical model (Figure 4.11, cross-section C-C'), the temperature range predicted is between  $500 - 600^\circ \text{C}$  from heat flow data (Jones, 1988). This temperature range is similar for all the Kaapvaal Craton at this depth (Jones, 1988). Also, the last thermal event in the emplacement of the Bushveld Complex occurred in the Archean (Begg et al., 2009; Rob L. Evans et al., 2011). With these pieces of evidence, this study, supporting the interpretation of Fouch et al. (2004), attributes the compositional change of the mantle material due to iron enrichment as the cause of high conductivity structure in the Bushveld Complex.

### **Congo Craton-Damara-Ghanzi-Chobe Belt**

Figure 4.12 shows the electrical conductivity model along cross-section D-D' in northwest Botswana. From the result, there exists a highly resistive and thick structure in the northwest of the profile. This structure has a cratonic signature, and it is interpreted as an extension of the Congo Craton. Next to this is a relatively conductive crustal structure, which is interpreted as the Damara-Ghanzi-Chobe Belt (DGC). Similarly, another cross-section E-E' taken in northwest Botswana (Figure 4.12) revealed the cratonic structure of Congo Craton and the high conductivity anomaly that corresponds to the DGC.



The region of northwest Botswana has thick Kalahari overburden that hinders the study of the basement rocks due to poor exposure. An earlier geological study of the terrane in northwest Botswana suggested that the lithosphere in this region is an extension of the Damara Belt from the few mapped outcrops (Key & Ayres, 2000). However, with the use of geophysical data, it is possible to image the Earth subsurface structure beneath the thick sediment cover. The result of this 3-D electrical conductivity model (Figure 4.12) shows an extension of the Congo Craton into the northwest tip of Botswana. The results of the electrical conductivity model of this study are consistent with an earlier MT study by Khoza et al. (2013) in delineating the Congo Craton extension into northwest Botswana (Figure 2.7). This result from the electrical model is confirmed by the recent seismic models by Fadel et al. (2020), which shows high-velocity anomaly, and the model of Yu et al. (2017), which shows high P and S wave signature in northwest Botswana. This high

seismic wave velocity, which is indicative of cratonic signature, is interpreted as an extension of the Congo Craton.

The DGC, which includes the ORZ, is a zone of weakness owing to past collision and reactivation processes. The structure of the DGC in the 3-D electrical model was imaged as a conductive structure (average of 50  $\Omega\text{m}$ ) (Figure 4.12). Previously imaged sections of DGC using MT data in northwest Botswana by Khoza et al. (2013) and in northeast Botswana by Miensopust et al. (2011) confirmed high conductivity structure within the DGC. The observation from the electrical conductivity model within the DGC is confirmed by previous seismic studies, which observed low velocities beneath the DGC and ORZ (Fadel et al., 2020; Ortiz et al., 2019; White-Gaynor et al., 2021).

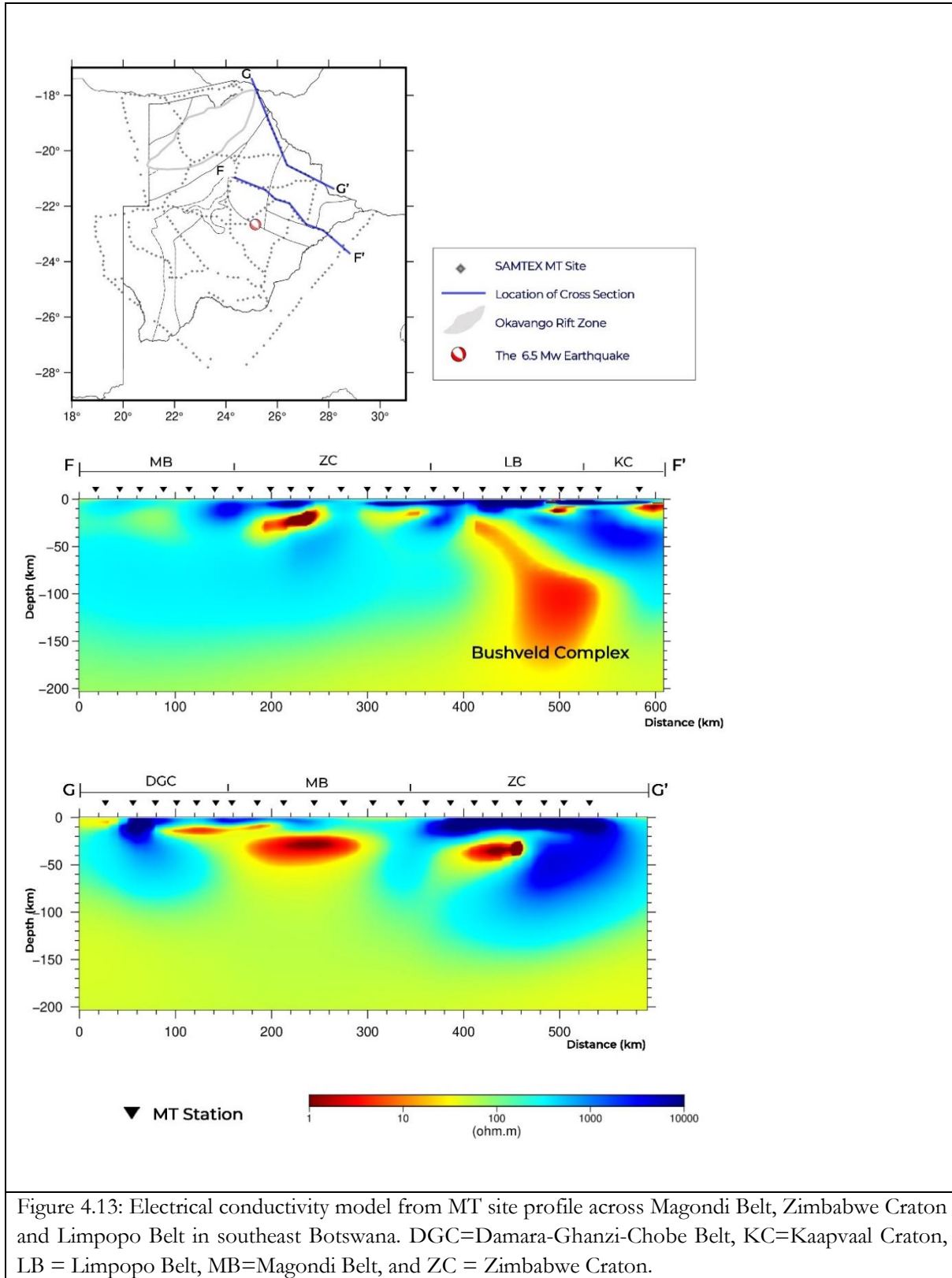
The well imaged conductive structure beneath the DGC from the new 3-D conductivity model, which also corresponds to low-velocity anomalies from seismic models, still need to be understood in terms of the cause of the structure. The DGC includes the ORZ, which is an important tectonic domain in Botswana due to the incipient rifting that is believed to be taking place in the ORZ. Understanding the cause of the conductive structure beneath this zone has implications on the understanding of the tectonic of the area as discussed next.

Khoza et al. (2013) argued that the combination of interconnected graphite and sulfide mineralization formed from the collision between the Congo and Kalahari Cratons is the most suitable explanation for the high conductivity structure beneath the DGC. On the contrary, Yu et al. (2016) attributed the structure beneath the DGC to the thermal anomaly related to the incipient rifting in the ORZ and not lithospheric thickness changes at the edge of the adjacent Kalahari Craton. In another view, Ortiz et al. (2019) suggest that the combination of thermal anomaly from rifting process in ORZ and thinning of the off-craton lithosphere beneath the DGC contribute to the low velocity/high conductivity structure. Following the interpretation of Ortiz et al. (2019), this study suggests that thermal anomalies from the incipient rifting in ORZ is the most probable cause of the high conductivity structure beneath the DGC.

### **Magondi Belt-Zimbabwe Craton-Limpopo Belt**

Figure 4.13 presents electrical conductivity model cross-sections across the Magondi Belt, Zimbabwe Craton and the Limpopo Belt. The Zimbabwe Craton is imaged as a highly resistive structure in cross-section F-F'. The Zimbabwe Craton is also well imaged in cross-section G-G' (Figure 4.13) as a highly resistive structure. The observed high resistivity structure of the Zimbabwe Craton is consistent with results from seismic models. There is a region of high-velocity anomalies beneath the Zimbabwe Craton (Fadel et al., 2020; Ortiz et al., 2019; White-Gaynor et al., 2021).

In the central part of the cross-section G-G' (Figure 4.13), the lithosphere beneath the Magondi Belt is imaged as a conductive structure. Miensopust et al. (2011), in a previous MT study in northeast Botswana, observed crustal conductors beneath the Magondi Belt. The previous deformation and reworking processes on the lithosphere beneath the Magondi Belt explain the very high conductivity values observed from the electrical model. The Magondi belt was accreted to the Kheis-Okwa Belt during the Eburnean Orogeny (Thomas et al., 1993), and the Kheis-Okwa-Magondi Belt composite was modified by the Bushveld event.



The Limpopo Belt is imaged as a moderately resistive structure (Figure 4.13, cross-section F-F'). The low resistivity region below the Limpopo Belt reflects the deformation that the zone has undergone, owing to the collision between the Kaapvaal and Zimbabwe Craton and other events such as the Bushveld Complex magmatic event. This observation is consistent with results from seismic studies. There is a region of low

velocity beneath the Limpopo Belt (Ortiz et al., 2019). Ortiz et al. (2019) support that this region of low velocity resulted from modification of the lithospheric and the mantle material by the Bushveld Complex magmatic event. Khoza et al. (2012), in an MT study, proposed a tectonic model of the evolution of the Limpopo Belt. According to Khoza et al. (2012), the Limpopo Belt has undergone a sequence of events; (1) subduction of oceanic lithosphere beneath the southern part of the Zimbabwe Craton between 2.7 – 2.6 Ga, (2) collision between the Kaapvaal and the Zimbabwe Craton, (3) transpression as a result of the movement of the Zimbabwe Craton relative to the Kaapvaal Craton (2.02 – 2.04 Ga), and (4) uplift as a result of Bushveld magmatic event (1.95 - 2.03 Ga).

#### **4.3.4. The Maltahohe Microcraton – Okavango Rift Zone – East African Rift System**

The structure beneath the Rehoboth Province in southwest Botswana, the ORZ, and the EARS in Botswana are the main tectonic domains that the second, third, and fourth objectives this study aims to investigate. Three cross-sections were taken to investigate the crust and upper mantle beneath these focus tectonic domains. The choices of the cross-section locations along or near the MT data sites were made to address the shortcoming of small horizontal adjustment length and make the interpretation of the models reliable. The results of the electrical conductivity model across these structures are presented in cross-sections H-H', I-I', and J-J' in Figure 4.14.

##### **4.3.4.1. The Maltahohe Microcraton**

To investigate the subsurface electrical structure in the area that correspond to the suggested location of the MC in southwest Botswana, a cross-section was taken across the area (cross-section H-H' in Figure 4.14). From the cross-section, the Kaapvaal craton is imaged as a highly resistive structure (approximately 10,000  $\Omega\text{m}$ ). There is a relatively conductive mantle structure beneath the Kaapvaal Craton, interpreted as the Bushveld Complex, as discussed previously. Also, the Kheis Belt is imaged next to the Kaapvaal Craton as a relatively less resistive and thin lithosphere. In the western part of the cross-section, the result shows a resistive structure with average resistivity of 1,000  $\Omega\text{m}$  beneath the Rehoboth Province between 30 km to 100 km depth. This signature is indicative of a cratonic composition. This structure may be interpreted as the MC. The MC structure in the model is resolved by multiple stations. There are three MT stations, which have depth sensitivities of 100 km, 120 km and 150 km (Figure 4.1) directly above the imaged resistive structure of the MC (Figure 4.14). This makes the interpretation of the MC structure reliable.

The result of the 3-D electrical model on the existence of the MC is confirmed by previous studies (e.g., Begg et al., 2009; Chisenga, Jianguo, et al., 2020; Fadel et al., 2020). Fadel et al. (2020), from their 3-D shear wave velocity study, observed a positive shear wave velocity in southwest Botswana beneath the Rehoboth Province between the depths of 50 km – 200 km, which is interpreted as the MC. The depth range of occurrence of the MC from the study by Fadel et al. (2020) is not consistent with the depth range (30 km – 100 km) resolved for the microcraton in the electrical conductivity model. Due to the low MT site coverage in the east of the imaged MC structure, the electrical model has a low spatial resolution in that area. Also, the intermediate depth of penetration of the three MT sites above the MC structure (100 km, 120 km, and 150 km) could limit the further imaging of the structure to deeper depths.

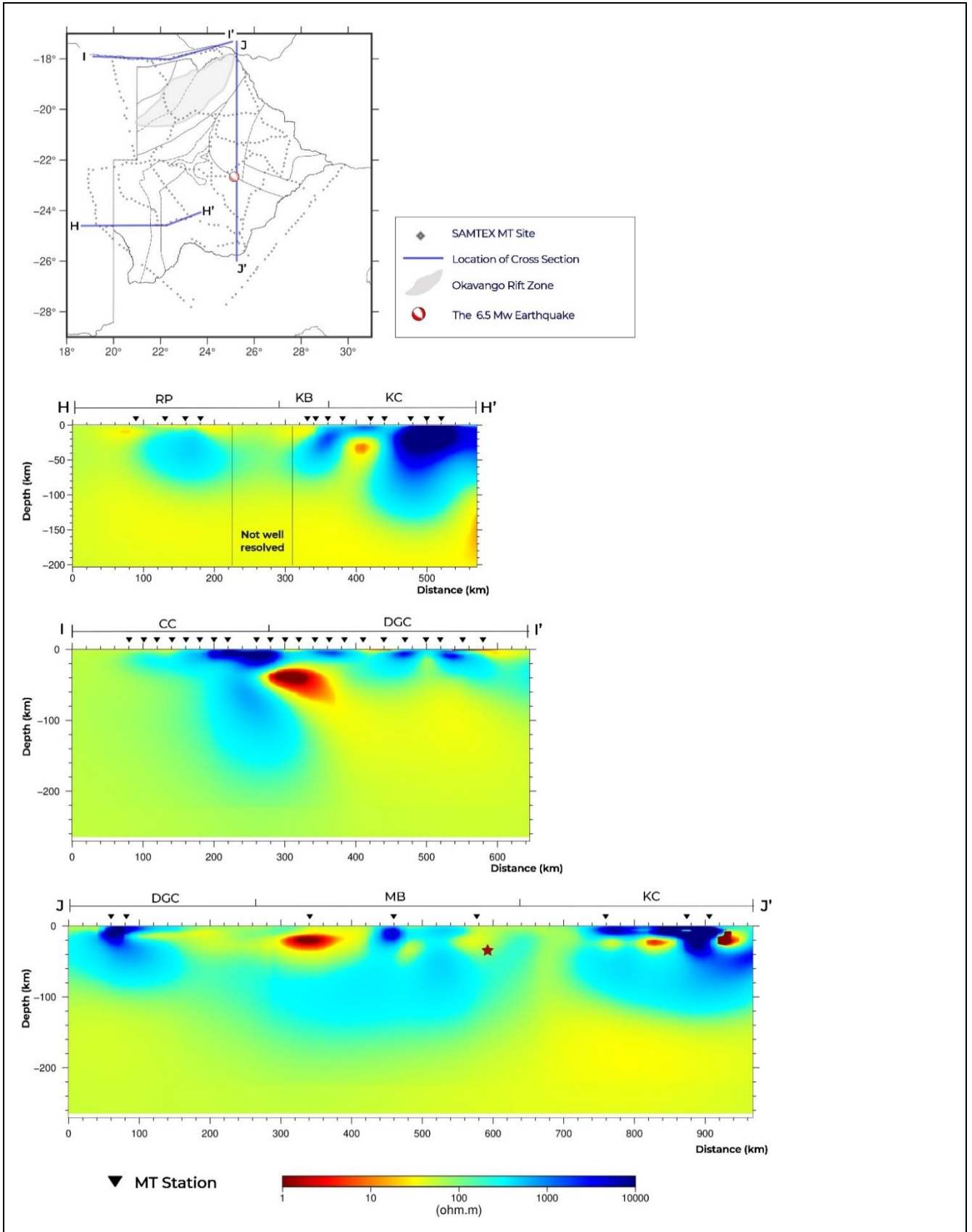


Figure 4.14: Electrical conductivity model cross-sections across southwest Botswana, ORZ, and Central Botswana. The red star = location of the 6.5 Mw earthquake in Central Botswana. CC=Congo Craton, DGC=Damara-Ghanzi-Chobe Belt, KC=Kaapvaal Craton, KB=Kheis Belt, MB=Magondi Belt, and RP=Rehoboth Province.

In an earlier active deep seismic study in southwest Botswana, Wright and Hall (1990) suggested that the cratonic structure beneath the Rehoboth Province is a thinned western extension of the Kaapvaal Craton. However, this interpretation by Wright & Hall (1990) is not consistent with the results from the new 3-D electrical conductivity model and recent seismic study by Fadel et al. (2020). While the electrical conductivity model of this study reveals a resistive cratonic structure beneath the Rehoboth Province, which is interpreted as the MC, it does not show a connection of the structure to the Kaapvaal Craton. The Kheis Belt is imaged as a relatively less resistive structure, which separates the MC from the Kaapvaal Craton. Similarly, the structure of the MC in the A-A' cross-section (Figure 4.11) is clearly imaged as a separate cratonic unit from the adjacent Kaapvaal Craton. The preferred interpretation of this study is that the MC is a separate cratonic structure from the Kaapvaal Craton. This interpretation of a separate MC from the electrical conductivity model is consistent with the results from the shear wave velocity model by Fadel et al. (2020).

The improved methodological approach of this study helped to investigate the MC better as compared to the previous MT study by Muller et al. (2009). The 3-D MT modelling approach prevents dimensionality distortion in the interpretation of the electrical model and also recovered the structure beneath the Rehoboth Province better as compared to the previous 2-D modelling by Muller et al. (2009).

#### 4.3.4.2. The Okavango Rift Zone and the East African Rift System

Figure 4.14 shows cross-section I-I' across the Congo Craton and DGC in northern Botswana. The cross-section reveals a distinctive high conductivity anomaly around the Okavango Rift Zone at depths corresponding to lower crust to upper mantle depth (30 km downward). In northeast Botswana, there exist a region of high conductivity from a depth of about 150 km and downward (east of the cross-section I-I').

The high conductive anomaly around the ORZ corresponds with the low-velocity anomaly revealed from the shear wave velocity study (Fadel et al., 2020), high  $V_p/V_s$  ratio revealed by receiver function studies (Fadel et al., 2018; Yu, Gao, et al., 2015) and shallow Curie depth from aeromagnetic data (Leseane et al., 2015). The result from the 3-D electrical conductivity model is consistent with the previously suggested hypothesis of hot fluids migration from the mantle into the crust through zones of weakness (e.g., suture zones associated with Damara-Ghanzi-Chobe orogeny) beneath the ORZ. According to Leseane et al. (2015) and references therein, it is suggested that the earthquakes in the ORZ are triggered by the migration of fluids from the mantle to the crust. The result of this study provides a piece of evidence for the role of ascending hot fluids, which leads to the weakening of the lithosphere, strain regime, and subsequent rifting in the ORZ.

There exist some contrary opinions on the mechanism of the incipient rifting in the ORZ (e.g., Khoza et al., 2013; and references therein). Khoza et al. (2013), in a previous MT study, argued that evidence of continental rifting such as thinned lithosphere and high conductivity mantle anomaly are not present in the ORZ. From their electrical conductivity model (OKA-WIN profile shown in Figure 2.7), Khoza et al. (2013) concluded that there is neither a thinned lithospheric structure nor high conductivity mantle anomalies beneath the ORZ. They go further to propose a model in which the incipient rifting in ORZ is initiated from the surface. However, at the northern end of imaged electrical conductivity model from their OKA-WIN profile (Figure 2.7), there exists a high conductivity signature that could indicate the presence of mantle anomaly. The limited spatial coverage of their model in this direction hindered further investigation of this anomaly. In the new 3-D electrical conductivity model, this area is well covered, and it reveals this high conductivity anomaly in the upper mantle clearly. The high conductivity structure continues downward up to a depth of about 200 km (Figure 4.14, cross-section I-I').

In the eastern end of the cross-section I-I' (Figure 4.14), there is a high conductivity anomaly revealed in the upper mantle. This highly conductive structure may be due to the EARS extension to northern Botswana. Also, it is observed that this high conductivity anomaly connects with the shallower high conductivity anomaly around the ORZ (Figure 4.14, cross-section I-I'). The southwestern branch of the EARS is often interpreted to have its terminus in northern Botswana by many previous studies (e.g., Fadel et al., 2020; Leseane et al., 2015; Modisi, 2000; Ortiz et al., 2019; Youqiang Yu, Gao, et al., 2015). Fadel et al. (2020), in a 3-D shear wave velocity modelling of Botswana, observed that the low-velocity anomaly beneath the ORZ seems to connect with a low-velocity anomaly in the mantle, which is interpreted as an expression of the EARS in northeast Botswana. The result of this 3-D electrical conductivity model supports the interpretation of the role of ascending fluids from the EARS in the rifting in the ORZ by Fadel et al. (2020) and Chisenga, Van der Meijde, et al. (2020).

The cross-section J-J' (Figure 4.14) cuts across geological terranes from northeast Botswana to the location of the 6.5 Mw earthquake in central Botswana and downward to southern Botswana. Due to the unavailability of closely spaced MT sites along the cross-section, the interpretation of the structures in areas that are not well resolved by MT sites cannot be relied on. However, at high depths approximately below 100 km, the MT response becomes more regional, and off MT data locations in the model can be reliably interpreted. From the result of the J-J' cross-section, at a location that corresponds to the 6.5 Mw earthquake, there exists a high conductivity anomaly at a depth of 30 km, which is resolved by at least one MT site. There is also a high conductivity anomaly in the northern part of this cross-section from the depth of about 100 km, which may be from the extension of the EARS to northern Botswana. Another feature of note is the conductive structure beneath the southern part of the cross-section from a depth of 120 km (beneath the Kaapvaal Craton), which may be due to the Bushveld magmatic emplacement. At a depth of about 200 km, the conductive structure in the northern part of the cross-section seems to connect to the further south conductive structure but not to the earthquake location. Again, the areas along this cross-section are sparsely covered by the MT sites, which reduces the spatial resolution possible along the cross-section. Consequently, the new 3-D electrical conductivity is not able to provide more insight into the connection between the EARS and the 6.5 Mw earthquake in central Botswana.

#### 4.4. Velocity-Conductivity Interpretation

In a recent seismic study, Fadel et al. (2020) presented a nationwide 3-D shear wave velocity model of Botswana. Their results included an investigation of important tectonic domains in Botswana, some of which were also considered in this study. In this section, a joint interpretation of the nationwide 3-D shear wave velocity model of Fadel et al. (2020) and the new 3-D electrical conductivity model is discussed. Figure 4.15 shows how the results of the 3-D shear wave velocity model compare with the new 3-D electrical conductivity model.

An east-west cross-section H-H' (Figure 4.15) across the southwest Botswana shows a separate high resistivity cratonic structure beneath the Rehoboth Province. This structure is similar to the interpreted high-velocity structure of the MC by Fadel et al. (2020) (cross-section HH-HH', Figure 4.15). However, in the unresolved section along the H-H' profile due to low MT site coverage, the conductivity model of this study could not image deeper sections of the supposed MC compared to the 3-D shear wave velocity model.

In the northern part of Botswana, to investigate the ORZ, cross-section I-I' (Figure 4.15b) was chosen along the MT site profile, where the resolution of the imaged electrical structure can be reliably interpreted. The I-I' cross-section is displaced to the north of the cross-section II-II' from the shear wave velocity model (Figure 4.15). However, the structures recovered from these two cross-sections are comparable. At the area

corresponding to the ORZ, there is a very high conductivity structure that connects to a deeper mantle high conductivity anomaly. The deeper high conductivity structure in northeast Botswana may be due to the extension of the EAR, which matches the last surface expression of the EARS rift lines (Figure 1.1). This interpretation is consistent with the shear wave velocity model across the ORZ, which shows a region of low velocity beneath the ORZ that seem to connect with a deeper low-velocity structure of the EARS in northeast Botswana (Fadel et al. 2020).

Cross-section JJ-JJ' (Figure 4.15a) in the shear wave velocity model shows a connection between a low-velocity anomaly beneath the area that corresponds to the epicentre of the 6.5 Mw earthquake and a deeper low-velocity anomaly that may be due to the EARS (Figure 4.15b). According to Fadel et al. (2020), the ascending fluids or melt from the EARS into the region below central Botswana may be the cause of the 6.5 Mw earthquake. To investigate the possible extension of the EARS into central Botswana, a cross-section J-J' was taken in the north-south direction in the electrical conductivity model (Figure 4.15b). The electrical conductivity model shows a region of high conductivity beneath the epicentre of the 6.5 Mw earthquake. The cross-section also reveals a high conductivity structure in the northern part of the cross-section, which may be due to the EARS extension in northeast Botswana. However, due to high spatial aliasing (poorly constrained features) because of low MT site cover along the cross-section, the electrical conductivity model of this study is not able to provide more insight into the connection between the EARS and the 6.5 Mw earthquake of 2017 in central Botswana.

From the shear wave velocity model (Figure 4.15a), the two main sedimentary basins in Botswana are clearly imaged. The Nosop Basin in the southwest and the Passarge Basin in central Botswana are distinctively imaged in the shear wave velocity model. However, the sedimentary basins are not clearly imaged in the electrical conductivity model (Figure 4.15b). This may be due to the large interstation spacings of the MT sites that do not allow for the high constraint of features that exist between the MT sites. At shallow depths, the horizontal adjustment length to which the MT data is sensitive is very small. Hence, near-surface features that are off the MT sites, such as the sedimentary basins are not well resolved in the new 3-D electrical model.

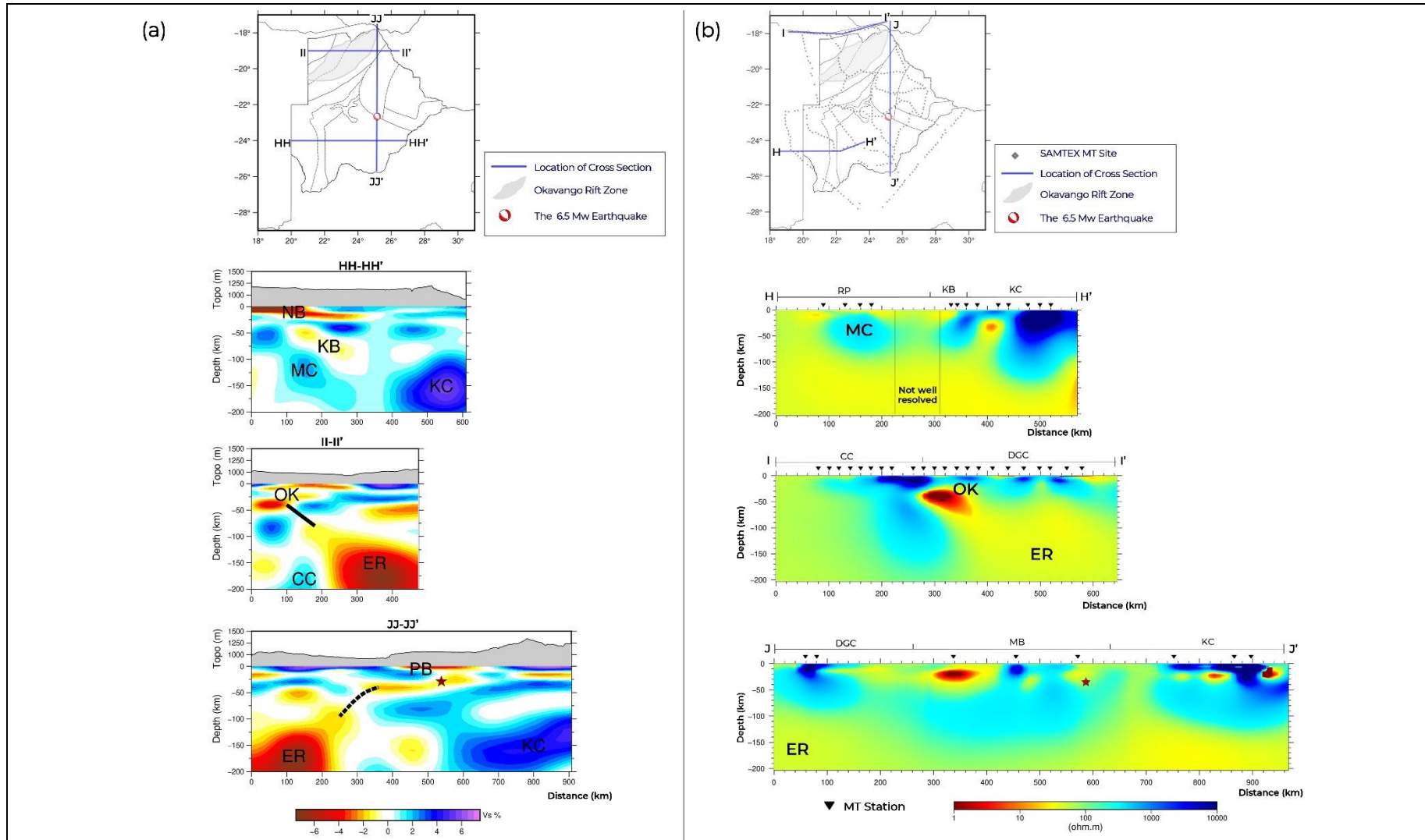


Figure 4.15: (a) The 3-D shear wave velocity model of Botswana after Fadel et al. (2020). (b) Electrical conductivity model derived from MT data. The red star = location of the 6.5 Mw earthquake in 2017. The cross-sections are shown in relative (left) and absolute (right) shear wave velocity. The highlighter features are; CC=Congo Craton, DGC=Damara-Ghanzi-Chobe Belt, ER = East African Rift System, KC=Kaapvaal Craton, KB=Kheis Belt, MB=Magondi Belt, MC = Maltahohe microcraton, NB = Nosop Basin, OK = Okavango Rift Zone, PB = Passarge Basin, and RP=Rehoboth Province.

## 5. CONCLUSION AND RECOMMENDATION

### 5.1. Conclusion

This study presents the first homogenous 3-D electrical model with an unprecedented spatial coverage over Botswana. The MT data used were corrected to remove distortions and errors to ensure high data quality, which consequently produced more accurate inversion results. Several inversions were done to explore the model space of the 3-D MT data inversion and determine appropriate inversion parameters. The study employed a robust 3-D modelling methodological scheme, which requires no assumption about the directionality of the subsurface structure. The results provide more straightforward, connected, and precise geologic interpretations about different arguments raised in the literature on the tectonics and structure of the crust and upper mantle beneath Botswana.

The result of this study highlights the main geologic terranes in Botswana, including the cratonic terranes - Congo, Kaapvaal, Zimbabwe Cratons and Rehoboth Province; and the mobile belts - Damara-Ghanz-Chobe, Limpopo, and Kheis-Okwa-Magondi Belts. Besides mapping these geologic terranes, this study provides an improved understanding of the current tectonic settings of Botswana and the deformation history. This study also presents the electrical conductivity model and interpretations on the existence of the MC and its connection with adjacent terranes in southwest Botswana for the first time using the MT data. Furthermore, the 3-D electrical conductivity model offers new insight into the incipient rifting process in the Okavango Rift Zone in northern Botswana, its link to the EARS. Finally, a joint velocity-conductivity interpretation of the structures beneath Botswana was done using the new 3-D electrical conductivity model and existing velocity model of Botswana. The joint interpretation validates findings and offers a more robust understanding of the geologic terrane and tectonic processes in Botswana from both MT and seismic data.

The results to investigate the research questions are:

1. What improvements does the nationwide 3-D electrical conductivity model from MT data add to the understanding of the geological provinces in Botswana?
  - The new nationwide 3-D electrical conductivity model offers precise imaging capability of the electrical structure of the Cratons and mobile belts in Botswana than previous 2-D electrical modelling efforts, which were limited by low spatial coverage and the need for assumption on the directionality of the subsurface structure.
2. Are there electrical structures that suggest the existence of the buried MC in southwest Botswana?
  - Yes, there exists a cratonic structure (resistive structure) beneath the Rehoboth Province in southwest Botswana that may be due to the MC structure.
3. If the presence of cratonic electrical structure is confirmed in southwest Botswana which suggests the existence of the buried MC, does it occur as a separate craton or as an extension of Kaapvaal Craton?
  - From the electrical conductivity model, the structure of the microcraton exists as a separate entity from the Kaapvaal Craton, with the Kheis Belt separating both terranes. This supports the interpretation that the MC is a separate cratonic structure from the Kaapvaal Craton.
4. Can the MT data with constraints from the available seismic models confirm or reject the hypothesis of rifting along the Okavango zone?
  - The 3-D electrical conductivity model reveals a high conductivity structure around the ORZ which seems to connect with a deeper high conductivity structure that may be due to the EARS' extension

- to northern Botswana. This gives a piece of evidence to the role of ascending hot fluids or melt, leading to weakening of the lithosphere and subsequent rifting in the ORZ.
5. Can the MT data, with constraints from the available seismic models, confirm or reject the hypothesis of rifting in central Botswana?
    - The 3-D electrical conductivity model showed a high conductivity structure beneath northeast Botswana, which is similar to the low-velocity structure from the shear wave velocity model. However, because of poor constrain of the electrical model due to lack of good MT site coverage, the results could not clearly verify the hypothesis of EARS extension to central Botswana.
  6. What is the role of the EARS in the 6.5Mw earthquake in central Botswana?
    - The 3-D electrical model could not establish the link between the high conductivity structures of the EARS in northern Botswana and central Botswana because of poor constrain of the model, which is due to sparse MT site distribution in the area.

The improvements in the understanding of the electrical structure of the crust and upper mantle beneath Botswana and the general southern Africa geodynamics from this study are significant contributions to the scientific community.

## 5.2. Research Limitations

The use of multiple 3-D inversion codes for MT data modelling is highly recommended for more reliable geologic interpretation of the resultant electrical conductivity models. However, only the ModEM 3-D inversion code was used, as it is available for use in academia (Egbert & Kelbert, 2012; Kelbert et al., 2014). Other known 3-D MT inversion codes are either very expensive to acquire or for private use only. The upside is that the ModEM is known as the most robust and widely used 3D MT inversion package both in academia and industry.

The 3-D modelling of MT data is computationally intensive and require high computational resources. The extensive spatial coverage of the 3-D electrical conductivity model of this study also makes the 3-D modelling computation more tedious and require more time. Also, several inversions with varying model parameters were required to explore the model space of the 3-D MT data inversion. Limited computational resources were available for this study, which makes large models run between tens of days to a couple of months (with up to 10 hours required per NLCG iteration in some cases). Also, several computational downtimes were experienced during this research. However, in the last quartile of this research work, access to the Dutch National Supercomputing Facilities, Cartesius, was granted (Grant Number: EINF-1468), which accelerated the computation of the 3-D electrical conductivity models and eventual successful completion of this study.

## 5.3. Recommendations

1. The velocity models of the crust and upper mantle structures are more robust, as MT data losses resolution with depth. The velocity models can be used as *a priori* information for constraining MT inversions. Constrained MT data inversion using velocity models would help reduce the unrealism and non-uniqueness of the geologic interpretation of the electrical model.
2. Whilst this study achieved a joint velocity-conductivity interpretation of the structure of the crust and upper mantle beneath Botswana, there is yet a need for joint inversion of MT and seismological data. Joint MT and seismological data inversion could be the focus of future research on the crust and upper mantle beneath Botswana.

## LIST OF REFERENCES

---

- Avdeev, D. B. (2005). Three-dimensional electromagnetic modelling and inversion from theory to application. In *Surveys in Geophysics* (Vol. 26). <https://doi.org/10.1007/s10712-005-1836-x>
- Bahr, K. (1988). Interpretation of the magnetotelluric impedance tensor: regional induction and local telluric distortion. *Journal of Geophysics - Zeitschrift Fur Geophysik*, 62(2), 119–127.
- Bahr, Karsten. (1991). Geological noise in magnetotelluric data: a classification of distortion types. *Physics of the Earth and Planetary Interiors*, 66(1–2), 24–38. [https://doi.org/10.1016/0031-9201\(91\)90101-M](https://doi.org/10.1016/0031-9201(91)90101-M)
- Becken, M., & Burkhardt, H. (2004). An ellipticity criterion in magnetotelluric tensor analysis. *Geophysical Journal International*, 159(1), 69–82. <https://doi.org/10.1111/j.1365-246X.2004.02376.x>
- Becken, M., Ritter, O., & Burkhardt, H. (2008). Mode separation of magnetotelluric responses in three-dimensional environments. *Geophysical Journal International*, 172(1), 67–86. <https://doi.org/10.1111/j.1365-246X.2007.03612.x>
- Becken, M., Ritter, O., Park, S. K., Bedrosian, P. A., Weckmann, U., & Weber, M. (2008). A deep crustal fluid channel into the San Andreas Fault system near Parkfield, California. *Geophysical Journal International*, 173(2), 718–732. <https://doi.org/10.1111/j.1365-246X.2008.03754.x>
- Becken, Michael, & Ritter, O. (2012). Magnetotelluric Studies at the San Andreas Fault Zone: Implications for the Role of Fluids. *Surveys in Geophysics*, 33(1), 65–105. <https://doi.org/10.1007/s10712-011-9144-0>
- Begg, G. C., Griffin, W. L., Natapov, L. M., O'Reilly, S. Y., Grand, S. P., O'Neill, C. J., ... Bowden, P. (2009). The lithospheric architecture of Africa: Seismic tomography, mantle petrology, and tectonic evolution. *Geosphere*, 5(1), 23–50. <https://doi.org/10.1130/GES00179.1>
- Bibby, H. M., Caldwell, T. G., & Brown, C. (2005). Determinable and non-determinable parameters of galvanic distortion in magnetotellurics. *Geophysical Journal International*, 163(3), 915–930. <https://doi.org/10.1111/j.1365-246X.2005.02779.x>
- Booker, J. R. (2014). The Magnetotelluric Phase Tensor: A Critical Review. *Surveys in Geophysics*, 35(1), 7–40. <https://doi.org/10.1007/s10712-013-9234-2>
- Brandt, M. B. C., Grand, S. P., Nyblade, A. A., & Dirks, P. H. G. M. (2011). Upper mantle seismic structure beneath Southern Africa : constraints on the buoyancy supporting the African superswell. *Pure and Applied Geophysics*, (March). <https://doi.org/10.1007/s00024-011-0361-8>
- Cagniard, L. (1953). Basic theory of the magnetotelluric method of geophysical prospecting. *Geophysics*, 605–635.
- Caldwell, T. G., Bibby, H. M., & Brown, C. (2004). The magnetotelluric phase tensor. *Geophysical Journal International*, 158(2), 457–469. <https://doi.org/10.1111/j.1365-246X.2004.02281.x>
- Company, J., Jones, A. G., Rath, V., Vozar, J., & Meqbel, N. (2016). The advantages of complementing MT profiles in 3-D environments with geomagnetic transfer function and interstation horizontal magnetic transfer function data : results from a synthetic case study. *Geophysical Journal International*, 1818–1836. <https://doi.org/10.1093/gji/ggw357>
- Carlson, R. W., Grove, T. L., De Wit, M. J., & Gurney, J. J. (1996). Program to study crust and mantle of the Archean craton in southern Africa. *Eos, Transaction, American Geophysical Union*, 77(29), 273–277. <https://doi.org/10.1029/96eo00194>
- Chave, A. D., & Jones, A. G. (2012). The magnetotelluric method: Theory and practice. In *The Magnetotelluric Method: Theory and Practice*. <https://doi.org/doi:10.1017/CBO9781139020138.004>
- Cherevatova, M., Smirnov, M. Y., Jones, A. G., Pedersen, L. B., Becken, M., Biolik, M., ... Smirnov, M. (2015). Magnetotelluric array data analysis from north-west Fennoscandia. *Tectonophysics*, 653, 1–19. <https://doi.org/10.1016/j.tecto.2014.12.023>
- Chisenga, C., Jianguo, Y., Fadel, I., Meijde, M. van der, & Atekwana, E. A. (2020). Updated tectonic terrane boundaries of Botswana determined from gravity and aeromagnetic data. *Episodes, Journal of International Geosciences*, 1–15. <https://doi.org/10.18814/epiugs/2020/020054>
- Chisenga, C., Van der Meijde, M., Yan, J., Fadel, I., Atekwana, E. A., Steffen, R., & Ramotoroko, C. (2020). Gravity derived crustal thickness model of Botswana: Its implication for the Mw 6.5 April 3, 2017, Botswana earthquake. *Tectonophysics*, 787(May). <https://doi.org/10.1016/j.tecto.2020.228479>
- Chorowicz, J. (2005). The East African rift system. *Journal of African Earth Sciences*, 43(1–3), 379–410. <https://doi.org/10.1016/j.jafrearsci.2005.07.019>
- Comeau, M. J., Becken, M., Käüfl, J. S., Grayver, A. V., Kuvshinov, A. V., Tserendug, S., ... Demberel, S.

- (2020). Evidence for terrane boundaries and suture zones across Southern Mongolia detected with a 2-dimensional magnetotelluric transect. *Earth, Planets and Space*, 72(1).  
<https://doi.org/10.1186/s40623-020-1131-6>
- Cooper, C. M., & Miller, M. S. (2014). Craton formation : Internal structure inherited from closing of the early oceans. *Lithosphere*, (February 2014). <https://doi.org/10.1130/L321.1>
- Corner, B., Durrheim, R. J., & Nicolaysen, L. O. (1990). Relationships between the Vredefort structure and the Witwatersrand basin within the tectonic framework of the Kaapvaal craton as interpreted from regional gravity and aeromagnetic data. *Tectonophysics*, 171(1–4), 49–61.  
[https://doi.org/10.1016/0040-1951\(90\)90089-Q](https://doi.org/10.1016/0040-1951(90)90089-Q)
- Dehkordi, B. H., Ferguson, I. J., Jones, A. G., Ledo, J., & Wennberg, G. (2019). Tectonics of the northern Canadian Cordillera imaged using modern magnetotelluric analysis. *Tectonophysics*, 765(May), 102–128.  
<https://doi.org/10.1016/j.tecto.2019.05.012>
- Delph, J. R., & Porter, R. C. (2015). Crustal structure beneath southern Africa: Insight into how tectonic events affect the Mohorovičić discontinuity. *Geophysical Journal International*, 200(1), 254–264.  
<https://doi.org/10.1093/gji/ggu376>
- Egbert, G. D., & Kelbert, A. (2012). Computational recipes for electromagnetic inverse problems. *Geophysical Journal International*, 189(1), 251–267. <https://doi.org/10.1111/j.1365-246X.2011.05347.x>
- Eglington, B. M., & Armstrong, R. A. (2004). The Kaapvaal Craton and adjacent orogens, southern Africa: A geochronological database and overview of the geological development of the craton. *South African Journal of Geology*, 107(1–2), 13–32. <https://doi.org/10.2113/107.1-2.13>
- Evans, R. L., Elsenbeck, J., Zhu, J., Abdelsalam, M. G., Sarafian, E., Mutamina, D., ... Jones, A. G. (2019). Structure of the Lithosphere Beneath the Barotse Basin, Western Zambia, From Magnetotelluric Data. *Tectonics*, 38(2), 666–686. <https://doi.org/10.1029/2018TC005246>
- Evans, Rob L., Jones, A. G., Garcia, X., Muller, M., Hamilton, M., Evans, S., ... Hutchins, D. (2011). Electrical lithosphere beneath the Kaapvaal craton, southern Africa. *Journal of Geophysical Research: Solid Earth*, 116(4), 1–16. <https://doi.org/10.1029/2010JB007883>
- Fadel, I. (2018). *Crustal and upper mantle structure of Botswana : is Botswana rifting?* (Faculty of Geoinformation Science and Earth Observation (ITC)-University of Twente).  
<https://doi.org/dx.doi.org/10.3990/1.9789036544641>
- Fadel, I., Paulssen, H., van der Meijde, M., Kwadiba, M., Ntibinyane, O., Nyblade, A., & Durrheim, R. (2020). Crustal and Upper Mantle Shear Wave Velocity Structure of Botswana: The 3 April 2017 Central Botswana Earthquake Linked to the East African Rift System. *Geophysical Research Letters*, 47(4). <https://doi.org/10.1029/2019GL085598>
- Fadel, I., van der Meijde, M., & Paulssen, H. (2018). Crustal Structure and Dynamics of Botswana. *Journal of Geophysical Research: Solid Earth*, 123(12), 10,659–10,671. <https://doi.org/10.1029/2018JB016190>
- Fouch, M. J., James, D. E., VanDecar, J. C., & van der Lee, S. (2004). Mantle seismic structure beneath the Kaapvaal and Zimbabwe Cratons. *South African Journal of Geology*, 107(1–2), 33–44.  
<https://doi.org/10.2113/107.1-2.33>
- Gao, S. S., Liu, K. H., Reed, C. A., Yu, Y., Massinque, B., Mdala, H., ... Reusch, A. M. (2013). Seismic Arrays to Study African Rift Initiation. *Eos, American Geophysical Union*, 94(24), 213–214.
- Gao, S. S., Silver, P. G., Liu, K. H., & Group, S. (2002). Mantle discontinuities beneath Southern Africa. *Geophysical Research Letters*, 29(10), 4–7.
- Gardonio, B., Jolivet, R., Calais, E., & Leclère, H. (2018). The April 2017 Mw6.5 Botswana Earthquake: An Intraplate Event Triggered by Deep Fluids. *Geophysical Research Letters*, 45(17), 8886–8896.  
<https://doi.org/10.1029/2018GL078297>
- Globig, J., Fernández, M., Vergés, J., Robert, A., & Faccenna, C. (2016). New insights into the crust and lithospheric mantle structure of Africa from elevation, geoid, and thermal analysis. *Journal of Geophysical Research: Solid Earth*, (Table 1), 5389–5424.  
<https://doi.org/10.1002/2016JB012972>.Received
- Groom, R. W., & Bailey, R. C. (1991). Analytic investigations of the effects of near-surface three-dimensional galvanic scatterers on MT tensor decompositions. *Geophysics*, 56(4), 496–518.  
<https://doi.org/10.1190/1.1443066>
- Groom, Ross W, & Bailey, R. C. (1989). Decomposition of magnetotelluric impedance tensors in the presence of local three-dimensional galvanic distortion. *Journal of Geophysical Research*, 94, 1913–1925.
- Haddon, I. G. (2005). The Sub-Kalahari Geology and Tectonic Evolution of the Kalahari Basin, Southern

- Africa. *PhD Thesis, Faculty of Science, University of the Witwatersrand, Johannesburg*, 1–360.
- Hamilton, M. P., Jones, A. G., Evans, R. L., Evans, S., Fourie, C. J. S., Garcia, X., ... Spratt, J. E. (2006). Electrical anisotropy of South African lithosphere compared with seismic anisotropy from shear-wave splitting analyses. *Physics of the Earth and Planetary Interiors*, 158(2–4), 226–239. <https://doi.org/10.1016/j.pepi.2006.03.027>
- Hansen, S. E., & Nyblade, A. A. (2013). The deep seismic structure of the Ethiopia / Afar hotspot and the African superplume. *Geophysical Journal International*, 118–124. <https://doi.org/10.1093/gji/ggt116>
- Hansen, S. E., Nyblade, A. A., & Benoit, M. H. (2012). Mantle structure beneath Africa and Arabia from adaptively parameterized P-wave tomography: Implications for the origin of Cenozoic Afro-Arabian tectonism. *Earth and Planetary Science Letters*, 319–320, 23–34. <https://doi.org/10.1016/j.epsl.2011.12.023>
- Hill, G. J., Caldwell, T. G., Heise, W., Chertkoff, D. G., Bibby, H. M., Burgess, M. K., ... Cas, R. A. F. (2009). Distribution of melt beneath Mount St Helens and Mount Adams inferred from magnetotelluric data. *Nature Geoscience*, 2(11), 785–789. <https://doi.org/10.1038/ngeo661>
- Hutchins, D. G., & Reeves, C. V. (1980). Regional geophysical exploration of the Kalahari in Botswana. *Test Tectonophysics*, 69(3–4), 201–220. [https://doi.org/10.1016/0040-1951\(80\)90211-5](https://doi.org/10.1016/0040-1951(80)90211-5)
- Jones, A.G., Evans, R. L., Muller, M. R., Hamilton, M. P., Miensopust, M. P., Garcia, X., ... Team, T. S. (2009). The SAMTEX Experiment: Overview and Preliminary Results. *11th SAGA Biennial Technical Meeting and Exhibition*. [https://doi.org/10.3997/2214-4609-pdb.241.jones\\_paper1](https://doi.org/10.3997/2214-4609-pdb.241.jones_paper1)
- Jones, Alan G., Fishwick, S., Evans, R. L., Muller, M. R., & Fullea, J. (2013). Velocity-conductivity relations for cratonic lithosphere and their application: Example of Southern Africa. *Geochemistry, Geophysics, Geosystems*, 14(4), 806–827. <https://doi.org/10.1002/ggge.20075>
- Jones, Alan G., & Garcia, X. (2006). Electrical resistivity structure of the Yellowknife River Fault zone and surrounding region. *Geological Association of Canada, Mineral Deposits Division*, 3(3), 126–141.
- Jones, Alan G., Ledo, J., & Ferguson, I. J. (2005). Electromagnetic images of the Trans-Hudson orogen: The North American Central Plains anomaly revealed. *Canadian Journal of Earth Sciences*, 42(4), 457–478. <https://doi.org/10.1139/e05-018>
- Jones, Alan G, Chave, A. D., Egbert, G., & Auld, D. O. N. (1989). A comparison of techniques for magnetotelluric response function estimation. *Journal of Geophysical Research*, 94, 201–213.
- Jones, Alan G, Evans, R. L., Muller, M. R., Hamilton, M. P., Miensopust, M. P., Garcia, X., ... Team, T. S. (2009). Area selection for diamonds using magnetotellurics: Examples from southern Africa. *LITHOS*, 112, 83–92. <https://doi.org/10.1016/j.lithos.2009.06.011>
- Jones, M. Q. W. (1988). Heat flow in the Witwatersrand basin and environs and its significance for the South African shield geotherm and lithosphere thickness. *Journal of Geophysical Research*, 93(B4), 3243–3260. <https://doi.org/10.1029/JB093iB04p03243>
- Kearey, P., Brooks, M., & Hill, I. (2002). *An introduction to geophysical exploration* (Third). Oxford, UK: Blackwell Science.
- Kebede, F., & Kulhánek, O. (1991). Recent seismicity of the East African Rift system. *Physics of the Earth and Planetary Interiors*, 68, 259–273.
- Kelbert, A., Meqbel, N., Egbert, G. D., & Tandon, K. (2014). ModEM: A modular system for inversion of electromagnetic geophysical data. *Computers and Geosciences*, 66, 40–53. <https://doi.org/10.1016/j.cageo.2014.01.010>
- Key, R. M., & Ayres, N. (2000). The 1998 edition of the National Geological Map of Botswana. *Journal of African Earth Sciences*, 30(3), 427–451. [https://doi.org/10.1016/S0899-5362\(00\)00030-0](https://doi.org/10.1016/S0899-5362(00)00030-0)
- Kgaswane, E. M., Rathod, G. W., & Saunders, I. (2018). Tectonic History of the Kaapvaal Craton: Constraints From Rheological Modeling. *Journal of Geophysical Research: Solid Earth*, 123(8), 6734–6768. <https://doi.org/10.1029/2018JB015631>
- Khoza, D., Jones, A. G., Muller, M. R., Evans, R. L., Webb, S. J., & Miensopust, M. (2012). Tectonic model of the Limpopo belt: constraints from magnetotelluric data. *Precambrian Research*, 226, 143–156. <https://doi.org/http://dx.doi.org/10.1016/j.precamres.2012.11.016>
- Khoza, D., Jones, A., Muller, M., Evans, R., Miensopust, M., & Webb, S. (2013). Lithospheric structure of an Archean craton and adjacent mobile belt revealed from 2-D and 3-D inversion of magnetotelluric data: Example from southern Congo craton in northern Namibia. *Journal of Geophysical Research: Solid Earth*, 118(8), 4378–4397. <https://doi.org/10.1002/jgrb.50258>
- Kinabo, B. D., Atekwana, E. A., Hogan, J. P., Modisi, M. P., Wheaton, D. D., & Kampunzu, A. B. (2007).

- Early structural development of the Okavango rift zone , NW Botswana. *Journal of African Earth Sciences*, 48, 125–136. <https://doi.org/10.1016/j.jafrearsci.2007.02.005>
- Kinabo, B. D., Hogan, J. P., Atekwana, E. A., Abdelsalam, M. G., & Modisi, M. P. (2008a). Fault growth and propagation during incipient continental rifting : insights from a combined aeromagnetic and Shuttle Radar Topography Mission digital elevation model investigation of the Okavango Rift Zone , northwest Botswana. *Tectonics*, 27, 1–16. <https://doi.org/10.1029/2007TC002154>
- Kinabo, B. D., Hogan, J. P., Atekwana, E. A., Abdelsalam, M. G., & Modisi, M. P. (2008b). Fault growth and propagation during incipient continental rifting: Insight from a combined aeromagnetic and Shuttle Radar Topography Mission digital elevation model investigation of the Okavango Rift Zone, northwest Botswana. *Tectonics*, 27(3), 1–16. <https://doi.org/10.1029/2007TC002154>
- Kirkby, A., Zhang, F., Peacock, J., Hassan, R., & Duan, J. (2019). The MTPy software package for magnetotelluric data analysis and visualisation. *Journal of Open Source Software*, 4(37), 1358. <https://doi.org/10.21105/joss.01358>
- Kolawole, F., Atekwana, E. A., Malloy, S., Stamps, D. S., Grandin, R., Abdelsalam, M. G., ... Shemang, E. M. (2017). Aeromagnetic, gravity, and Differential Interferometric Synthetic Aperture Radar analyses reveal the causative fault of the 3 April 2017 Mw 6.5 Moiyabana, Botswana, earthquake. *Geophysical Research Letters*, 44(17), 8837–8846. <https://doi.org/10.1002/2017GL074620>
- Krieger, L., & Peacock, J. R. (2014). MTPy: A Python toolbox for magnetotellurics. *Computers and Geosciences*, 72, 167–175. <https://doi.org/10.1016/j.cageo.2014.07.013>
- Le Pape, F., Jones, A. G., Vozar, J., & Wenbo, W. (2012). Penetration of crustal melt beyond the Kunlun Fault into northern Tibet. *Nature Geoscience*, 5(5), 330–335. <https://doi.org/10.1038/ngeo1449>
- Ledo, J. (2005). 2-D versus 3-D magnetotelluric data interpretation. *Surveys in Geophysics*, 26(5), 511–543. <https://doi.org/10.1007/s10712-005-1757-8>
- Ledo, J., Queralt, P., Martí, A., & Jones, A. G. (2002). Two-dimensional interpretation of three-dimensional magnetotelluric data: An example of limitations and resolution. *Geophysical Journal International*, 150(1), 127–139. <https://doi.org/10.1046/j.1365-246X.2002.01705.x>
- Lenardic, A. (2003). Longevity and stability of cratonic lithosphere : insights from numerical simulations of coupled mantle convection and continental tectonics. *Journal of Geophysical Research*, 108, 1–15. <https://doi.org/10.1029/2002JB001859>
- Leseane, K., Atekwana, E. A., Mickus, K. L., Abdelsalam, M. G., Shemang, E. M., & Atekwana, E. A. (2015). Thermal perturbations beneath the incipient Okavango Rift Zone, northwest Botswana. *Journal of Geophysical Research: Solid Earth*, 3782–3803. <https://doi.org/10.1002/2014JB011029>
- Luchs, T., Brey, G. P., Gerdes, A., & Höfer, H. E. (2013). The lithospheric mantle underneath the Gibeon Kimberlite field (Namibia): A mix of old and young components—Evidence from Lu-Hf and Sm-Nd isotope systematics. *Precambrian Research*, 231, 263–276. <https://doi.org/10.1016/j.precamres.2013.03.006>
- Mackie, R. L., Madden, T. R., & Wannamaker, P. E. (1993). Three-dimensional magnetotelluric modeling using difference equations - theory and comparisons to integral equation solutions. *Geophysics*, 58(2), 215–226. <https://doi.org/10.1190/1.1443407>
- Malservisi, R., Hugentobler, U., Wonnacott, R., & Hackl, M. (2013). How rigid is a rigid plate? Geodetic constraint from the TrigNet CGPS network, South Africa. *Geophysical Journal International*, 918–928. <https://doi.org/10.1093/gji/ggs081>
- McCourt, S., Armstrong, R. A., Jelsma, H., & Mapeo, R. B. M. (2013). New U-Pb SHRIMP ages from the Lubango region, SW Angola: Insights into the Palaeoproterozoic evolution of the Angolan Shield, southern Congo Craton, Africa. *Journal of the Geological Society*, 170(2), 353–363. <https://doi.org/10.1144/jgs2012-059>
- McNeice, G. W., & Jones, A. G. (2001). Multisite, multifrequency tensor decomposition of magnetotelluric data. *Geophysics*, 66(1), 158–173. <https://doi.org/10.1190/1.1444891>
- McPherron, R. L. (2005). Magnetic pulsations: Their sources and relation to solar wind and geomagnetic activity. *Surveys in Geophysics*, 26(5), 545–592. <https://doi.org/10.1007/s10712-005-1758-7>
- Meqbel, N. M., Egbert, G. D., Wannamaker, P. E., Kelbert, A., & Schultz, A. (2014). Deep electrical resistivity structure of the northwestern U.S. derived from 3-D inversion of USArray magnetotelluric data. *Earth and Planetary Science Letters*, 402(C), 290–304. <https://doi.org/10.1016/j.epsl.2013.12.026>
- Meqbel, N., Weckmann, U., Muñoz, G., & Ritter, O. (2016). Crustal metamorphic fluid flux beneath the Dead Sea Basin: Constraints from 2-D and 3-D magnetotelluric modelling. *Geophysical Journal*

- International*, 207(3), 1609–1629. <https://doi.org/10.1093/gji/ggw359>
- Midzi, V., Saunders, I., Manzunzu, B., Kwadiba, M. T., Jele, V., Mantsha, R., ... Zulu, B. S. (2018). The 03 April 2017 Botswana M6.5 earthquake: Preliminary results. *Journal of African Earth Sciences*, 143, 187–194. <https://doi.org/10.1016/j.jafrearsci.2018.03.027>
- Miensopust, M. P., Jones, A. G., Muller, M. R., Garcia, X., & Evans, R. L. (2011). Lithospheric structures and Precambrian terrane boundaries in northeastern Botswana revealed through magnetotelluric profiling as part of the Southern African Magnetotelluric Experiment. *Journal of Geophysical Research*, 116, 1–21. <https://doi.org/10.1029/2010JB007740>
- Miensopust, Marion P., Queralt, P., Jones, A. G., Avdeev, D., Avdeeva, A., Börner, R. U., ... Vozar, J. (2013). Magnetotelluric 3-D inversion—a review of two successful workshops on forward and inversion code testing and comparison. *Geophysical Journal International*, 193(3), 1216–1238. <https://doi.org/10.1093/gji/ggt066>
- Modisi, M. P. (2000). Fault system at the southeastern boundary of the Okavango Rift, Botswana. *Journal of African Earth Sciences*, 30(3), 569–578. [https://doi.org/10.1016/S0899-5362\(00\)00039-7](https://doi.org/10.1016/S0899-5362(00)00039-7)
- Modisi, M. P., Atekwana, E. A., Kampunzu, A. B., & Ngwisanyi, T. H. (2000). Rift kinematics during the incipient stages of continental extension: Evidence the nascent Okavango rift basin, Northwest Botswana. *Geology*, 28(10), 939–942. [https://doi.org/10.1130/0091-7613\(2000\)28<939:RKDTIS>2.0.CO;2](https://doi.org/10.1130/0091-7613(2000)28<939:RKDTIS>2.0.CO;2)
- Moorkamp, Jones, A. G., & Eaton, D. W. (2007). Joint inversion of teleseismic receiver functions and magnetotelluric data using a genetic algorithm: Are seismic velocities and electrical conductivities compatible? *Geophysical Research Letters*, 34(16), 3–7. <https://doi.org/10.1029/2007GL030519>
- Moorkamp, M., Fishwick, S., Walker, R. J., & Jones, A. G. (2019). Geophysical evidence for crustal and mantle weak zones controlling intra-plate seismicity – the 2017 Botswana earthquake sequence. *Earth and Planetary Science Letters*, 506, 175–183. <https://doi.org/10.1016/j.epsl.2018.10.048>
- Muller, M. R., Jones, A. G., Evans, R. L., Grütter, H. S., Hatton, C., Garcia, X., ... Wasborg, J. (2009). Lithospheric structure, evolution and diamond prospectivity of the Rehoboth Terrane and western Kaapvaal Craton, southern Africa: Constraints from broadband magnetotellurics. *Lithos*, 112, 93–105. <https://doi.org/10.1016/j.lithos.2009.06.023>
- Newman, G. A., & Alumbaugh, D. L. (2000). Three-dimensional magnetotelluric inversion using non-linear conjugate gradients. *Geophysical Journal International*, 140(2), 410–424. <https://doi.org/10.1046/j.1365-246X.2000.00007.x>
- Niblett, E. R., & Sayn-wittgenstein, C. (1960). Variation of electrical conductivity with depth by the magnetotelluric method. *Geophysics*.
- Nyblade, A., Dirks, P., Durrheim, R., Webb, S., Jones, M., Cooper, G., & Graham, G. (2008). AfricaArray: Developing a geosciences workforce for Africa’s natural resource sector. *The Leading Edge*, 27(10), 1358–1361. <https://doi.org/10.1190/1.2996547>
- Ortiz, K., Nyblade, A., Meijde, M. Van Der, Paulssen, H., Kwadiba, M., Ntibinyane, O., ... Homman, K. (2019). Upper mantle P and S wave Velocity structure of the Kalahari Craton and surrounding Proterozoic terranes, southern Africa Geophysical Research Letters. *Geophysical Research Letters*, 9509–9518. <https://doi.org/10.1029/2019GL084053>
- Panza, G. F., Peccerillo, A., Aoudia, A., & Farina, B. (2006). Geophysical and petrological modelling of the structure and composition of the crust and upper mantle in complex geodynamic settings: the Tyrrhenian sea and surroundings. *Earth Science Reviews*. <https://doi.org/10.1016/j.earscirev.2006.08.004>
- Parker, E. N. (1958). Dynamics of the interplanetary gas and magnetic fields. *American Astronomical Society*, 664–676.
- Pastier, A. M., Dauteuil, O., Murray-Hudson, M., Moreau, F., Walpersdorf, A., & Makati, K. (2017). Is the Okavango Delta the terminus of the East African Rift System? Towards a new geodynamic model: Geodetic study and geophysical review. *Tectonophysics*, 712–713, 469–481. <https://doi.org/10.1016/j.tecto.2017.05.035>
- Pretorius, D. A. (1984). *The Kalahari Foreland, its marginal troughs and overthrust belts, and the regional structure of Botswana*. Johannesburg, South Africa: University of Witwatersrand.
- Reeves, C. V. (1972). Rifting in the Kalahari? *Nature*, 95–96. <https://doi.org/10.1038/237095a0>
- Reeves, C. V., & Hutchins, D. G. (1982). A progress report on the geophysical exploration of the Kalahari in Botswana. *Geoexploration*, 20(3–4), 209–224. [https://doi.org/10.1016/0016-7142\(82\)90022-9](https://doi.org/10.1016/0016-7142(82)90022-9)

- Reilly, S. Y. O., & Griffin, W. L. (2006). *Imaging global chemical and thermal heterogeneity in the subcontinental lithospheric mantle with garnets and xenoliths: Geophysical implications*. 416, 289–309. <https://doi.org/10.1016/j.tecto.2005.11.014>
- Rikitake, T. (1946). Notes on the electromagnetic induction within the Earth. *Earthquake Research Institute*, 1–9.
- Ring, U. (2014). The East African rift system. *Austrian Journal of Earth Sciences*, 107/1, 132–146.
- Ritter, P., & Banks, R. J. (1998). Separation of local and regional information in distorted GDS response functions by hypothetical event analysis. *Geophysical Journal International*, 135(3), 923–942. <https://doi.org/10.1046/j.1365-246X.1998.t01-1-00674.x>
- Robertson, K., Thiel, S., & Meqbel, N. (2020). Quality over quantity: on workflow and model space exploration of 3D inversion of MT data. *Earth, Planets and Space*. <https://doi.org/10.1186/s40623-019-1125-4>
- Rodi, W. L., & Mackie, R. L. (2001). Nonlinear conjugate gradients algorithm for 1D magnetotelluric inversion. *Geophysics*, 53(6), 752–759. <https://doi.org/10.3969/j.issn.1000-1441.2014.06.017>
- Saria, E., Calais, E., Stamps, D. S., Delvaux, D., & Hartnady, C. J. H. (2014). Present-day kinematics of the East African Rift. *Journal of Geophysical Research: Solid Earth*, 3584–3600. <https://doi.org/10.1002/2013JB010901.Abstract>
- Schluter, T. (2008). *Geological atlas of Africa* (Vol. 53). Berlin, Germany: Springer.
- Schmitz, M. D., Bowring, S. A., de Wit, M. J., & Gartz, V. (2004). Subduction and terrane collision stabilize the western Kaapvaal craton tectosphere 2.9 billion years ago. *Earth and Planetary Science Letters*, 222(2), 363–376. <https://doi.org/10.1016/j.epsl.2004.03.036>
- Scholz, C. H., Koczyński, T. A., & Hutchins, D. G. (1976). Evidence for Incipient Rifting in Southern Africa. *Geophysical Journal of the Royal Astronomical Society*, 44(1), 135–144. <https://doi.org/10.1111/j.1365-246X.1976.tb00278.x>
- Simpson, F., & Bahr, K. (2005). *Practical magnetotellurics*. Cambridge, UK: Cambridge University Press.
- Singletary, S. J., Hanson, R. E., Martin, M. W., Crowley, J. L., Bowring, S. A., Key, R. M., ... Krol, M. A. (2003). Geochronology of basement rocks in the Kalahari Desert, Botswana, and implications for regional Proterozoic tectonics. *Precambrian Research*, 121(1–2), 47–71. [https://doi.org/10.1016/S0301-9268\(02\)00201-2](https://doi.org/10.1016/S0301-9268(02)00201-2)
- Smith, J. T. (1995). Understanding telluric distortion matrices. *Geophysical Journal International*, 122(1), 219–226. <https://doi.org/10.1111/j.1365-246X.1995.tb03549.x>
- Telford, W. M., Geldart, L. P., & Sheriff, R. E. (2004). *Applied Geophysics* (Second). Cambridge, UK: Cambridge University Press.
- Thomas, R. J., von Veh, M. W., & McCourt, S. (1993). The tectonic evolution of southern Africa: an overview. *Journal of African Earth Sciences*, 16(1–2), 5–24. [https://doi.org/10.1016/0899-5362\(93\)90159-N](https://doi.org/10.1016/0899-5362(93)90159-N)
- Tikhonov, A. N. (1950). On determining electrical characteristics of the deep layers of the Earth's crust. *Geophysical Institute Academy of Science*, 73(2), 295–297.
- Türkoğlu, E., Unsworth, M., Çağlar, İ., Tuncer, V., & Avşar, Ü. (2008). Lithospheric structure of the Arabia-Eurasia collision zone in eastern Anatolia: Magnetotelluric evidence for widespread weakening by fluids? *Geology*, 36(8), 619–622. <https://doi.org/10.1130/G24683A.1>
- Unsworth, M. (2010). Magnetotelluric studies of active continent-continent collisions. *Surveys in Geophysics*, 31(2), 137–161. <https://doi.org/10.1007/s10712-009-9086-y>
- Unsworth, M., & Rondenay, S. (2012). Mapping the distribution of fluids in the crust and lithospheric mantle utilizing geophysical methods. In D. E. Harlov & H. Austrheim (Eds.), *Metasomatism and the chemical transformation of rock, Lecture Notes in Earth System Sciences* (pp. 535–598). <https://doi.org/10.1007/978-3-642-28394-9>
- Van Schijndel, V., Cornell, D. H., Frei, D., Simonsen, S. L., & Whitehouse, M. J. (2014). Crustal evolution of the reboth province from archaean to mesoproterozoic times: Insights from the reboth basement inlier. *Precambrian Research*, 240, 22–36. <https://doi.org/10.1016/j.precamres.2013.10.014>
- Van Schijndel, V., Cornell, D. H., Hoffmann, K. H., & Frei, D. (2011). Three episodes of crustal development in the Rehoboth Province, Namibia. *Geological Society Special Publication*, 357(1), 27–47. <https://doi.org/10.1144/SP357.3>
- Vozoff, K. (1991). The magnetotelluric method. In M. N. Nabighian (Ed.), *Electromagnetic Methods in Applied Geophysics* (1st ed., pp. 641–712). <https://doi.org/10.1190/1.9781560802686.ch8>

- Wannamaker, P. E., Hasterok, D. P., Johnston, J. M., Stodt, J. A., Hall, D. B., Sodergren, T. L., ... Unsworth, M. J. (2008). Lithospheric dismemberment and magmatic processes of the Great Basin–Colorado Plateau transition, Utah, implied from magnetotellurics. *Geochemistry, Geophysics, Geosystems*, 9(5), 1–38. <https://doi.org/10.1029/2007GC001886>
- Weaver, J. T., Agarwal, A. K., & Lilley, F. E. M. (2000). Characterization of the magnetotelluric tensor in terms of its invariants. *Geophysical Journal International*, 141(2), 321–336. <https://doi.org/10.1046/j.1365-246X.2000.00089.x>
- Wei, W., Unsworth, M., Jones, A., Booker, J., Tan, H., Nelson, D., ... Roberts, B. (2001). Detection of widespread fluids in the Tibetan crust by magnetotelluric studies. *Science*, 292(5517), 716–718. <https://doi.org/10.1126/science.1010580>
- Wessel, P., Luis, J. F., Uieda, L., Scharroo, R., Wobbe, F., Smith, W. H. F., & Tian, D. (2019). The Generic Mapping Tools Version 6. *Geochemistry, Geophysics, Geosystems*, 20(11), 5556–5564. <https://doi.org/10.1029/2019GC008515>
- White-Gaynor, A. L., Nyblade, A. A., Durrheim, R. J., Raveloson, R., van der Meijde, M., Fadel, I., ... Sitali, M. (2021). Shear-Wave Velocity Structure of the Southern African Upper Mantle: Implications for Craton Structure and Plateau Uplift. *Geophysical Research Letters*, 48(7), 1–10. <https://doi.org/10.1029/2020GL091624>
- Wright, J. A., & Hall, J. (1990). Deep Seismic profiling in the Nosop Basin, Botswana: cratons, mobile belts and sedimentary basins. *Tectonophysics*, 173(1–4), 333–343. [https://doi.org/10.1016/0040-1951\(90\)90228-Z](https://doi.org/10.1016/0040-1951(90)90228-Z)
- Xue, S., Bai, D., Chen, Y., Ma, X., Chen, L., Li, X., & Yan, Y. (2019). Contrasting crustal deformation mechanisms in the Longmenshan and West Qinling orogenic belts, NE Tibet, revealed by magnetotelluric data. *Journal of Asian Earth Sciences*, 176, 120–128. <https://doi.org/10.1016/j.jseaes.2019.01.039>
- Youssof, M., Thybo, H., Artemieva, I. M., & Levander, A. (2015). Upper mantle structure beneath southern African cratons from seismic finite-frequency P- and S-body wave tomography. *Earth and Planetary Science Letters*, 420, 174–186. <https://doi.org/10.1016/j.epsl.2015.01.034>
- Yu, Y., Liu, K. H., Reed, C. A., Moidaki, M., Mickus, K., Atekwana, E. A., & Gao, S. S. (2015). A joint receiver function and gravity study of crustal structure beneath the incipient Okavango Rift, Botswana. *Geophysical Research Letters*, 42(20), 8398–8405. <https://doi.org/10.1002/2015GL065811>
- Yu, Youqiang, Gao, S. S., Moidaki, M., Reed, C. A., & Liu, K. H. (2015). Seismic anisotropy beneath the incipient Okavango rift: Implications for rifting initiation. *Earth and Planetary Science Letters*, 430, 1–8. <https://doi.org/10.1016/j.epsl.2015.08.009>
- Yu, Youqiang, Liu, K. H., Huang, Z., Zhao, D., Reed, C. A., Moidaki, M., ... Gao, S. S. (2016). Mantle structure beneath the incipient Okavango rift zone in southern Africa. *Geosphere*, 13(1), 102–111. <https://doi.org/10.1130/GES01331.1>
- Yu, Youqiang, Liu, K. H., Moidaki, M., Reed, C. A., & Gao, S. S. (2015). No thermal anomalies in the mantle transition zone beneath an incipient continental rift : evidence from the first receiver function study across the Okavango Rift Zone, Botswana. *Geophysical Journal International*, 1407–1418. <https://doi.org/10.1093/gji/ggv229>

# APPENDIX 1

## Electrical Conductivity Model across Kaapvaal Craton and Bushveld Complex

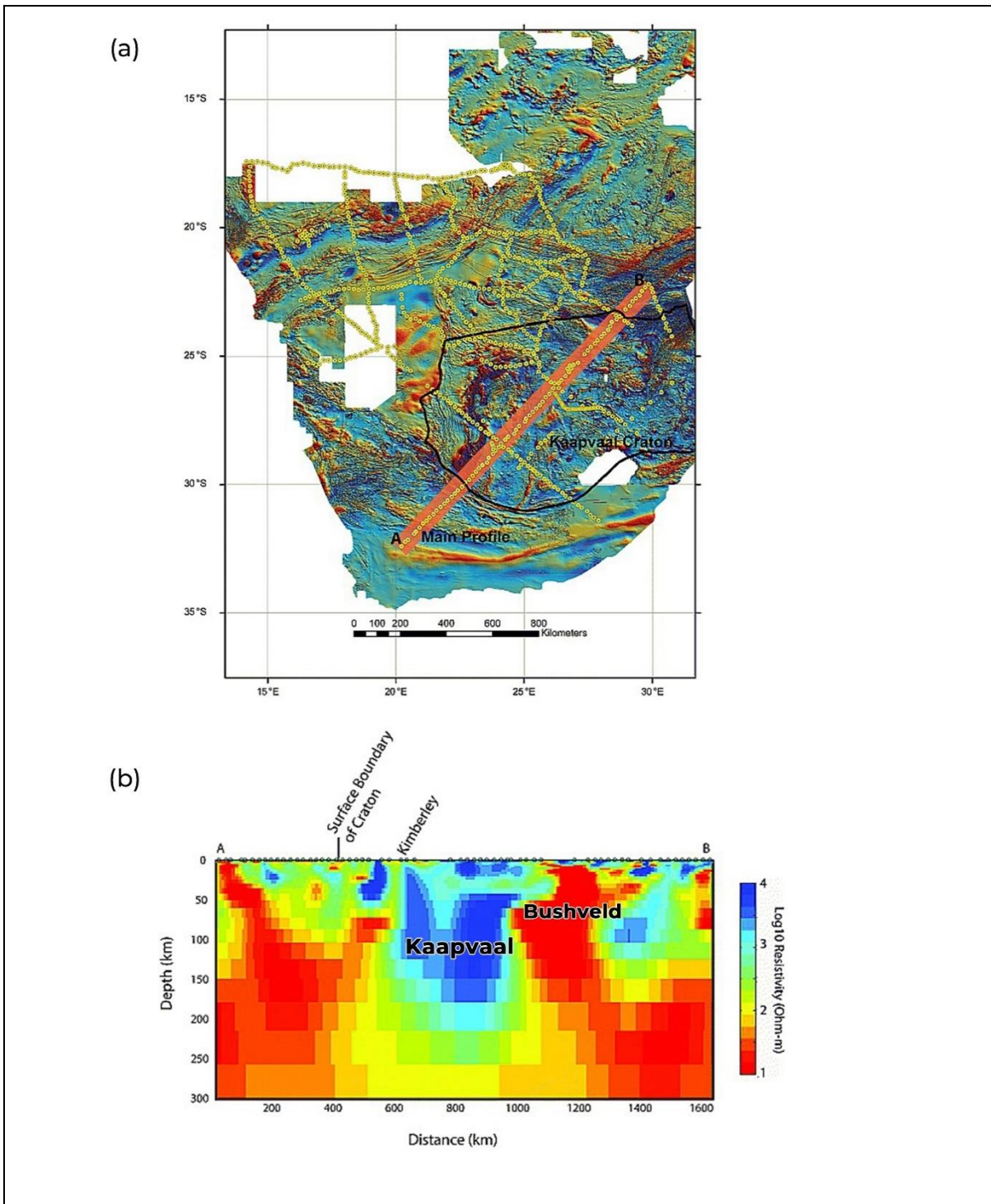


Figure A1: (a) A map of southern Africa aeromagnetic data and SAMTEX MT stations (yellow dots), the black lines shows the outline of the Kaapvaal Craton (Begg et al., 2009). (b) Electrical conductivity model across the main profile A-B highlighted in (a) showing the Kaapvaal Craton and Bushveld Complex structure labelled. The figure is after (Evans et al., 2011).

## APPENDIX 2

### Electrical Conductivity Model around Location of 03 April Earthquake in Central Botswana

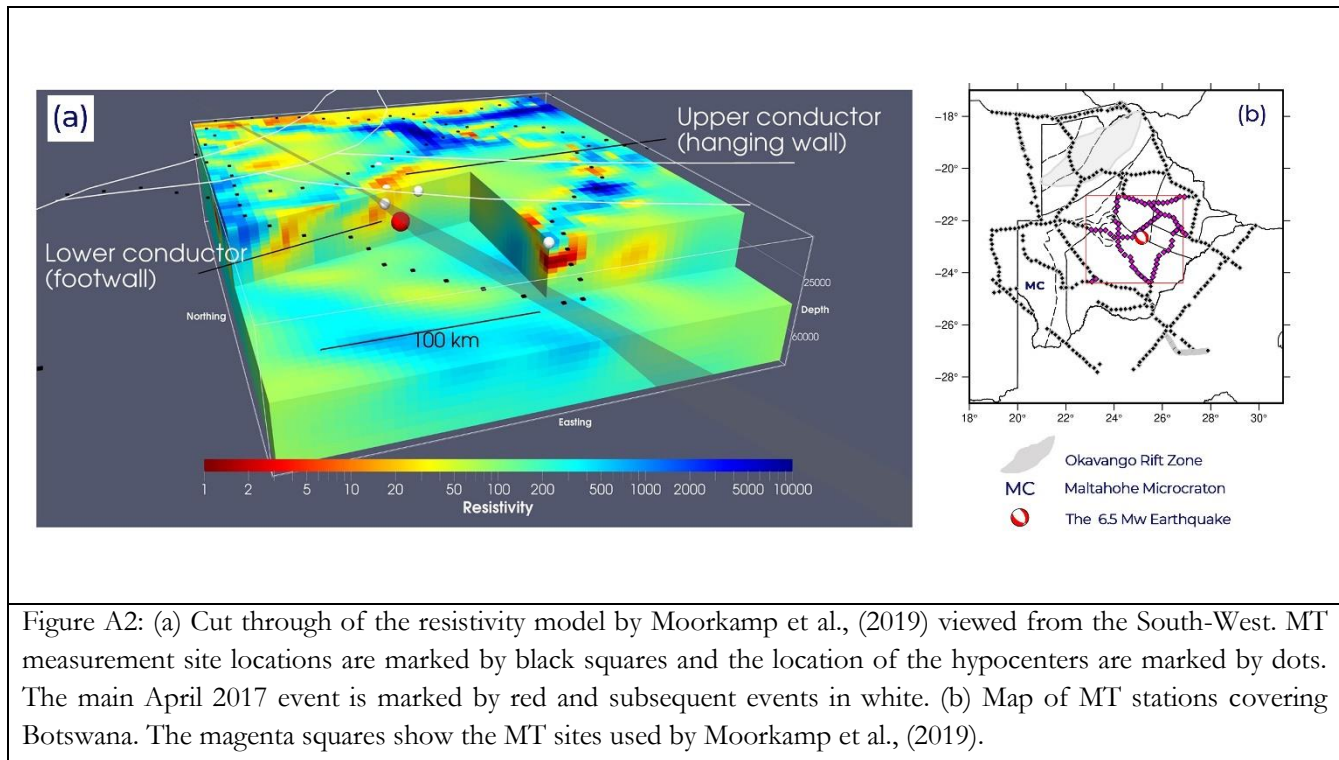


Figure A2: (a) Cut through of the resistivity model by Moorkamp et al., (2019) viewed from the South-West. MT measurement site locations are marked by black squares and the location of the hypocenters are marked by dots. The main April 2017 event is marked by red and subsequent events in white. (b) Map of MT stations covering Botswana. The magenta squares show the MT sites used by Moorkamp et al., (2019).

## APPENDIX 3

### The Phase Tensor Representation

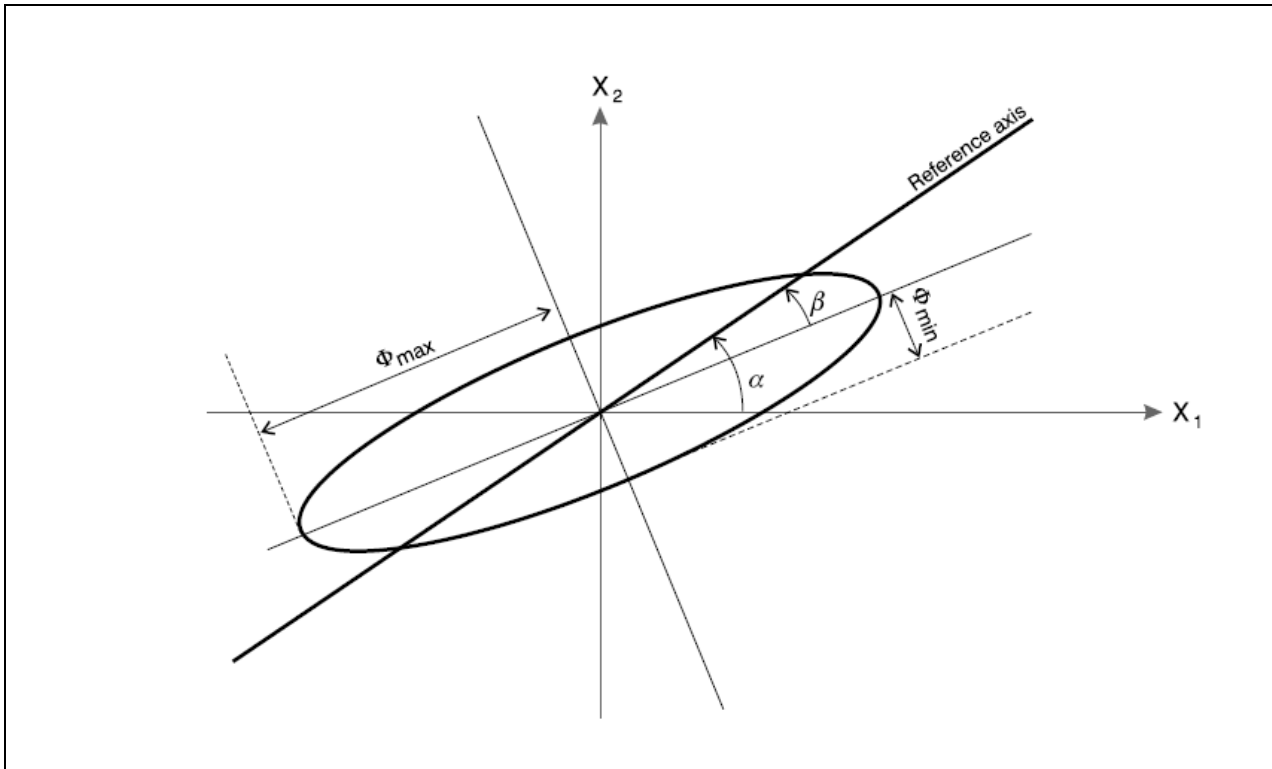
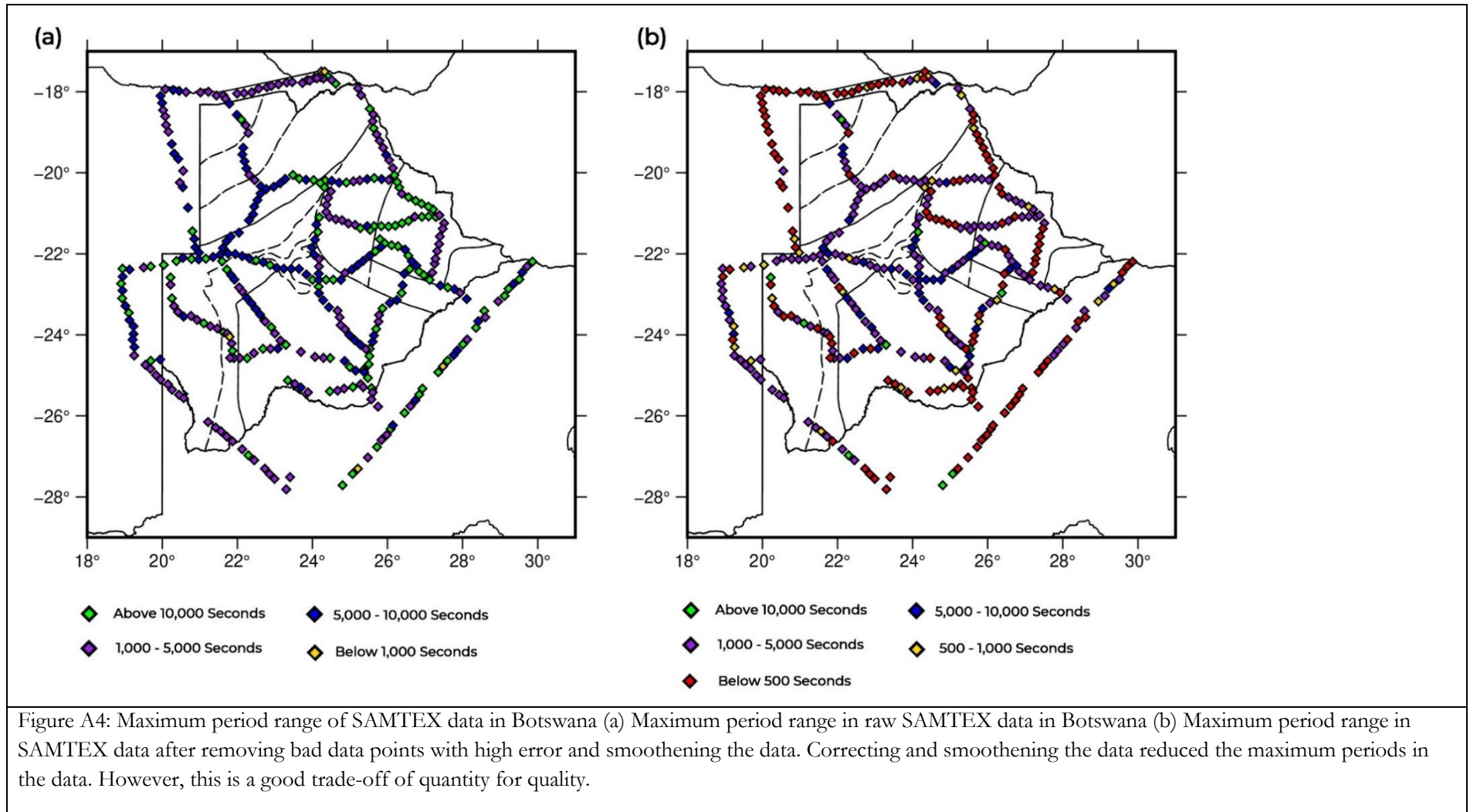


Figure A3: The graphical representation of a phase tensor as an ellipse (see Appendix). The semi-major and semi-minor axes of the ellipse are defined by the coordinate invariants  $\Phi_{min}$  and  $\Phi_{max}$ , respectively. The intrinsic physical properties of the phase tensor are: Skew =  $\beta$ ,  $\Phi_{min}$  and  $\Phi_{max}$ , and they are not dependent on the reference frame (Bibby et al., 2005).

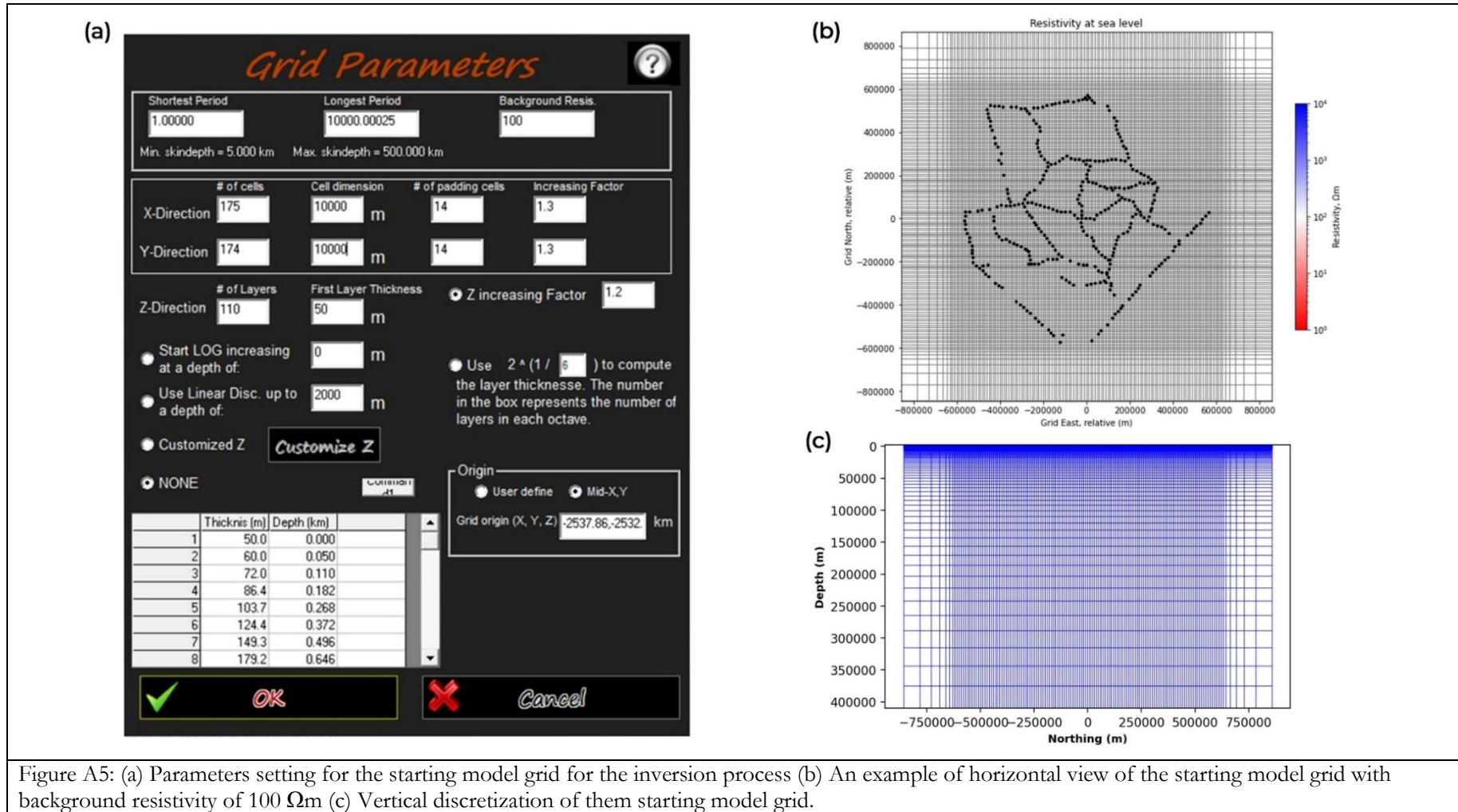
## APPENDIX 4

### Period Range of SAMTEX Data in Botswana



# APPENDIX 5

## Model Grid Parameters and Model Mesh



# APPENDIX 6

## Sensitivity Tests and Nationwide Inversions

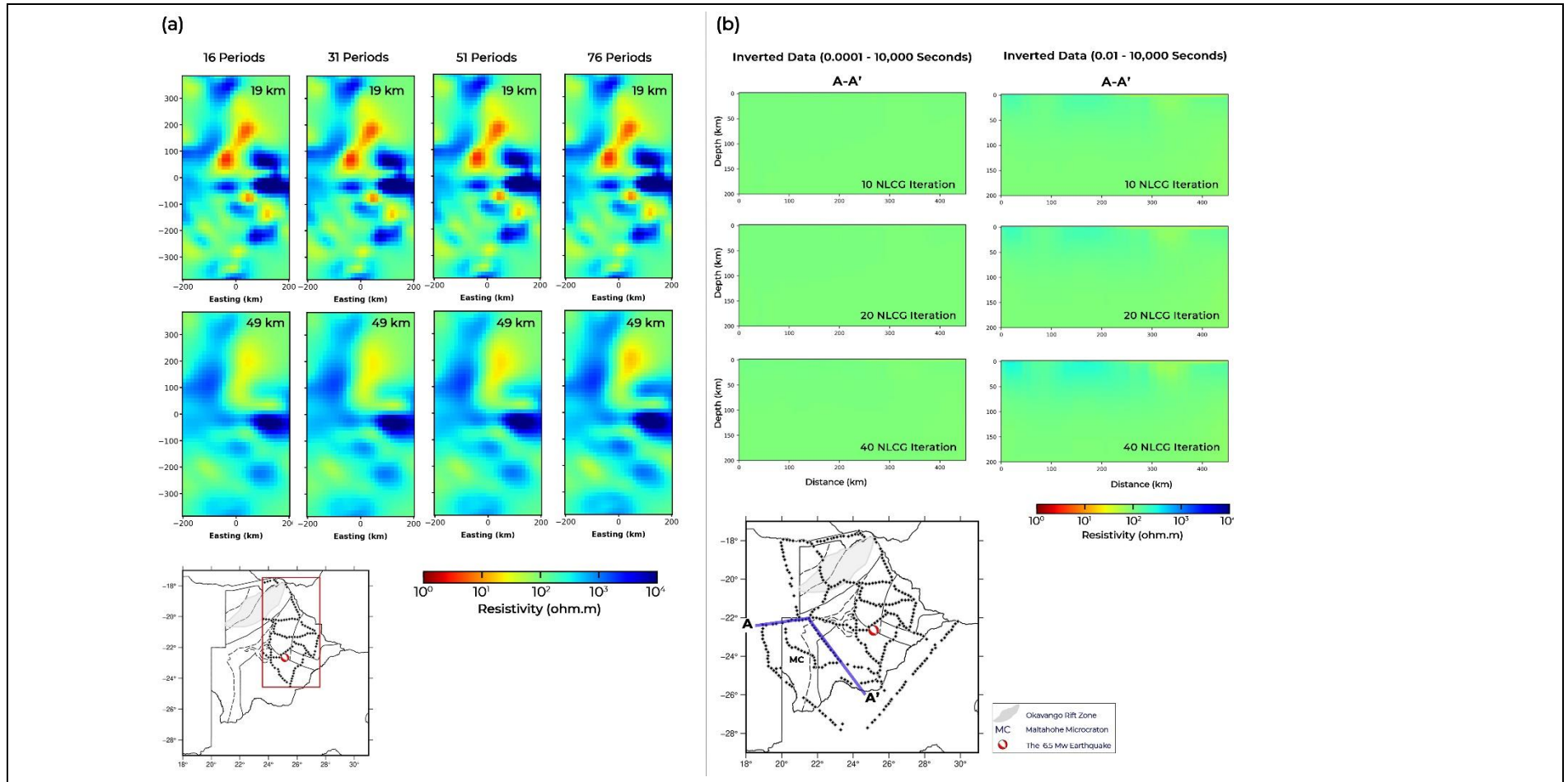


Figure A6: (a) Plan view of electrical conductivity model depth slices at 19 km and 49 km derived for four models with 16, 31, 51, and 76 periods data. Red bounding box shows the location of models presented. (b) Vertical sections across A-A' showing model development in inversion with short period data

# APPENDIX 7

## Dimensionality Analysis using Phase Tensor

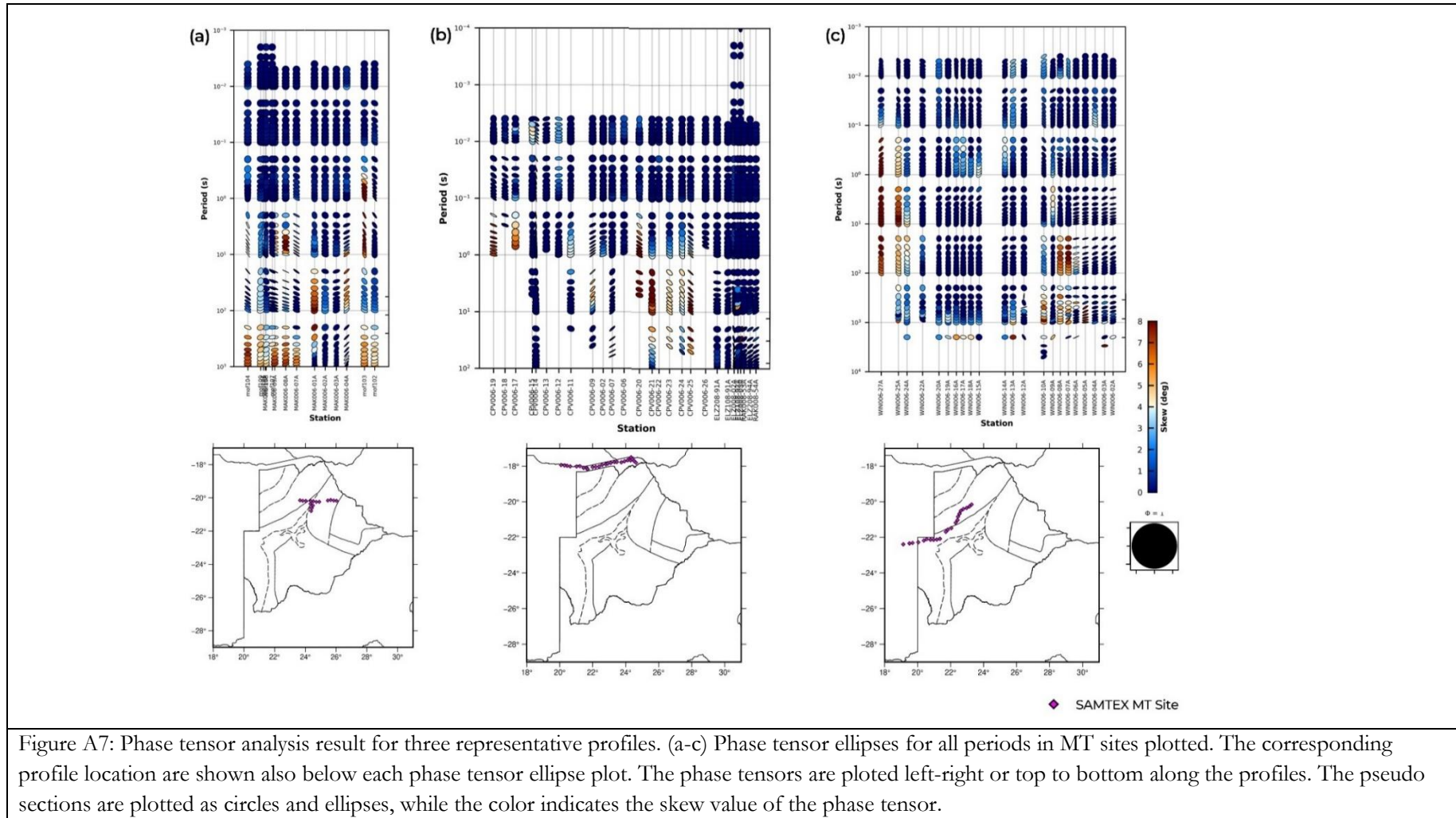


Figure A7: Phase tensor analysis result for three representative profiles. (a-c) Phase tensor ellipses for all periods in MT sites plotted. The corresponding profile location are shown also below each phase tensor ellipse plot. The phase tensors are plotted left-right or top to bottom along the profiles. The pseudo sections are plotted as circles and ellipses, while the color indicates the skew value of the phase tensor.

## APPENDIX 8

### nRMS per Station for Components of Impedance Tensor and VTFs (3-D Nationwide Electrical Model of Botswana)

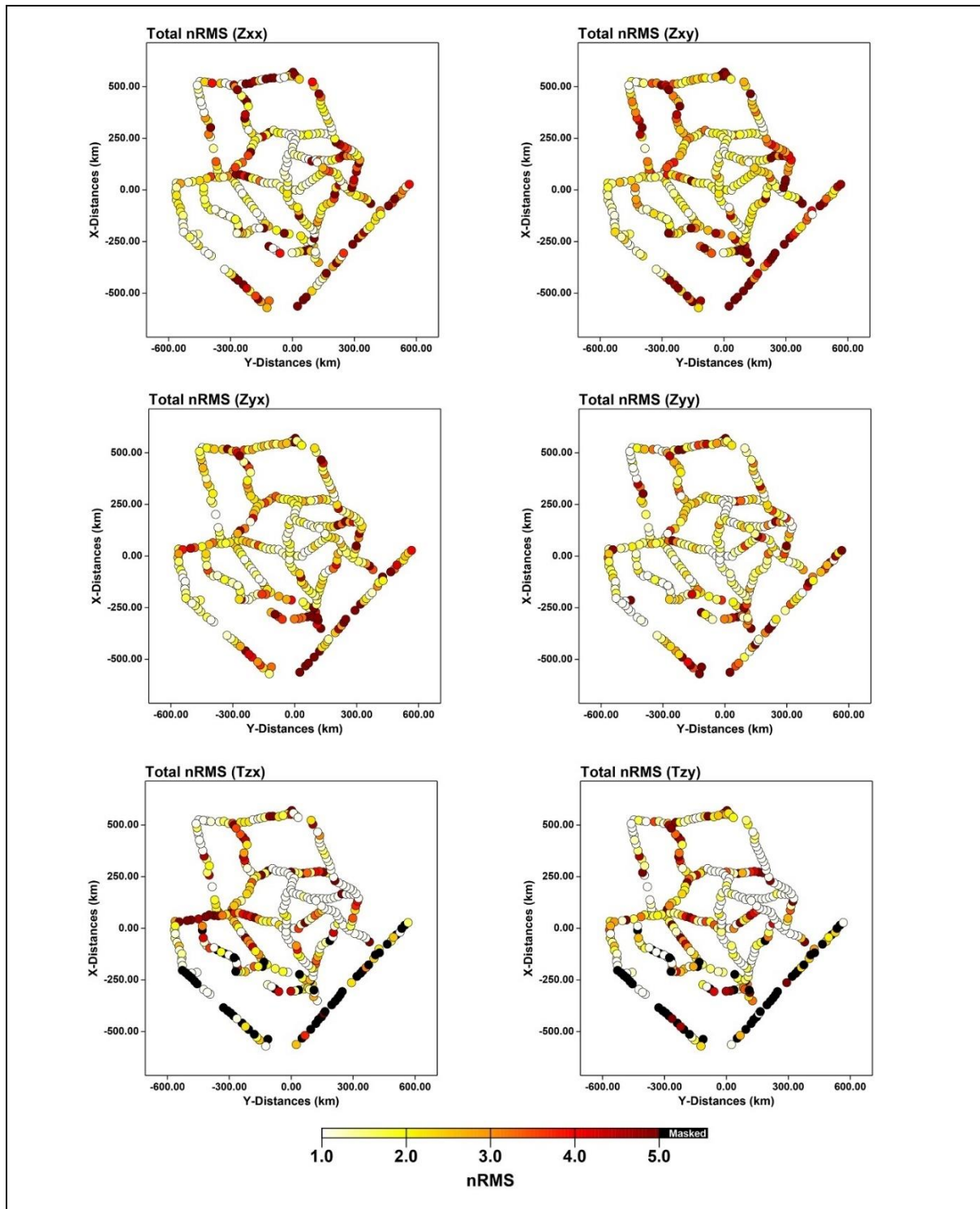


Figure A8: nRMS plot per station for each component of the impedance tensor and VTFs for the 3-D nationwide electrical model of Botswana. The MT sites are represented in circles and the corresponding nRMS are indicated by the colour. Masked (shown in black colour) = no data.

# APPENDIX 9

## Observed and Predicted Responses for Representative MT Sites

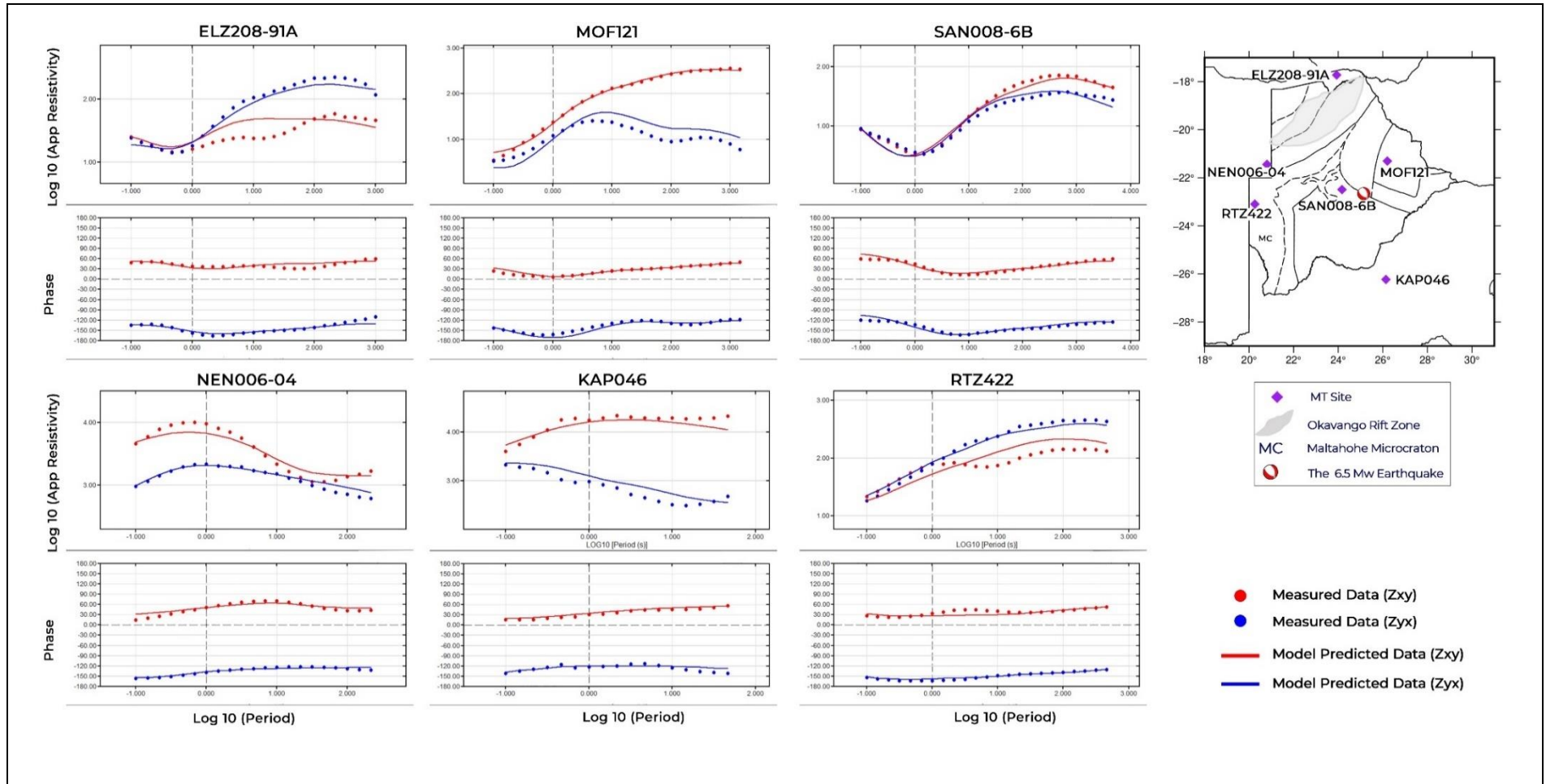


Figure A9: Observed and predicted responses for six representative MT Sites. Location maps shows the MT sites analysed.

# APPENDIX 10

## nRMS per Station for Data Period Sensitivity Test Model

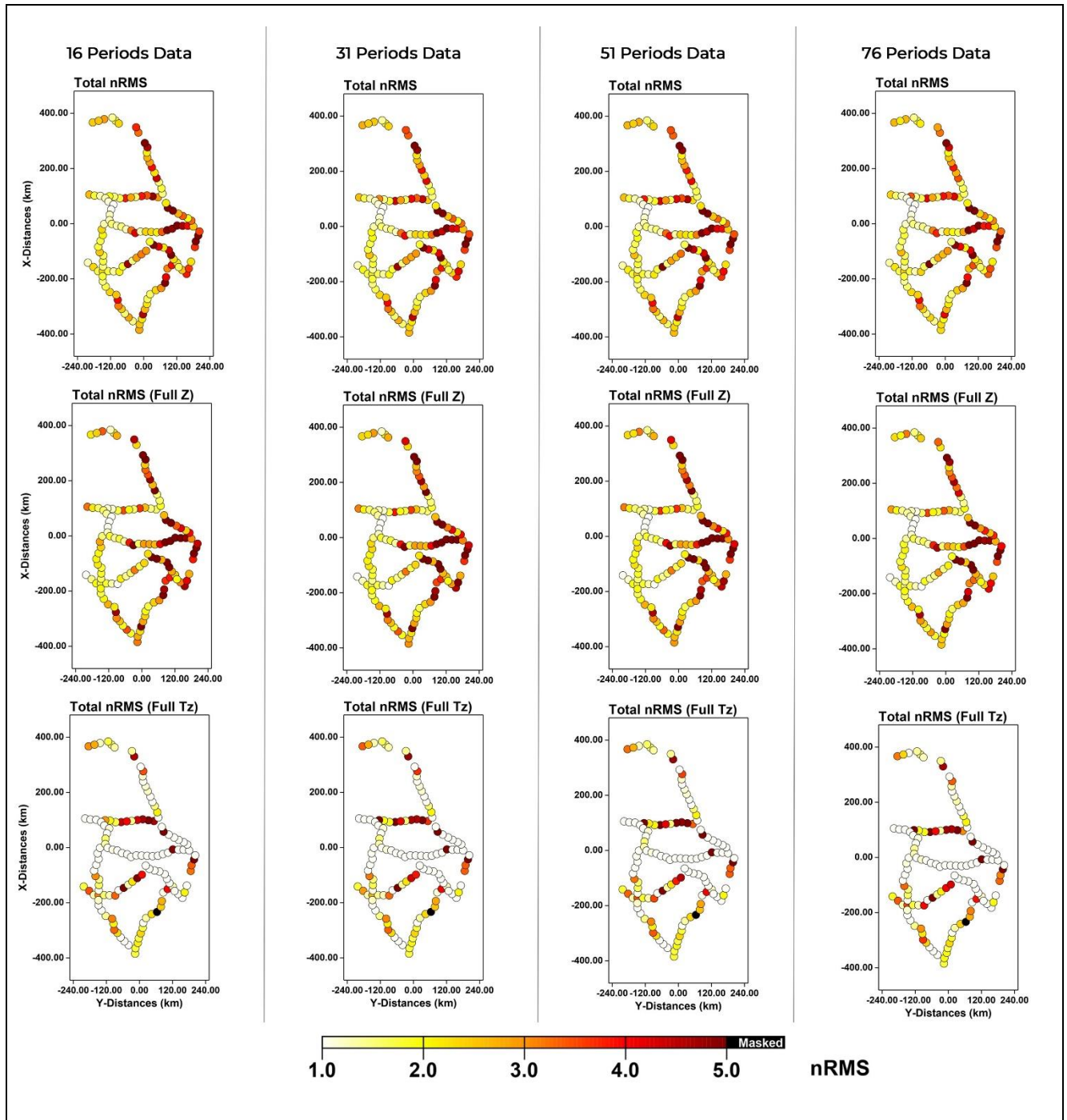


Figure A10: nRMS plot per station for total impedance, impedance tensor, and VTFs data components for models derived from 16, 31, 51 and 76 periods data. The MT sites are represented in circles and the corresponding nRMS are indicated by the colour. Masked (shown in black colour) =no data.